UNIVERSITY OF CALIFORNIA

Santa Barbara

Investigating the Aggregation of the ALS-Related Proteins TDP-43 and SOD1 Utilizing Atomic Force Microscopy

A dissertation submitted in partial satisfaction of the

requirements for the degree Doctor of Philosophy

in Chemistry

by

Dezmond Bishop

Committee in charge:

Professor Steven K. Burrato, Chair

Professor Michael T. Bowers

Professor Mattanjah S. de Vries

Professor Stuart C. Feinstein

December 2022

The dissertation of Dezmond Bishop is approved.

_____

Michael T. Bowers

_____

Mattanjah S. de Vries

_____

Stuart C. Feinstein

_____

Steven K. Buratto, Committee Chair

September 2022

Investigating the Aggregation of the ALS-Related Proteins TDP-43 and SOD1 Utilizing Atomic Force Microscopy

by

Dezmond Bishop

Acknowledgements

First and foremost, I would like to thank my advisor Prof. Steve Buratto for his guidance and mentorship throughout my PhD studies. Steve provided me with the flexibility to work on interesting projects outside the historic direction of the group. He has always been incredibly supportive and helpful, particularly in the development of presentation skills. I also had the opportunity to collaborate heavily with Prof. Mike Bowers, who is a wealth of knowledge relating to protein aggregation and neurodegenerative diseases. His influence is a major factor that has enabled the projects I have been involved with to flourish. I would also like to thank Prof. Mattanjah de Vries and Prof Stu Feinstein for serving on my committee and extending their guidance.

While I did not have the opportunity to work closely with them, Prof. Kristi Lazar Cantrell and Prof. Ambuj Singh were essential contributors to the projects I worked on. Kristi was responsible for the synthesis of many of the peptides I studied throughout my PhD and during our few meetings she was always an extremely positive person and seemed excited about our work. Ambuj is responsible for the design of the inhibitor drug molecules investigated in this work and collaborating with him has provided an exciting and promising avenue of research.

One of the biggest contributors to my PhD work at UCSB was Dr. Veronica Laos, a former member of the Bowers research group. Working with Veronica, I gained access to a wealth of knowledge and cemented the collaboration between our two research groups. All of the major projects I have worked on started with Veronica's work, and without her none of

the work presented here would have been possible. Perhaps most importantly, I truly enjoyed working with her.

I also had the pleasure of working with many other members of my research group as well as the Bowers research group who assisted me throughout my PhD studies. Yingying Jin and Sadia Nowshin both worked with me in studying TDP-43(307-319) before joining the Buratto research group as graduate students. Former Buratto group members Dr. Austin Barnes, Dr. Cynthia Cooper, and Dr. Max Giammona all offered guidance to me as a new graduate student. Xikun Liu in the Bowers research group instructed me on the use of their home-built ion mobility-mass spectrometer.

Finally, I would like to extend my sincere gratitude to the friends and family who have supported me throughout my PhD studies. Both my parents have provided me with unconditional love and support and have always encouraged me to excel. Knowing that they are there for me no matter what happens has been a stabilizing effect in sometimes tumultuous times. My fellow graduate students at UCSB have also been instrumental in my success. In particular, my former roommates Sheng-Ping Liang, Pavel Shapturenko, Kalin Hansen, and Sam Jacobs have all helped to make my studies a more enjoyable experience.

VITA OF DEZMOND BISHOP

December 2022

EDUCATION

B.A. in Chemistry (Honors), Connecticut College, New London, CT: Fall 2012-Spring 2016

Ph.D in Chemistry, University of California, Santa Barbara, Santa Barbara, CA: Fall 2016-Fall 2022 (expected)

PROFESSIONAL EMPLOYEMENT

Graduate Student Researcher, University of California Santa Barbara, Department of Chemistry and Biochemistry: Fall 2016-Fall 2022
Teaching Assistant, University of California Santa Barbara, Department of Chemistry and Biochemistry: Fall 2016-Spring 2022

- General Chemistry Lab TA
- Physical Chemistry Lecture TA
- Biophysical Chemistry Lecture TA

Undergraduate Student Researcher, Connecticut College, Department of Chemistry Summer 2015-Spring 2016

PUBLICATIONS

Bishop, D.; Laos, V.; Cantrell, K. L.; Buratto, S. K.; Bowers, M. T. Characterizing the Oligomeric Assembly of SOD1: Links to Familial Amyotrophic Lateral Sclerosis (ALS). *In Preparation.*

Laos, V.; Do, T. D.; Bishop, D.; Jin, Y.; Marsh, N. M.; Quon, B.; Fetters, M.; Cantrell, K. L.; Buratto, S. K.; Bowers, M. T. Characterizing TDP-43(307-319) Oligomeric Assembly to Elucidate Mechanistic and Structural Implications Involved in the Etiology of ALS. *ACS Chem. Neurosci.* **2019**, *10* (9), 4112−4123.

Laos, V.; Bishop D.; Ganguly P.; Schonfeld, G.; Trapp, E.;Cantrell, K. L.; Buratto, S. K.; Shae, J. E.; Bowers, M. T. Catalytic Cross Talk between Key Peptide Fragments That Couple Alzheimer's Disease with Amyotrophic Lateral Sclerosis. *J. Am. Chem. Soc.* **2021,** *143* (9), 3494-3502.

Laos, V.; Bishop, D.; Lang, A. C.; Marsh, N. M.; Cantrell, K. L.; Buratto, S. K.; Singh, A. K.; Bowers, M. T. Modulating ALS-Related Amyloidogenic TDP-43$_{307-319}$ Oligomeric Aggregation with Computationally Derived Therapeutic Molecules. *Biochemistry*. **2020**, *59* (4), 499-508.

ABSTRACT

Investigating the Aggregation of the ALS-Related Proteins TDP-43 and SOD1 Utilizing Atomic Force Microscopy

by

Dezmond Bishop

Protein misfolding has been implicated in a number of neurodegenerative diseases, including Alzheimer's Disease (AD), Parkinson's Disease, and amyotrophic lateral sclerosis (ALS). In these diseases, one or more proteins adopt a non-native conformation that is prone to aggregate into small soluble oligomers and larger fibrils, which typically present as abnormal protein deposits in the afflicted cells or tissues. Understanding the aggregation of these proteins is essential to the development of effective disease-modifying therapeutics.

TAR DNA binding protein of 43 kDa (TDP-43) is one such protein that is believed to play a causative role in sporadic ALS and tau- and alpha synuclein-negative frontotemporal lobar degeneration (FTLD-TDP), and is also observable in a significant percentage of individuals with AD, where it is associated with increased cognitive decline. Atomic force microscopy (AFM) was used as a complementary technique to ion mobility-mass spectrometry (IM-MS) to elucidate the early-stage aggregation of the amyloidogenic core region of TDP-43, TDP-43(307-319). TDP-43(307-319) aggregation was shown to progress via a bifurcated pathway, with toxic oligomers off pathway from fibrillization. Two ALS-

related mutations of TDP-43 increase aggregation while a synthetic non-toxic mutant prevents oligomerization but does not suppress fibrilization. Similar experiments with a fragment of the familial ALS-related protein superoxide dismutase-1, SOD1(28-38), show that the formation of ordered, non-fibrillar aggregates was tied to the presence of a potentially toxic corkscrew oligomer.

TDP-43(307-319) aggregation was also modulated using two methods. First, computationally generated inhibitors molecules developed using the Join Pharmacophore Space (JPS) were shown to disrupt oligomers believed to play a toxic role in ALS but were not observed to impact off-pathway fibrillization. Further refinement of the JPS algorithm will be required if fibril disruption is shown to be necessary for effective treatment of ALS. Next, TDP-43(307-319) was co-aggregated with a fragment of the AD-implicated protein amyloid beta, Aβ(25-35). Coaggregation of TDP-43(307-319) and Aβ(25-35) results in increased formation of toxic oligomers for both peptides. Coaggregation was also conducted with a mutation of TDP-43(307-319) that suppresses toxic oligomers, and potentially toxic Aβ(25-35) oligomers were observed to increase fibrilization of TDP-43. These results indicate that cross talk between amyloidogenic proteins must be considered in the development of therapeutics for related diseases.

Table of Contents

I. Introduction

A number of natively occurring proteins are believed to play a causative role in neurodegenerative diseases including Alzheimer's disease, amyotrophic lateral sclerosis (ALS), and Parkinson's disease. In patients with these diseases, one or more proteins are observed to misfold and aggregate into soluble oligomers and insoluble fibrils. Extracellular and/or intracellular fibrillar deposits are pathological hallmarks in most neurodegenerative diseases. While the exact mechanisms of these diseases remain to be elucidated, toxicity has been linked to the soluble oligomer species. Understanding the full aggregation pathways of implicated proteins is likely essential to producing effective therapies for neurodegenerative diseases.

1.1 Protein Misfolding Diseases

Protein misfolding diseases are a class of diseases in which abnormal structural changes to native protein result in a loss of normal function or a toxic gain of function. Protein misfolding diseases largely overlap with neurodegenerative diseases, characterized by progressive damage to neurons. An estimated 50 million people are currently living with a protein misfolding neurodegenerative disease, a number expected to increase to over 80 million by 2030 and over 150 million by 2050.[1,2]

The leading cause of neurodegeneration is Alzheimer's disease (AD), a form of dementia that causes impairment in learning and memory, behavioral changes, and a loss of independence, and ultimately leads death. AD is the seventh leading cause of death in the United States, accounting for over 130,000 deaths in 2020.[2,3] AD is also associated with a significant economic cost, with the total cost of treatment reaching $305 billion in 2020.[4] While less prevalent, other protein misfolding diseases such as Lewy body dementia,

frontotemporal dementia, and Huntington's disease may also cause dementia.[2] Other neurodegenerative diseases can effect physical functions, such as Parkinson's disease and amyotrophic lateral sclerosis (ALS), or Lou Gehrig's disease, which afflict basal ganglia and motor neurons respectively. Both of these diseases may copresent with cognitive impairment.[5,6]

Unfortunately, protein misfolding diseases are fatal and do not have effective treatments or cures. The current standard of treatment focuses on temporarily alleviating symptoms and has not been conclusively shown to prolong life. As such, it is imperative to expand the current understanding of protein misfolding diseases in the search for effective therapeutics. The similar pathology of abnormal protein aggregates shared by these diseases suggests that advancements in one disease may lead to similar advancements in treatment of all protein misfolding diseases.[7,8]

While the exact mechanism of pathology has yet to be determined, one or more proteins have been implicated in each protein misfolding disease due to their presence in abnormal protein deposits. Extracellular Amyloid beta and tau plaques and intracellular tau neurofibrillary tangles are found in AD, α-synuclein Lewy bodies are found in the basal ganglia in Parkinson's disease, and TAR DNA binding protein-43 (TDP-43) inclusion bodies are associated with frontotemporal lobar degeneration with ubiquitin-positive inclusions and sporadic ALS.[5,6,9,11] TDP-43 aggregates are also present in a notable portion of patients with AD, increasing up to 75% for late-stage AD. Coupled with the cognitive impairment experienced by a subset of ALS patients, this suggests that there may be important interactions between proteins related to these different diseases. [12-16]

Abnormal protein deposits often contain protein fragments instead of full-length proteins. Amyloid beta denotes a 36-43 amino acid polypeptide chain that is a product from the proteolysis of the amyloid precursor protein. Amyloid beta(25-35) has been shown to be physiologically present and toxic. C-terminal fragments of TDP-43 are the main component of sporadic ALS inclusion bodies. Additionally, studies have shown that specific, small regions of these proteins drive aggregation. Cleavage, post translational modification, or mutation of proteins may open access to these segments. This, along with the fact that full length proteins are too large for certain experimental and modeling techniques, has led a significant portion of research to focus on the aggregation of specific fragments of these proteins. [10,11,17-19]

This work will primarily focus on the aggregation mechanism of TDP-43(307-319). This fragment is found in the low complexity C-terminal domain, which is largely disordered. Research has identified this fragment as being sufficient and necessary for fibril formation and was capable of inducing axon neural death.[19] This region also contains two ALS-related point mutations, A315E and A315T. [20-21] This work also investigates SOD1(28-38), identified for its propensity to form toxic, beta sheet-rich oligomers. Mutations of SOD1 are associated with familial ALS and some studies suggest WT SOD1 may play a role in sporadic ALS as well.[22-28]

1.2 Protein Structure

A protein's propensity to aggregate is intrinsically tied to its structure. Proteins are polymers of amino acids, referred to as polypeptides, which can be described in four levels of structure. Protein primary structure refers to the sequence of amino acids. During protein synthesis, the amine group of one amino acid or polypeptide chain reacts with the carboxylic

acid of another single amino acid to form a peptide bond, releasing water in the process (**Figure 1.1**). The N-terminus of the resulting polypeptide chain refers to the free amine group at one end of the peptide backbone, while the C-terminus refers to the free carboxylic acid at the other end. Proteins are synthesized from the N-terminus to the C-terminus, and primary sequence is conventionally written the same way, with the N-terminus on the left and the C-terminus on the right. Protein primary structure is ultimately determined by the sequence of DNA that encodes for that protein. Messenger RNA (mRNA) is copied from the associated DNA in a process known as transcription. Ribosomes then translate the mRNA, with triplet nucleotide codons transcribed as a specific amino acid. Genetic mutations in the encoding DNA genes are therefore expressed as mutations in the primary structure of the associated protein. Primary structure determines how a protein folds, and therefore dictates higher levels of protein structure.[29]

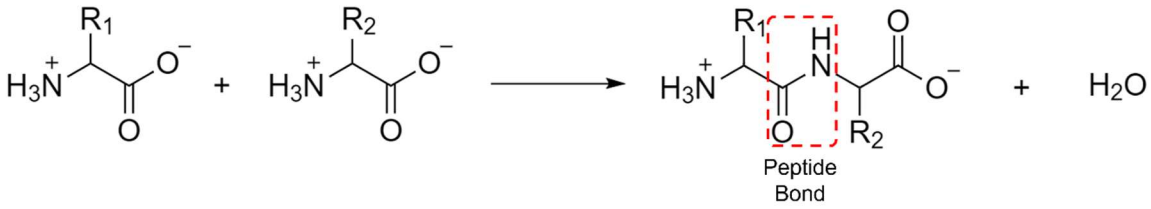

Figure 1.1 Formation of a peptide bond between two amino acids. R_1 and R_2 represent side chains and are specific to each amino acid. Amino acids and the dipeptide are in their zwitterionic form, typical at a physiological pH of 7.4, with the free amine groups protonated and the free carboxylic acid groups deprotonated.

Protein secondary structure describes the local three-dimensional structure of a protein. Proteins commonly contain structural motifs that form spontaneously as a result of intramolecular forces dependent on the primary structure of the protein. These structural motifs are typically defined based on the arrangement of hydrogen bonds. Of particular

interest with respect to amyloid proteins is the beta sheet motif, which consists of two or more rows of peptides where the amine groups of one row forms hydrogen bonds with the carbonyl groups of another row (**Figure 1.2**). In amyloid proteins, these beta sheets are often composed of a large number of hydrophobic residues which create a hydrophobic interface. In order to minimize contact with water, these interfaces may associate with one another, resulting in beta sheet stacking that is often a driving force behind protein aggregation.[29,39]

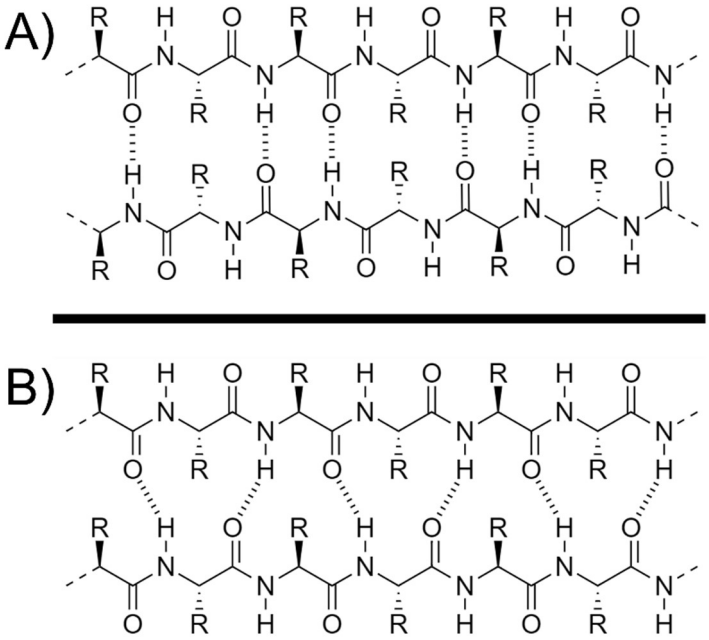

Figure 1.2 Antiparallel (A) and parallel (B) beta sheets comprised of two beta strands. In antiparallel beta sheets the two beta strand backbones are offset from one another. This allows for optimal hydrogen bonding between the N-H of one strand and the O of another strand. In parallel beta sheets the beta strand backbones are in line with one another. As a result, hydrogen bonding is slightly less optimal.

Protein tertiary structure is the complete three-dimensional structure of a single polypeptide chain. A protein in its normal functional conformation is said to be in its native state and is typically at or near a thermodynamic energy minimum. A protein that is unable to

adopt its native conformation is described as misfolded. Many proteins related to protein misfolding diseases can be described as intrinsically disordered.[8,19] These proteins, while usually having conserved regions, lack a complete fixed or well-defined tertiary structure and may adopt different conformations while remaining functional. It is believed that in at least some protein misfolding diseases this flexibility allows the protein to adopt an aggregation-prone conformation that can be stabilized by protein-protein interactions and potentially induce the same conformation onto other members of the same protein in a prion-like effect.[29,30]

Some proteins in their native state are complexes of either like or different polypeptides chains. For proteins that are comprised of two or more polypeptide chains, protein quaternary structure describes the oligomerization of these polypeptide chains. Oligomerization that is not associated with the native function of a protein is implicated in protein misfolding diseases. Non-protein cofactors such as metals may also play an important role in protein structure and function. Some studies suggest that depletion of cofactors may be related to an increase in the toxicity of disease-related proteins.[29,31,32]

1.3 Protein Aggregation

Protein aggregation begins with protein misfolding.[8] While the exact trigger of misfolding is unknown, it is believed that intrinsically disordered regions and certain mutant proteins are particularly prone to aggregation and changing cellular conditions such as increased oxidative stress (often associated with aging) may play a role.[20,21,33] **Figure 1.3** is a simplified schematic of protein aggregation. Under conditions such as those stated above, a protein may adopt a misfolded, aggregation-prone, and typically beta sheet-rich conformation. This protein may then associate with other proteins to stabilize this

conformation through hydrophobic interactions present in beta sheet stacking, forming oligomers. Additional association of proteins results in oligomeric growth. Continuous association and a strengthening of the intermolecular interactions between proteins may lead to fibrilization.

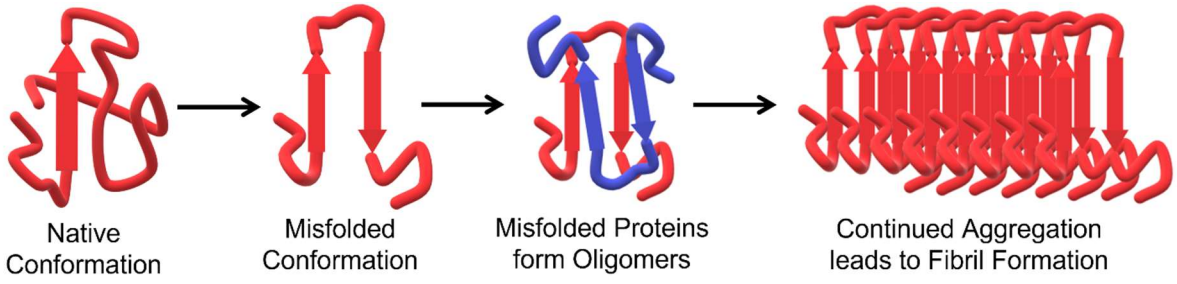

Figure 1.3. Cartoon of the protein aggregation pathway. A native protein may adopt a misfolded, aggregation prone conformation. This conformation can be stabilized through association with other proteins, often through beta sheet stacking. Continuous association and beta sheet stacking can lead to fibril formation.

Amyloid fibrils are the primary component of the amyloid protein deposits and were the first pathological hallmark of protein misfolding diseases. Because of this, fibrils have been the main focus and therapeutic target of research until recently, when new studies indicated that small soluble oligomers are the likely toxic agent in these diseases.[34-37] Fibrils nonetheless remain an important point of study in protein misfolding diseases due to their inherent equilibrium with soluble oligomers. Understanding when and why oligomers form fibrils and how fibrils relate to potential toxic agents is essential to understanding the overall aggregation pathway involved in these diseases. In some cases, toxic oligomers have been shown to even seed fibril formation.[38]

Fibrils can be defined as nonbranching, ribbon-like nanoscale features with a common cross-beta spine. Along the spine, side chains from adjacent beta sheets form what

has been termed a 'steric zipper' by Eisenberg et al in which interlocking side chains create a dry interface. Fibrils comprised of parallel or antiparallel beta sheets have both been observed, along with a variety of different stacking orientations, all of which contain the steric zipper interface.[39]

Interestingly, the cylindrin beta barrel structural motif has been observed in oligomers of a number of different systems.[40,41] Eisenberg et al isolated the hexameric cylindrin (**Figure 1.4A**) from a fragment of αB crystallin (**Table 1.1**) which consists of 6 antiparallel beta strands that form a cylindrical barrel with a hydrophobic core.[42] Each pair of beta strands in the cylindrin are out of register with one another, creating strong interfaces within a pair and weak interfaces between pairs. Cylindrin-like structures and the closely related corkscrew[43,44] (**Figure 1.4B**) have emerged as attractive areas of study because of their similarities and toxic nature.

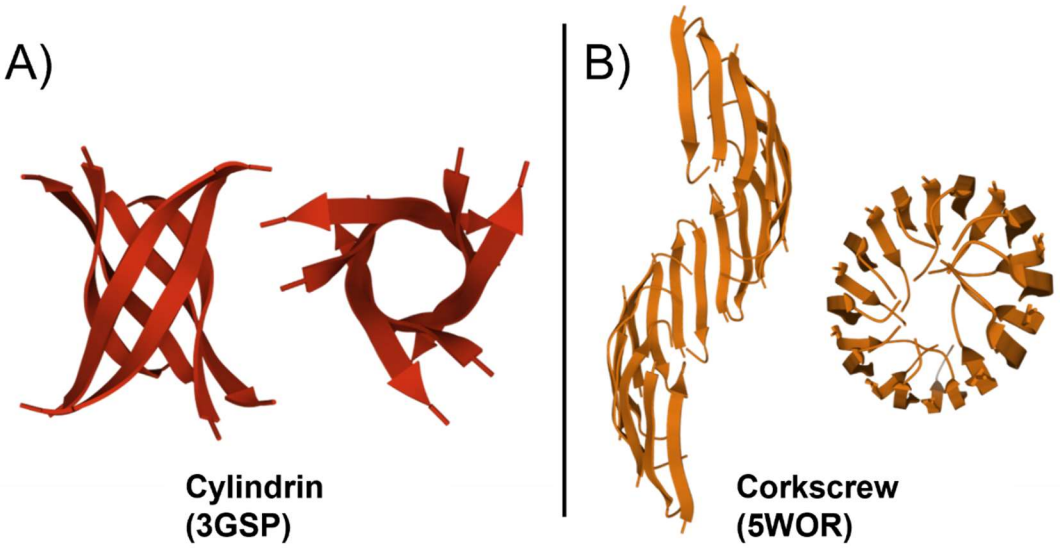

Figure 1.4 Side and top view of (A) the αB-crystallin(90-100) cylindrin (PDB 3GSP) [42] **and (B) the SOD1(28-38) P28KG37R mutant corkscrew (PDB 5WOR).** [44]

An important residue of cylindrin-like structures and corkscrews is the central glycine residue (**Table 1.1**). In several systems mutations of this residue prevent the formation of the cylindrin-like structure or corkscrew and greatly reduces the extent of oligomerization.[40,44] This has been attributed to the high flexibility of glycine, which is the amino acid with the smallest side chain, allowing the protein to accommodate the curvature exhibited in these structures. Additionally, these mutations are observed to be non-toxic, lending significant credence to the importance of these structures in protein misfolding diseases.

αB-Crystallin(90-100)	**K V K V L G D V I E V**
TDP-43(307-319)	**M G G G M N F G A F S I N**
SOD1(28-38)	**P V K V W G S I K G L**
Aβ(25-35)	**G S N K G A I I G L M**

Table 1.1 Primary sequence of peptides shown to adopt or be compatible with cylindrin-like structures or corkscrews. The central glycine residue, highlighted in red, has been shown to be important to the stability of these structures.

It should also be noted that cylindrin-like structures and fibrils are not necessarily on the same mechanistic pathway. Fibrils are typically in-register, while cylindrin-like structures are out of register.[39] That means that in order for a cylindrin-like structure to form a fibril it would need to at least partially dissociate, breaking several hydrogen bonds. This is energetically unfavorable and may suggest that other oligomers are responsible for the formation of fibrils.[40]

1.4 References

1. Alzheimer's Disease International. 2018. *World Alzheimer's Report 2018 – The state of the art dementia research: New Frontiers*. London: Alzheimer's Disease International.
2. World Health Organization. *Fact Sheets: Dementia*. World Health Organization, September 2021. ://www.who.int/en/news-room/fact-sheets/detail/dementia. (Accessed 2022-09-07).
3. Murphy, S. L.; Kochanek, K.D.; Xu, J. Q.; Arias, E. *Mortality in the United States, 2020.* NCHS Data Brief, no 427. Hyattsville, MD: National Center for Health Statistics. 2021.
4. Alzheimer's Association Report. 2020 Alzheimer's disease facts and figures. *Alzheimers Dement.* **2020**, 16, 391-460.
5. Bloem, R. B.; Okun, M. S.; Klein, C. Parkinson's Disease. *Lancet*. **2021**, *397* (10291), 2284-2303.
6. Masrori, P.; Van Damme, P. Amyotrophic lateral sclerosis: a clinical review. *Eur. J. Neurol*. **2020,** *27* (10), 1918-1929.
7. Hartl, F. U. Protein Misfolding Diseases. *Annu. Rev. Biochem.* **2017,** *20*, (86), 21-26.
8. Chiti F.; Dobson C. M. Protein Misfolding, Amyloid Formation, and Human Disease: A Summary of Progress Over the Last Decade. *Annu. Rev. Biochem.* **2017,** *20*, (86), 27-68.
9. Trejo-Lopez, J. A.; Yachnis, A. T.; Prokop, S. Neuropathology of Alzheimer's Disease. *Neurotherapeutics.* **2022**, *19*, 173–185.
10. Neumann M.; Sampathu D.M.; Kwong L.K.; Truax A.C.; Micsenyi M. C.;, Chou T.T.; Bruce J.; Schuck T.; Grossman M.; Clark C. M.; McCluskey L.F.; Miller B. L.; Masliah E.; Mackenzie I. R.; Feldman H.; Feiden W.; Kretzschmar H.A.; Trojanowski J.Q.; Lee V.M. Ubiquitinated TDP-43 in frontotemporal lobar degeneration and amyotrophic lateral sclerosis. *Science*. **2006,** *314* (5796), 130-3.
11. Arai T.; Hasegawa M.; Akiyama H.; Ikeda K.; Nonaka T.; Mori H.; Mann D.; Tsuchiya K.; Yoshida M.; Hashizume Y.; Oda T. TDP-43 is a component of ubiquitin-positive tau-negative inclusions in frontotemporal lobar degeneration and amyotrophic lateral sclerosis. *Biochem. Biophys. Res. Commun.* **2006,** *351* (3), 602-11.

12. Josephs, K. A.; Whitwell, J. L.; Weigand, S. D.; Murray, M. E.; Tosakulwong, N.; Liesinger, A. M.; Petrucelli, L.; Senjem, M. L.; Knopman, D. S.; Boeve, B. F.; Ivnik, R. J.; Smith, G. E.; Jack, C. R.; Parisi, J. E.; Petersen, R. C.; Dickson, D. W. TDP-43 is a key player in the clinical features associated with Alzheimer's disease. *Acta. Neuropathol.* **2014**, *127* (6), 811−824.
13. Josephs, K. A.; Murray, M. E.; Whitwell, J. L.; Parisi, J. E.; Petrucelli, L.; Jack, C. R.; Petersen, R. C.; Dickson, D. W. Staging TDP-43 pathology in Alzheimer's disease. *Acta. Neuropathol.* **2014**, *127* (3), 441−450.
14. Jo, M.; Lee, S.; Jean, Y.-M.; Kim, S.; Kwon, Y.; Kim, H.-J. The Role of TDP-43 propagation in neurodegenerative diseases: Integrating insights from clinical and experimental studies. *Exp. Mol. Med.* **2020**, *52*, 1652−1662.
15. Huang, W.; Zhou, Y.; Tu, L.; Ba, Z.; Huang, J.; Huang, N.; Luo, Y. TDP-43: From Alzheimer's disease to limbic-predominant age-related TDP-43 encephalopathy. *Front. Mol. Neurosci.* **2020**, *13*, 1−7.
16. Shih, Y.-S.; Tu, L.-H.; Chang, T.-Y.; Ganesan, K.; Chang, W.-W.; Chang, P.-S.; fang, Y.-S.; Lin, Y.-T.; Jin, L.-W.; Chen, Y.-R. TDP-43 interacts with amyloid-beta, inhibits fibrillization, and worsens pathology in a model of Alzheimer's disease. *Nat. Commun.* **2020**, *11*, 5950−5965.
17. Millucci, L.; Ghezzi, L.; Bernardini, G.; Santucci, A. Conformations and Biological Activities of Amyloid Beta Peptide 25-35. *Curr. Protein Pept. Sci.* **2010**, *11*, 54-67.
18. Pike, C. J.; Walencewicz-Wasserman, A. J.; Kosmoski, J.; Cribbs, D. H.; Glabe, C. G.; Cotman, C. W. Structure-activity analyses of β-amyloid peptides: contributions of the β 25–35 region to aggregation and neurotoxicity. *J. Neurochem.* **1995**, *64*, 253–265.
19. Zhu, L.; Xu, M.; Yang, M.; Yang, Y.; Li, Y.; Deng, J.; Ruan, L.; Liu, J.; Du, S.; Liu, X.; Feng, W.; Fushimi, K.; Bigio, E. H.; Mesulam, M.; Wang, C.; Wu, J. Y. An ALS-mutant TDP-43 neurotoxic peptide adopts an anti-parallel beta-structure and induces TDP-43 redistribution. *Hum. Mol. Genet.* **2014**, *23* (1), 6863−6877.
20. Gitcho, M. A.; Baloh, R. H.; Chakraverty, S.; Mayo, K.; Norton, J. B.; Levitch, D.; Hatanpaa, K. J.; White, C. L. 3rd; Bigio, E. H.; Caselli, R.; Baker, M.; Al-Lozi, M. T.;

Morris, J. C.; Pestronk, A.; Rademakers, R.; Goate, A. M.; Cairns, N. J. TDP-43 A315T mutation in familial motor neuron disease. *Ann. Neurol.* **2008**, *63* (4), 535−8.

21. Fujita, Y.; Ikeda, M.; Yanagisawa, T.; Senoo, Y.; Okamoto, K. Different clinical and neuropathologic phenotypes of familial ALS with A315E TARDBP mutation. *Neurology.* **2011**, *77* (15), 1427−31.
22. Pasinelli, P.; Brown, Robert H. B. Molecular Biology of Amyotrophic Lateral Sclerosis: Insight from Genetics. *Nat Rev Neurosci* **7**, 710-23. https://doi.org/10.1038/nrn1971
23. Chattopadhyay, M.; Valentine, J. S. Aggregation of Copper-Zinc Superoxide Dismutase in Familial and Sporadic ALS. *Antioxid Redox Signal*. **2009**, *11* (7), 1603-1614.
24. Blokhuis, A. M.; Groen, E. J. N.; Koppers, M.; van den Berg, L. H.; Pasterkamp, R. J. Protein aggregation in amyotrophic lateral sclerosis. *Acta Neuropathol* **2013**, *125*, 777-794.
25. Gagliardi, S.; Cova, E.; Davin, A.; Guareschi, S.; Abel, K.; Alvisi, E.; Laforenza, U.; Ghidoni, R.; Cashman, J. R.; Ceroni, M.; Cereda, C. SOD1 mRNA expression in sporadic amyotrophic lateral sclerosis. *Neurobiol Dis* **2010**, *39* (2), 198-203.
26. Forsberg, K.; Jonsson, P. A.; Anderson, P. M.; Bergemalm, D.; Graffmo, K. S.; Hultdin, M.; Jacobsson, J.; Rosquist, R.; Marklund, S. L.; Brännström, T. Novel Antibodies Reveal Inclusions Containing Non-Native SOD1 in Sporadic ALS Patients. *PLoS One* **2010** *5* (7), e11552.
27. Rotunno, M. S.; Bosco, D. A. An emerging role for misfolded wild-type SOD1 in sporadic ALS pathogenesis. *Front Cell Neurosci* **2013**, *7*.
28. Ivanova, M. I.; Sievers, S. I.; Guenther, E. L.; Johnson, L. M.; Winkler, D. D.; Galaleldeen, A.; Saway, M. R.; Hart, P. J.; Eisenberg, D. S. Aggregation-triggered segments of SOD1 fibril formation support a common pathway for familial and sporadic ALS. *Proc Natl Acad Sci USA* **2014** *111* (1), 197-210.
29. Nelson, D. L.; Cox, M. M. *Lehinger Principles of Biochemistry,* 5th ed.; W. H. Freeman and Company, 2008.
30. Ross, C.; Poirier, M. Protein aggregation and neurodegenerative disease. *Nat. Med.* **2004,** 10 (Suppl 7), S10–S17.

31. Uversky, V. N.; Oldfield, C. J.; Dunker, A. K. Intrinsically Disordered Proteins in Human Diseases: Introducing the D^2 Concept. *Annu. Rev. Biophys.* **2008**, (37) 215-246.
32. Martinez-Limon, A.; Alriquet, M.; Lang, W.-H.; Calloni, G.; Wittig, I.; Vabulas, R. M. Recognition of enzymes lacking bound cofactor by protein quality control. *Proc. Natl. Acad. Sci.* **2016,** 113 (43), 12156-12161.
33. Squire, T. C.; Oxidative Stress and Protein Aggregation During Biological Aging. *Exp. Gerontol.* **2001**, *36* (9), 1539-50.
34. Proctor, E. A.; Fee, L. Tao, Y. Redler, R. L.; Fay, J. M.; Zhang, Y.; Lv, Z.; Mercer, I. P.; Deshmukh, M.; Lyubchenko, Y. L.; Dokholyan, N. V. Nonnative SOD1 trimer is toxic to motor neurons in a model of amyotrophic lateral sclerosis. *Proc Natl Acad Sci USA* **2015**, *113* (3) 614-9.
35. Sengupta, U.; Nilson, A. N.; Kayed, R. The Role of Amyloid-β Oligomers in Toxicity, Propagation, and Immunotherapy. *EBioMedicine* **2016**, *6*, 42-9.
36. Fang Y.S.; Tsai K. J.; Chang Y. J.; Kao P.; Woods R.; Kuo P. H.; Wu C. C.; Liao J. Y.; Chou S. C.; Lin V.; Jin L. W.; Yuan H. S.; Cheng I. H.; Tu P. H.; Chen Y. R. Full-length TDP-43 forms toxic amyloid oligomers that are present in frontotemporal lobar dementia-TDP patients. *Nat Commun* **2014,** *5,* 4824.
37. Ghag,G.; Bhatt, N.; Cantu, D. V.; Guerrero-Munoz, M. J.; Ellsworth, A.; Sengupta, U.; Kayed, R. Soluble tau aggregates, not large fibrils, are toxic species that display seeding and cross-seeding behavior. *Protein Sci* **2018**, *27* (11), 1901-9.
38. Economou, N. J.; Giammona, M. J., Do, T. D.; Zheng, X.; Teplow, D. B.; Buratto, S. K.; Bowers, M. T. Amyloid β-Protein Assembly and Alzheimer's Disease: Dodecamers of Aβ42, but Not of Aβ40, Seed Fibril Formation. *J. Am. Chem. Soc.* **2016**, *138* (6), 1772-5.
39. Sawaya, M.; Sambashivan, S.; Nelson, R.; Samashivan, S.; Nelson, R.; Ivonova, M. I.; Sievers, S. A.; Apostol, M. I. Thompson, M. J.; Balbirnie, M.; Wilzius, J. J. W.; McFarlane, H. T.; Madeson, A.; Riekel, C.; Eisenberg, D. Atomic structures of amyloid cross-β spines reveal varied steric zippers. *Nature*. **2007**, *447*, 453–457.
40. Laos, V.; Bishop, D.; Lang, A. C.; Marsh, N. M.; Cantrell, K. L.; Buratto, S. K.; Singh, A. K.; Bowers, M. T. Modulating ALS-Related Amyloidogenic TDP-43 307-319

Oligomeric Aggregation with Computationally Derived Therapeutic Molecules. *Biochemistry*. **2020**, *59* (4), 499-508.

41. Do T.D., LaPointe N.E., Nelson R., Krotee P., Hayden E.Y., Ulrich B., Quan S., Feinstein S.C., Teplow D.B., Eisenberg D., Shea J.E., Bowers M.T.. Amyloid β-Protein C-Terminal Fragments: Formation of Cylindrins and β-Barrels. *J Am Chem Soc.* **2016** *138* (2),549-57.
42. Laganowsky, A.; Liu, C.; Saway, M. R.; Whitelegge, J. P.; Park, J.; Zhao, M.; Pensalfini, A.; Soriaga, A. B.; Landau, M.; Teng, P. K.; Cascio, D.; Glabe, C.; Eisenberg, D.; Atomic View of a Toxic Amyloid Small Oligomer. *Science* **2012** *355* (6073), 1228-31.
43. Laganowsky, A.; Liu, C.; Saway, M. R.; Whitelegge, J. P.; Park, J.; Zhao, M.; Pensalfini, A.; Soriaga, A. B.; Landau, M.; Teng, P. K.; Cascio, D.; Glabe, C.; Eisenberg, D.; Atomic View of a Toxic Amyloid Small Oligomer. *Science* **2012** *355* (6073), 1228-31.
44. Do, T. D.; LaPOinte, N. E.; Nelson, R.; Krotee, P.; Hayden, E. Y.; Ulrich, B.; Quan, S.; Feinstein, S. C.; Teplow, D. B.; Eisenberg, D.; Shea, J.; Bowers, M. T. Amyloid β-Protein C-terminal Fragments: Formation of Cylindrins and β-Barrels. *J Am Chem Soc* **2016** *138* (2), 549-57.

II. Experimental Techniques

2.1 Atomic Force Microscopy

Atomic force microscopy (AFM) is a high-resolution form of scanning probe microscopy adept at imaging nanoscale features. In the study of disease-related protein aggregation, AFM is particularly effective at studying the transition from the soluble oligomer phase to insoluble fibrils due to its excellent resolution and relatively gentle imaging methods. As such, it complements ion mobility-mass spectrometry[1] (IM-MS), which elucidates information on oligomer assembly, and transmission electron microscopy[2-5] (TEM), which has been effectively used to characterizing mature fibrils but is severely limited by the requirement of coating or staining biological samples.

2.1A Instrumentation

The Asylum Research (Santa Barbara, CA) MFP-3D AFM was used to collect all AFM data presented in this work.[6] A simplified schematic of this AFM is provided in **Figure 2.1**. The MFP-3D AFM principally operates by tracking the position of a cantilever with a sharp tip using a low coherence light source (~860 nm). When the height of the sample changes, the change in the angle of deflection of the light is detected by a segmented photodiode. The calibrated piezoelectric actuator in the Z-stage then adjusts the Z-height of the cantilever and tracking apparatus to restore a set point, with the z-piezo position being converted to a height output channel. A height image is constructed by ortho scanning the sample utilizing piezoelectronics located in the XY-scanning stage. A typical image presented in this work consists of measurements at 512 points in a line, with 512 lines.

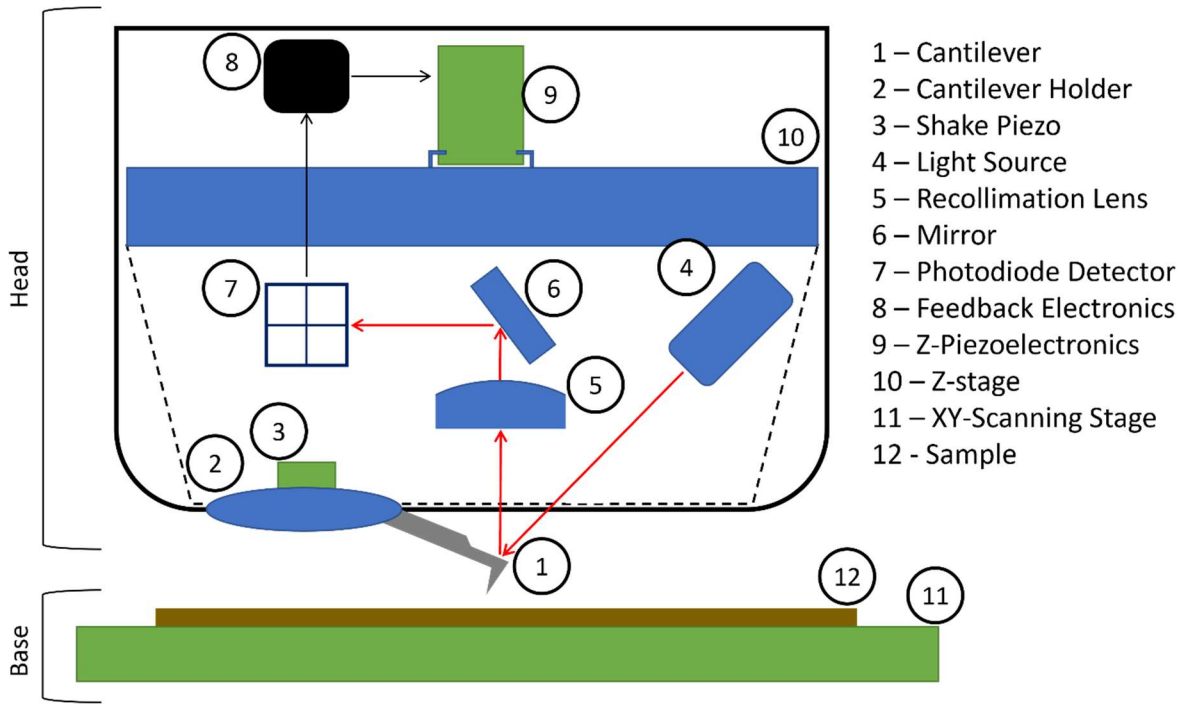

Figure 2.1 Schematic of the Asylum Research MFP-3D AFM. The tip of the cantilever interacts with the sample, causing a change in position that is tracked using a light source and photodiode detector. Feedback electronics and piezoelectronics raise the Z-stage to adjust the height of the cantilever and tracking apparatus to restore the original position of the cantilever. Piezoelectronics in the XY-scanning state ortho scan the position of the sample with respect to the tip in order to construct an image.

2.1B Imaging Modes

AFMs can operate in either contact mode or tapping mode (also called intermittent contact or AC mode). In contact mode, the tip of the cantilever continuously tracks the surface of the sample. This mode is primarily used for imaging hard surfaces and has several drawbacks. Rapid changes in the height of the sample may cause the cantilever to crash, damaging the tip. Because contact mode requires relatively strong forces between the tip and the sample, softer samples are significantly more difficult to image and may also be damaged

in the process. The tip may also shift movable features on the surface. As a result, contact mode is not ideal for imaging biological samples. These drawbacks can be alleviated by using tapping mode. In tapping mode, an alternating current is applied to the shake piezo, driving the cantilever to oscillate at a desired frequency and amplitude. This results in only periodic interaction between the tip and the sample, greatly reducing frictional forces and therefore sample damage and tip degradation.[7]

Both contact mode and tapping mode both utilize the same style of feedback loop illustrated in **Figure 2.2**. The position of the light source on the photodiode is calibrated to the middle of the detector. In tapping mode, the AC drive causes the position of the light source to oscillate at a set amplitude. When the bend of the cantilever changes, caused by a change in the height of the sample, the deflection angle of the light changes as well. This causes the signal in the top half of the detector to change relative to the signal in the bottom half of the detector. Feedback electronics than change the voltage applied to the z-piezo to adjust the height and restore the set point position (in contact mode) or amplitude of oscillation (in tapping mode) of the light source on the photodiode.

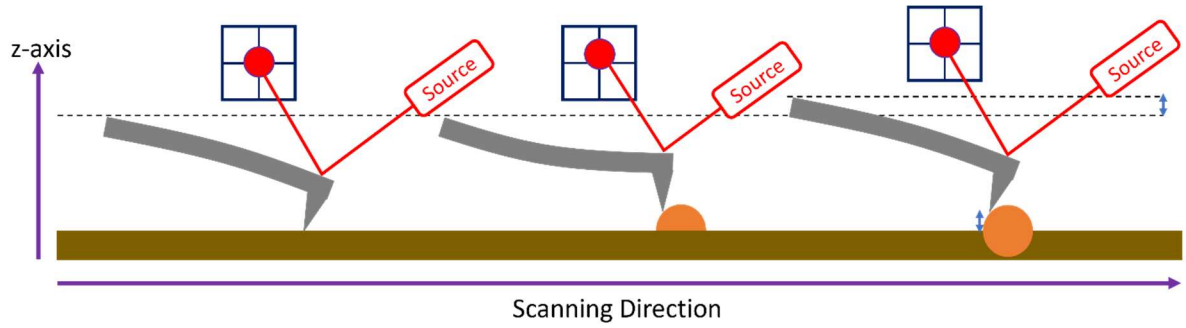

Figure 2.2 Illustration of the feedback loop employed by AFM. (Top) Changes in the cantilever concavity change the location of the light source reflection on the photodiode

detector. (Bottom) The height of the cantilever is then adjusted to restore the position or amplitude of oscillation of the light source on the photodiode.

In addition to being more adapted for imaging biological samples, tapping mode can also provide interesting information on the mechanical properties of the sample through phase imaging. Phase is the delay between the driving oscillation and the response of the cantilever, as detailed in **Figure 2.4A**. A cantilever driven at its resonance frequency has a phase of 90°. Interactions with the sample surface typically cause a change in the phase. For larger distances between the sample and the cantilever tip, longer-range attractive forces dominate. This causes the cantilever to bend down towards the sample at the bottom of the oscillation cycle, resulting in an increased phase >90°. As the tip-sample distance decreases, repulsive forces will eventually become dominant. These forces repel the tip at the bottom of the oscillation cycle, resulting in a decreased phase <90°.

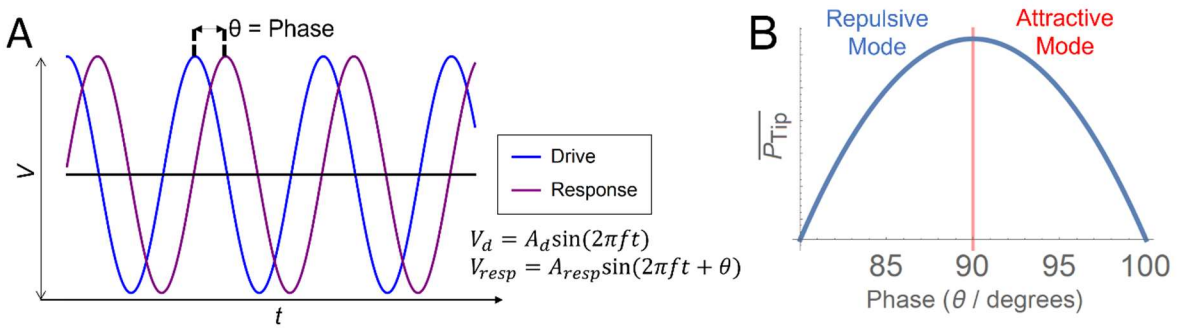

Figure 2.3 (A) Illustration of the definition of phase based off the difference in the drive voltage (blue) and the cantilever response voltage (purple). (B) Plot of the power dissipation curve at the AFM tip as a function of the phase.

Because of the feedback loop, tip-sample distance should be held constant throughout an image scan. Therefore, changes in the phase can be assigned to changes in the mechanical properties of the sample. The phase change can be interpreted by looking at power

dissipation at the tip.8 Power dissipation can be related to the phase, cantilever properties, and imaging parameters through the **Equation (1)**.

$$\overline{P_{Tip}} = \frac{1}{2}\frac{kA^2\omega_0}{Q}\left[\left(\frac{A_0}{A}\right)\sin\theta - 1\right] \quad (1)$$

where k is the force constant of the cantilever, Q is the quality factor of the cantilever, ω_0 is the drive frequency, A is the set point amplitude, A_0 is the free air amplitude, and θ is the phase angle. Because the cantilever properties and imaging parameters are fixed, changes in the phase can directly be attributed to changes in the power dissipation at the tip, as shown in **Figure 2.3B**. For the purposes presented in this work, this is interpreted as a measure of hardness, with softer samples dissipating more power and having a phase closer to 90° and harder samples dissipating less power and having a phase further from 90°.

2.1C Probe Selection and Resolution

AFM has excellent height resolution on the order of ~50 pm but suffers from relatively poor lateral resolution which can be attributed to tip geometry. AFM tips vary in size depending on the desired application. Conventional tip width and resolution is around 10 nm, which can be improved to 1 nm for high resolution tips. The HQ:XSC11/Al BS (NanoAndMore USA Corp, Watsonville, CA) AFM probe was primarily used in this work and has an estimated tip width of 8 nm. Because the features observed in the studied systems are often smaller than this width, significant lateral distortion is observed. **Figure 2.4** simulates a comparison between the actual morphology of a sample and the AFM output image. Tips with a large width can make it difficult to distinguish closely positioned features and makes smaller features appear significantly larger in the lateral dimension. Both effects are diminished when a tip with a smaller width is utilized, but it is impossible to completely remove them. As such, height measurements are generally much more precise than lateral

measurements and will be primarily used to describe features throughout this work. Because the excellent height resolution between a conventional and super sharp tip is consistent, it is often just as practical and notably more cost effective to use tips with a larger width.

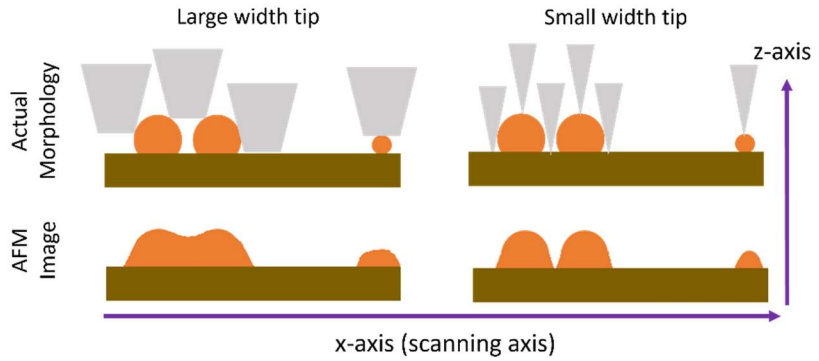

Figure 2.4 An illustration of how tip geometry affects the height observed in an AFM height image. Large width tips may have trouble distinguishing nearby features and may noticeably inflate the size of smaller features. This effect can be minimized (but not eliminated) by using sharper tips.

It is also important to consider cantilever properties when choosing an AFM probe, most notably the force constant and the resonance frequency. This choice can be highly dependent on the system being studied. In general, lower force constants and resonance frequencies are preferable when imaging softer samples in tapping mode, while the opposite is true for harder samples. Very low force constants are desirable when imaging in contact mode. Manufacturer recommended cantilevers for imaging biological samples in tapping mode typically have force constants in the range of ~0.5-15 N/m and resonance frequencies in the range of ~50-200 kHz.[9,10] Cantilever C of the HQ:XSC11/Al BS AFM probe was utilized in this work and has an estimated force constant of 7 N/m and an estimated resonance frequency 155 kHz.

2.1D Sample Preparation

Preparing samples for AFM imaging is exceptionally facile. High grade V1 muscovite mica discs are a nonreactive substrate that is both inexpensive and can be reused by cleaving the top layers of the disc using tape, making them ideal for use with AFM. These discs are atomically flat, allowing for accurate measurement of feature heights and preventing undue edge influences on deposition or aggregation. Because AFM imaging relies only on tip-sample interactions coating or staining the sample is not required as it can be for electron microscopy. Solution phase samples can be deposited on the mica substrate and either imaged in liquid or dried before imaging in air. For the purposes of studying protein aggregation, imaging dried samples essentially allows the aggregation to be frozen at specified time points, allowing for a time study of the aggregation pathway.

Figure 2.5 shows an example **(A)** height image and **(B)** repulsive mode phase image of a protein solution that was deposited onto a mica substrate and dried in a vacuum desiccator. Brighter features in the height image have a larger height, while darker features in the phase image are harder, which is an indication of a greater quantity of beta sheet formation. It is important to note that the background is not the bare mica substrate. Mica is a hard substrate and would be expected to be significantly harder than any protein structure. It can therefore be concluded that the background is a film of largely disordered protein, which will be present in all AFM images presented in this work.

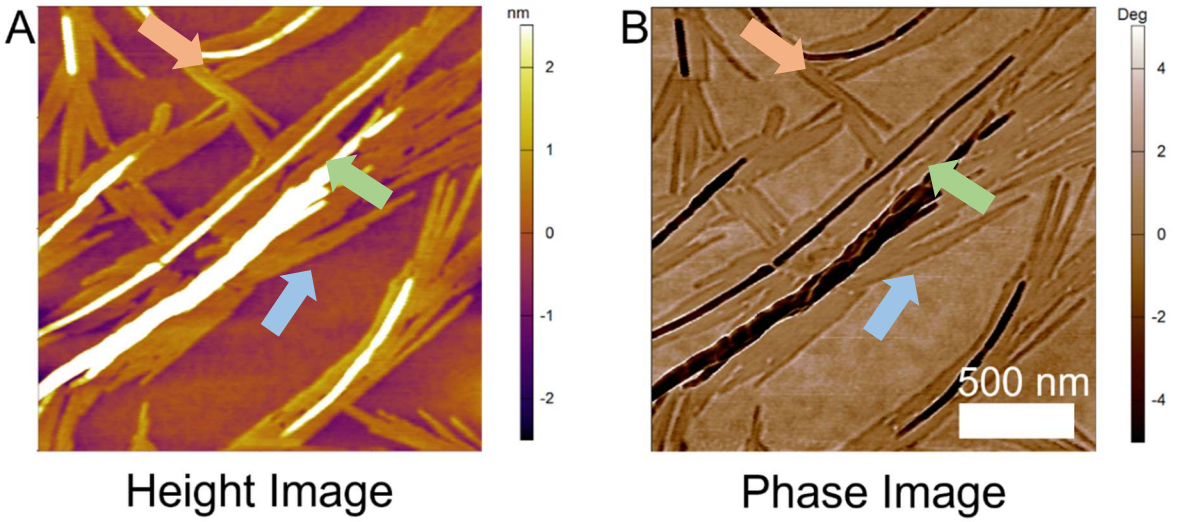

Figure 2.5 Example 2 µm x 2 µm AFM (A) height image and (B) repulsive mode phase image exhibiting fibrils (green arrow), non-fibular aggregates (orange arrow), and a background peptide film (blue arrow). Phase scale bar is defined such that the average phase of the image is 0°.

2.2 Ion Mobility Mass Spectrometry

IM-MS is a powerful tool that allows for the separation of ions with the same mass to charge ratio. This makes the technique particularly useful in elucidating the soluble oligomeric assembly observed in protein aggregation. Time evolution IM-MS, in tandem with AFM, can correlate oligomers with the formation of larger structures such as fibrils. Additionally, IM-MS derived collision cross sections (CCS) can be used to corroborate crystal structures and theoretically derived molecular dynamics structures.

In IM-MS experiments, ions of a specific mass to charge ratio are pulsed through a drift cell containing a buffer gas and a uniform weak electric field. For ions with the same mass, extended structures will travel slower than compact structures as a result of more

collisions with the buffer gas, resulting in the compact structures arriving at the detector before the extended structures (**Figure 2.6A**). For oligomers with different masses (but still the same mass to charge ratio), higher order oligomers will arrive first because the charge, and therefore propulsion in the electric field, grows faster while the CCS and number of buffer gas collisions (**Figure 2.6B)**.[11]

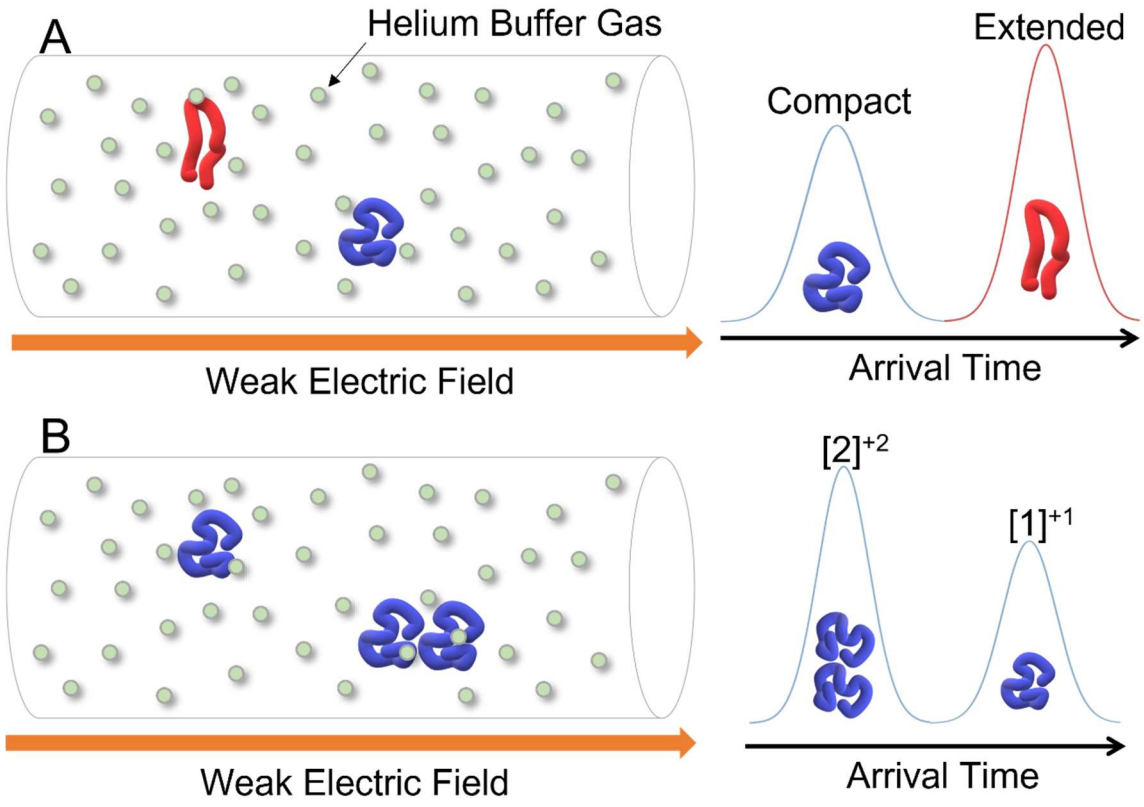

Figure 2.6 Separation of ions based in a drift cell. Ions travel through the drift cell at a constant velocity as a result of a weakly applied electric field. (A) Extended conformations (red structure) experience more collisions with the helium buffer gas (light green circles) than compact conformations (blue structure) and as a result compact conformations arrive first. (B) A dimer has twice the charge as a monomer but

experiences less than twice the number of helium buffer gas collisions and will therefore arrive before a monomer.

An ions mobility, K, is inversely proportional to the amount of time it takes for it to pass through the drift cell and inversely proportional to the CCS.[12,13] While the mobility is dependent on temperature and pressure, the reduced mobility – the mobility at standard temperature (273 K) and pressure (760 torr) – is constant. Reduced mobility is inversely proportional to the dependence of the arrival time on the ratio of pressure to drift voltage (P/V). Arrival time distributions (ATDs) are acquired at several pressure to drift voltage ratios to determine the reduced mobility. CCS are then calculated from **Equation 2.1**.

$$\sigma \approx \frac{3q}{16N}\left(\frac{2\pi}{\mu k_B T}\right)^{\frac{1}{2}}\frac{1}{K_0} \tag{2.1}$$

where q is the ion charge, N is the buffer gas number density, is the reduced mass, k_B is the Boltzmann constant, T is the temperature within the drift cell, and K_0 is the reduced mobility.

The theoretical peak shape on an ATD of an ion cloud with a single CCS is given by **Equation 2.2**.

$$\varphi(0,z,t) \approx \frac{sae^{-\alpha t}}{4(\pi D_L t)^{\frac{1}{2}}}\left(v_d + \frac{z}{t}\right)\left(1 - e^{-\frac{r_0}{4D_T t}}\right)e^{-\frac{(z-v_d t)^2}{4D_T t}} \tag{2.2}$$

where z is the distance travelled by the ion, t is the arrival time, s is the initial ion density, a is the area of the exit aperture, α is the loss of ions due to reactions in the drift cell (assumed to be zero in for data presented in this work), D_L and D_T are the longitudinal and transverse diffusion coefficients, v_d is the drift velocity, and r_0 is the radius of the initial ion packet.[12] The theoretical peaks are superimposed as colored lines over experimental data in the ATDs.

Experimental peaks larger than the theoretical distribution may be an indication of variations in the conformations.

In order to compare crystal structures and molecular dynamics simulation structures to IM-MS experimental data, it is necessary to be able to computationally derive the CCS for those structures. The projected superposition approximation (PSA) algorithm was designed by Bleiholder et al to overcome the inaccuracies and extensive computational requirement that other algorithms experience when working with biomolecules and other macromolecules.[14-17] PSA approximates the molecular momentum transfer integral as an orientation average projection error to account for size effects and corrects for deviation from full convexity using a shape factor. For deriving CCS, the PSA method was shown to be more accurate than the projection approximation (PA) method and computationally much faster than the trajectory method (TJM) while retaining accuracy. PSA is free and available online at http://PSA.chem.fsu.edu/.

2.3 Bulk Secondary Structure Characterization

While AFM is adept at studying the nuances of protein aggregation, bulk secondary structure analysis can be useful as a quantitative analysis of the overall level of aggregation. Far UV circular dichroism (CD) and the thioflavin T (ThT) fluorescence assay are both commonly employed to measure the levels of beta sheet formation in an aggregated protein sample.

CD operates on the principle that right circularly polarized light and left circularly polarized light will be absorbed to different degrees by optically active molecules. Protein secondary structures have unique CD signatures in the far UV range of light that can be used to measure their relative proportions in solution.[18] Most relevant to protein aggregation is that

beta sheets are characterized by a negative band centered around 216-218 nm and a positive band around 195 nm. Monitoring these peaks is a useful indication of the overall level of aggregation present in a bulk protein sample, although it cannot definitively prove the presence of fibrils.

ThT Fluorescence is a similarly useful technique for monitoring fibril formation.[19,20] ThT is a fluorescent dye that, as an aqueous solution, undergoes excitation at a maximum 385 nm and emission at a maximum 445 nm. However, when bound to amyloid fibrils, ThT undergoes a significant increase in fluorescence and a red shift in both excitation and emission, with respective maxima of 450 nm and 482 nm. This is believed to be caused by the immobilization of the C-C bond connecting ThT's two ring structures upon intercalating with fibrillar structures **(Figure X.X)**. Since this effect was described in 1959, the ThT fluorescence assay has become a mainstay in detecting and monitoring fibril formation due to its ease of use and efficacy under many experimental conditions. Despite its prominence ThT is not perfectly specific; it has been shown in rare circumstances to not bind to some amyloid fibrils and bind to some non-amyloid fibril structures. Nonetheless, ThT remains an important and useful tool when studying protein misfolding diseases.

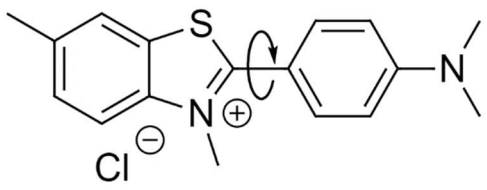

Figure 2.7 Thioflavin T. Upon binding to amyloid fibrils, rotation of the indicated C-C bond connecting the two ring structures is immobilized, leading to an increase in fluorescence.

2.4 References

1. Bleiholder C.; Bowers M.T. The Solution Assembly of Biological Molecules Using Ion Mobility Methods: From Amino Acids to Amyloid β-Protein. *Annu. Rev. Anal. Chem. (Palo Alto Calif).* **2017**, *10* (1), 365-386.
2. Guenther, E. L.; Ge, P.; Trinh, H.; Sawaya, M. R.; Cascio, D.; Boyer, D. R.; Gonen, T.; Zhou, Z. H.; Eisenberg, D. S. Atomic-level evidence for packing and positional amyloid polymorphism by segment from TDP-43 RRM2. *Nat. Struct. Mol. Biol.* **2018**, *25*, 311–319.
3. Arseni, D.; Hasegawa, M.; Murzin, A. G.; Kametani, F.; Arai, M.; Yoshida, M.; Ryskeldi-Falcon, B. Structure of pathological TDP-43 filaments from ALS with FTLD. *Nature*. **2022,** *601*, 139–143.
4. Li, Q., Babinchak, W. M.; Surewicz, W. K. Cryo-EM structure of amyloid fibrils formed by the entire low complexity domain of TDP-43. *Nat. Commun*. **2021,** *12*, 1620.
5. Cao, Q.; Boyer, D. R.; Sawaya, M. R.; Ge, P.; Eisenberg, D. S. Cryo-EM structures of four polymorphic TDP-43 amyloid cores. *Nat. Struct. Mol. Biol.* **2019**, *26*, 619–627.
6. Asylum Research. (2008). *MFP-3D: Installation and Operations Manual*. Santa Barbara, CA: Author.
7. Dufrêne, Y.; Ando, T.; Garcia, R. Alsteens, D.; Martinez-Martin, D.; Engles, A.; Gerber, C.; Muller, D. J. Imaging modes of atomic force microscopy for application in molecular and cell biology. *Nature Nanotech.* **2017,** *12*, 295–307.
8. Cleveland, J. P.; Anczykowski, B.; Schmid, A. E.; Elings, V. B. Energy Dissipation in Tapping Mode Atomic Force Microscopy. *Appl. Phys. Lett.* 1998, *72*, 2613.
9. NanoAndMore USA. *Relation between AFM Cantilever Geometry and Application Mode*. https://www.nanoandmore.com/more-about-afm-cantilevers
10. MikroMasch. *How to Choose AFM Probes by Application: Life Science.* https://www.spmtips.com/how-to-choose-afm-probes-by-applications-life-science.html

11. Wyttenbach, T.; Kemper, P. R.; Baykut, G.; Park, M. A.; Bowers, M. T. A new instrument with high mass and high ion mobility resolution. *Int J of Mass Spectrom* **2018** *434*, 108-115. https://doi.org/10.1016/j.ijms.2018.09.008
12. Mason, E. A. Transport Properties of Ions in Gases, 99th ed. John Wiley & Sons, **1988**.
13. Gidden, J.; Ferzoco, A.; Baker, E. S.; Bowers, M. T. Duplex Formation and the Onset of Helicity in Poly d(CG)n Oligonuceotides in a Solvent-Free Environment. *J Am Chem Soc* **2004** *126* (46), 15132-15140
14. Bleiholder, C.; Wyttenbach, T. Bowers, M. T. A novel projection approximation algorithm for the fast and accurate computation of molecular collision cross sections (I). Method. *Int J Mass Spectrom* **2011** *308* (1), 1-10.
15. Bleiholder, C.; Contreras, S.; Do, T. D.; Bowers, M. T. A novel projection approximation algorithm for the fast and accurate computation of molecular collision cross sections (I). Model parameterization and definition of empirical shape factors for proteins. *Int J Mass Spectrom* **2013** *345-347*, 89-96.
16. Anderson, S. E.; Bleiholder, C.; Brocker, E. R.; Stand, P. J.; Bowers, M. T. A novel projection approximation algorithm for the fast and accurate computation of molecular collision cross sections (III): Applications to supramolecular coordination-driven assemblies with complex shapes. *Int J Mass Spectrom* **2012** *330-332*, 78-84.
17. Bleiholder, C.; Contreras, S.; Bowers, M. T. A novel projection approximation algorithm for the fast and accurate computation of molecular collision cross sections (IV). Application to polypeptides. *Int J Mass Spectrom* **2013** *354-355*, 275-80.
18. Sabate, R.; Ventura, S. Cross-β-Sheet Supersecondary Structure in Amyloid Folds: Techniques for Detection and Characterization. In: Kister, A. (eds) Protein Supersecondary Structures. Methods in Molecular Biology, vol 932. Humana Press 2012, Totowa, NJ.
19. Khurana, R.; Coleman, C.; Ionescu-Zanetti, C.; Carter, S. A.; Krishna, V.; Grover, R. K.; Roy, R.; Singh, S.; Mechanism of thioflavin T binding to amyloid fibrils. *J Struct Biol* **2005** *3* (141), 229-38.

20. Williams, A. T. R.; Winfield, S. A.; Miller, J. N. Relative Fluorescence Quantum Yields Using a Computer-controlled Luminescence Spectrometer. *Analyst* **1983** *108*, 1067-71.

III. Self-Assembly of the ALS-Related Protein TDP-43(307-319)

3.1 Introduction

Amyotrophic lateral sclerosis (ALS) is the most common motor neuron disease, with an estimated prevalence of 5 in 100,000 in the United States.[1,2] Effecting both upper and lower motor neurons, it results in a progressive weaking of voluntary muscles leading to eventual paralysis, respiratory failure, and death. Following the onset of symptoms, the mean life expectancy is 3-5 years, though some patients may live significantly longer.[3,4] ALS has no cure, and the current standard of care is focused on treating symptoms without having a significant impact on prognosis.

Abnormal protein deposits of TAR DNA binding protein of 43 kDa (TDP-43) are the main pathological hallmark of sporadic ALS (sALS), accounting for approximately 95% of cases where the cause is unknown. The remaining cases are familial ALS (fALS), where a specific genetic factor can be implicated in the disease and causes a different protein to form aggregates.[5-7] The role of superoxide dismutase 1 (SOD1) in fALS will be discussed in Chapter 6. TDP-43 aggregation has also been associated with tau- and alpha synuclein-negative frontotemporal lobar degeneration (FTLD-TDP),[6,7] and a subset of patients with Alzheimer's disease.[8-12] Understanding TDP-43 aggregation is imperative for the development of therapeutic agents to treat these neurodegenerative diseases.

TDP-43 is 414 amino acid residue protein that forms a homodimer in its native state via interactions involving the N-terminus. TDP-43 has two RNA-binding motifs that enable it to bind to RNA and DNA, where it functions in several roles related to mRNA, including

regulation of transcription, translation, splicing, and stability. TDP-43 also plays a role in repairing DNA double-strand breaks. While primarily found in the nucleus, TDP-43 is also involved in cellular shuttling between the nucleus and the cytoplasm, and mislocalization of TDP-43 is exhibited in ALS. It is currently unclear whether disease is caused by a loss of normal function or a toxic gain of function, although *in vitro* experiments have shown that TDP-43 can be toxic to neurons.[13-16]

The C-terminal domain of TDP-43 is largely disorder, glycine-rich and shares significant homogeneity with the prion protein. These similarities are common among disease-related proteins. The C-terminal domain regulates protein solubility and is important for the role of TDP-43 in the formation of protective stress granules. However, the C-terminus is also believed to drive TDP-43 aggregation in neurodegenerative diseases. Hyper-phosphorylated and ubiquitinated C-terminal fragments of TDP-43 are a major component of the abnormal protein deposits seen in this disease. [6,7,13,17] The work of J. Y. Wu et al identified the C-terminal fragment at residues 307-319, herein designated TDP-43(307-319), as the minimal amyloidogenic core region capable of both forming fibrils and expressing neurotoxicity. They also identify the glycine at residue 314 as being important for aggregation and show that a G314V mutation eliminates toxicity.[18] TDP-43(307-319) also hosts two mutations, A315T and A315E, that have been found in ALS patients. A315T in particular is associated with more sever neurotoxicity and neurodegeneration as compared to wild type (WT) TDP-43.[19,20]

Peptide		Primary Structure													
WT	307	M	G	G	G	M	N	F	**G**	A	F	S	I	N	319
A315T	307	M	G	G	G	M	N	F	**G**	T	F	S	I	N	319
A315E	307	M	G	G	G	M	N	F	**G**	E	F	S	I	N	319
A315G	307	M	G	G	G	M	N	F	**V**	A	F	S	I	N	319

Table 3.1 Primary sequence of WT TDP-43(307-319), the ALS-related mutation A315T and A315E, and the synthetic non-toxic mutant G314V. Mutations are given in red. The central glycine at residue 314 is in bold. Amino acids highlighted in beige have hydrophobic side chains, Amino acids highlighted in green have polar side chains, and the amino acid highlighted in grey-blue has a positively charged side chain.

Several studies utilizing cryo-electron microscopy have detailed the structure of mature TDP-43 fibrils.[1-5] However, evidence suggests that small soluble oligomers, not fibrils, are the primary toxic agent in many protein misfolding diseases.[21-24] As such, it is essential to understand the early stages of aggregation in which these transient species are formed. Here, we aim to elucidate the assembly pathway of WT TDP-43(307-319), the ALS related mutations A315T and A315E, and the synthetic non-toxic mutation G314V using a combination of ion mobility-mass spectrometry (IM-MS) and atomic force microscopy (AFM). IM-MS is a powerful tool capable of separating ions with the same mass-to-charge ratio based on their ionic mobility and is adept at studying soluble species such as oligomers.[25] In order to visualize larger structures that cannot be seen via IM-MS, AFM is used in tandem. Time dependent studies enable oligomers to be correlated with the formation

of larger structures such as fibrils to obtain a complete picture of the early-stage assembly pathways peptides, which will hopefully aid in the development of future therapeutic agents.

3.2 Materials and Methods

3.2A Peptide Synthesis and Purification

TDP-43(307−319) WT peptide 307[MGGGMNFGAFSIN]319 was synthesized using standard 9-fluorenylmethoxycarbonyl (Fmoc) chemistry using 2-(1H-benzotriazol-1-yl)-1,1,3,3-tetramethyluronium hexafluorophosphate/hydroxybenzotriazole (HBTU/HOBT) manual solid phase peptide synthesis. The peptide was amidated with an Fmoc-Rink Amide resin (Anaspec). The peptide was cleaved from the resin using 94% TFA, 5% triisopropylsilane, and 1% phenol for 2 h at 295 K. The crude peptide was purified by reverse phase high-performance liquid chromatography (RP-HPLC) on a semipreparative C18 column (Phenomenex) using gradients of water [0.1% (v/v) TFA] and acetonitrile [0.1% (v/v) TFA]. The peptide was dissolved in 6 M guanidine hydrochloride (GdnHCl) prior to injection due to its insolubility in water and acetonitrile. The peptide purity was >93% as determined by analytical RP-HPLC. The molecular mass of the peptide was verified by ESI mass spectrometry. Peptide synthesis was performed by Nicole M. Marsh, Brady Quon and Megan Fetters and overseen by Prof. Kristi Lazar Cantrell (Westmont College, Santa Barbara, CA).

3.2B Ion Mobility-Mass Spectrometry

Ion mobility-mass spectrometry (IM-MS) was used to study oligomerization of TDP-43(307-319) peptides. IM-MS separates species of a specific $[m]^{+z}$ (m = mass, z = charge) with different $[n]^{+z}$ (n = oligomer number) by measuring arrival time distributions (ATDs). Experiments were performed on a home-built ion mobility mass spectrometer consisting of a

nano-electrospray ionization source, home-built ion funnel, 4.503 cm-long drift cell, quadrupole mass filter, and conversion dynode and electron multiplier detector. Ions are generated at the source, captured and stored in the ion funnel, and pulsed into the drift cell filled with approximately 3 Torr of helium gas. Ions exiting the drift cell are filtered by the quadrupole mass analyzer and finally reach the detector.[25] All ion mobility experiments were performed by Dr. Veronica Laos (University of California – Santa Barbara, Santa Barbara, CA).

3.2C Thioflavin T Fluorescence Assay

Thioflavin T stock solutions were prepared using the method described by Khurana et al.[26] WT TDP-43(307-319), A315T, and A315E peptides were prepared at a concentration 100 μM peptide and 98 μM thioflavin T in 10 mM ammonium acetate, pH 7.4, with 2% HFIP. Peptides were then analyzed using the thioflavin T fluorescence assay every 30 minutes for 10 hours. Fluorescence was measured (λex = 446 nm, λem = 460-540 nm) on a ThermoSpectronic Aminco Bowman Series 2 Luminescence Spectrometer with excitation and emission bandwidths set to 2 nm and a photomultiplier voltage of 600. Samples were pipetted gently at the beginning of the experiment. An increase in the fluorescence of thioflavin T at 490 nm is associated with the formation of β-sheet amyloid fibrils. The buffer background at 490 nm was subtracted from all data points. A standard consisting of a 100 μM thioflavin T solution in dimethylformamide was run prior to each experiment and the fluorescence intensity at 490 nm was used to normalize the data.[27] Secondary structure characterization was performed by Nicole M. Marsh, Brady Quon and Megan Fetters and overseen by Prof. Kristi Lazar Cantrell (Westmont College, Santa Barbara, CA).

3.2D Far-UV Circular Dichroism

WT TDP-43(307-319), A315T, and A315E were prepared at 100 μM in 10 mM ammonium acetate, pH 7.4, with 2% HFIP. Circular dichroism (CD) data was collected on a Jasco J-810 CD spectrometer. Measurements were collected at 0.5 nm interval from 260 to 190 nm with a response time of 4 s and a bandwidth of 1 nm. All spectra were obtained utilizing a 1 mm quartz cuvette at 295 K. A buffer baseline was subtracted from the spectra and the curves were baseline corrected. Secondary structure characterization was performed by Nicole M. Marsh, Brady Quon and Megan Fetters and overseen by Prof. Kristi Lazar Cantrell (Westmont College, Santa Barbara, CA).

3.2E Atomic Force Microscopy

Atomic force microscopy (AFM) was used to characterize TDP-43(307-319) fibril growth and morphology, and correlate these with oligomeric assembly. Experiments were conducted using an MFP-3D AFM (Asylum Research, Goleta, CA) and Cantilever C on HQ:XSC11/Al BS AFM probes (NanoAndMore USA Corp, Watsonville, CA). Images were acquired in air using repulsive tapping mode. Samples were prepared for imaging by depositing 5 μL of solution on freshly cleaved V1-grade muscovite mica discs (Ted Pella, Edding, CA) and drying in a vacuum desiccator. Samples were visibly dry in approximately 5 minutes but were allowed to dry over-night.

3.3 Results and Discussion

3.3A Ion Mobility-Mass Spectrometry

Ion-Mobility Mass-Spectrometry experiments revealed extensive oligomerization of WT TDP-43(307-319). WT TDP-43(307-319) was incubated at a concentration of 100 uM in ammonium acetate buffer, pH 7.4, with 2% HFIP and the oligomeric assembly was monitored using IM-MS. MS shows two major ion peaks corresponding to the $[1]^{+1}$ and $[1]^{+2}$

charge several minor peaks (**Figure 3.1A**). Additionally, a raised baseline and decrease in signal to noise ratio is observed after 3 hours, indicating extensive aggregation (**Figure 3.1B**). ATDs reveal the most extensive oligomeric growth is observed in the $[1]^{+1}$ charge state. At 15 minutes, the $[1]^{+1}$ charge state demonstrates three peaks corresponding to the monomer ($[1]^{+1}$), dimer ($[2]^{+2}$), and trimer ($[3]^{+3}$) in decreasing intensities (**Figure 3.2A**). Time evolution studies show that by three hours, tetramer ($[4]^{+4}$), hexamer ($[6]^{+6}$), and octamer ($[8]^{8+}$) peaks develop and that the dimer replaces the monomer as the dominant species (**Figure 3.2B**).

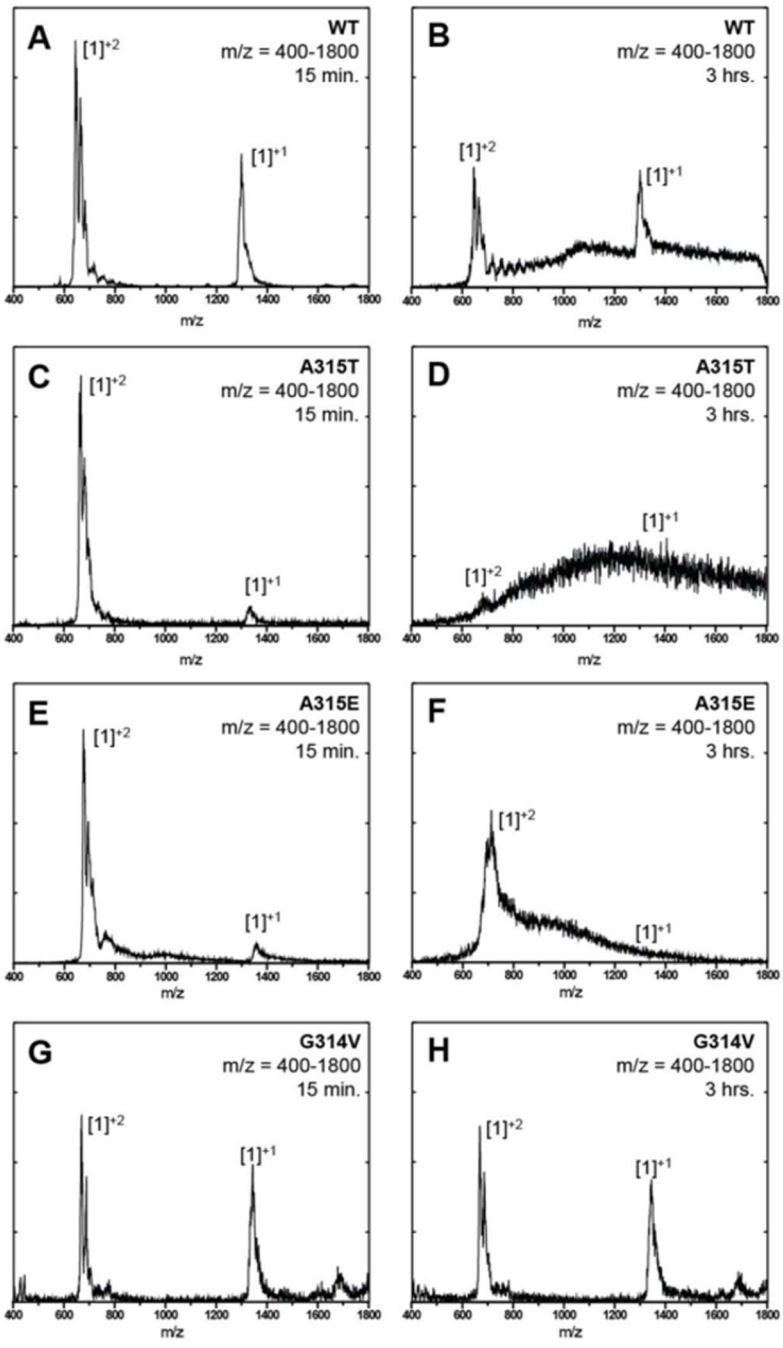

Figure 3.1 Mass spectra of (A, B) WT TDP-43(307-319), (C, D) A315T, (E, F) A315E, and (G, H) G314V at 15 minutes and 3 hours. The $[1]^{+1}$ peak was shown via IM-MS to display the most extensive oligomerization. WT, A315T, and A315E all experience a

raised base line after 3 hours, indicative of significant aggregation, while the non-toxic mutant G314V does not. Experiments performed by Dr. Veronica Laos.[28]

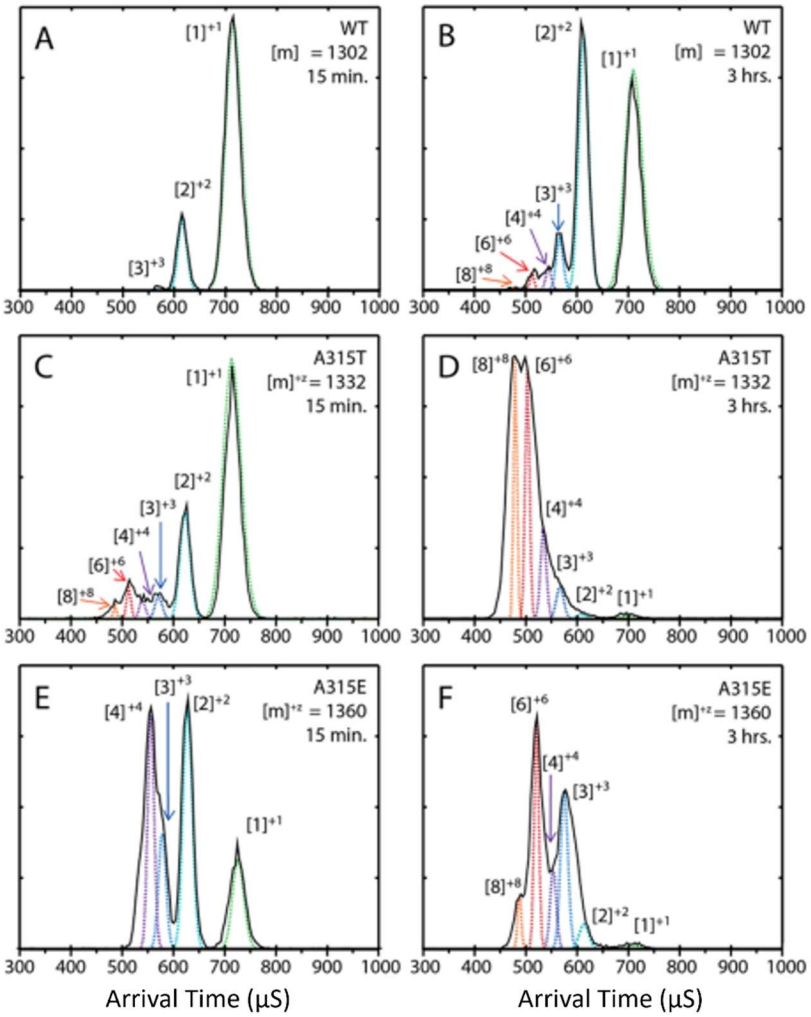

Figure 3.2 Arrival time distributions of the $[1]^{+1}$ mass spectral peak of WT TDP-43(307-319), A315E and A315T at 15 minutes and 3 hours. (A) WT demonstrates monomer, dimer, and trimer at 15 minutes. (B) By 3 hours, dimer and trimer populations have increased and tetramer, hexamer, and octamer are present. (C) A315E demonstrates monomer, dimer, trimer, tetramer, hexamer, and octamer at 15 minutes. (D) By 3 hours, the population shifts towards octamer and hexamer. (E) A315E demonstrates monomer, dimer, trimer, and tetramer at 15 minutes. (F) By 3

hours octamer and hexamer are observable, with the hexamer as the dominant peak. Experiments performed by Dr. Veronica Laos.[28]

Mutations of TDP-43(307-319) were shown to have a profound effect on the oligomeric distribution of the $[1]^{+1}$ charge state. The fALS mutations A315T and A315E were incubated under the same conditions as WT TDP-43(307-319). MS similarly shows the same two major peaks and an even more egregious raised baseline and lose in signal to noise ratio after 3 hours (**Figure 3.1C-F**). ATDs of the $[1]^{+1}$ charge state reveal both fALS related mutations form the same sized oligomers as the WT but with a notable bias towards higher order oligomers. The A315T mutation exhibits behavior that could be interpretated as accelerating the aggregation observed in the WT. Peaks corresponding to monomer, dimer, trimer, tetramer, hexamer, and octamer are observed in decreasing intensities at 15 minutes (**Figure 3.2C**). This distribution flips by 3 hours, with the octamer and hexamer becoming the dominant oligomers (**Figure 3.2D**). In the A315E mutation, tetramer and dimer are the dominant oligomers at 15 minutes, in addition to significant quantities of trimer and monomer (**Figure 3.2E**). After 3 hours the hexamer becomes the dominant species followed by the trimer, accompanied by the emergence of an octamer peak (**Figure 3.2F**). Trimer and tetramer appear to be more favorable structures for A315E than for A315T or the WT, suggesting slight differences in the assembly process.

The synthetic non-toxic mutation G314V was designed to disrupt TDP-43(307-319) oligomerization by removing the flexible central glycine residue that should be necessary for forming the cylindrin beta barrel motif. To combat poor solubility G314V was dissolved in a 50:50 mixture of 10 mM ammonium acetate, pH 7.4, and acetonitrile with 1% formic acid. G314V was observed to have the desired effect of destabilizing higher order aggregation. MS

base line remains constant over 3 hours (**Figure 3.1G, H**). Monomer, dimer, and trimer oligomers are present at 15 minutes and no larger oligomers are observed through 1 week. The relative populations of these oligomers are largely consistent over 1 week, with no major change in the oligomeric populations (**Figure 3.3**).

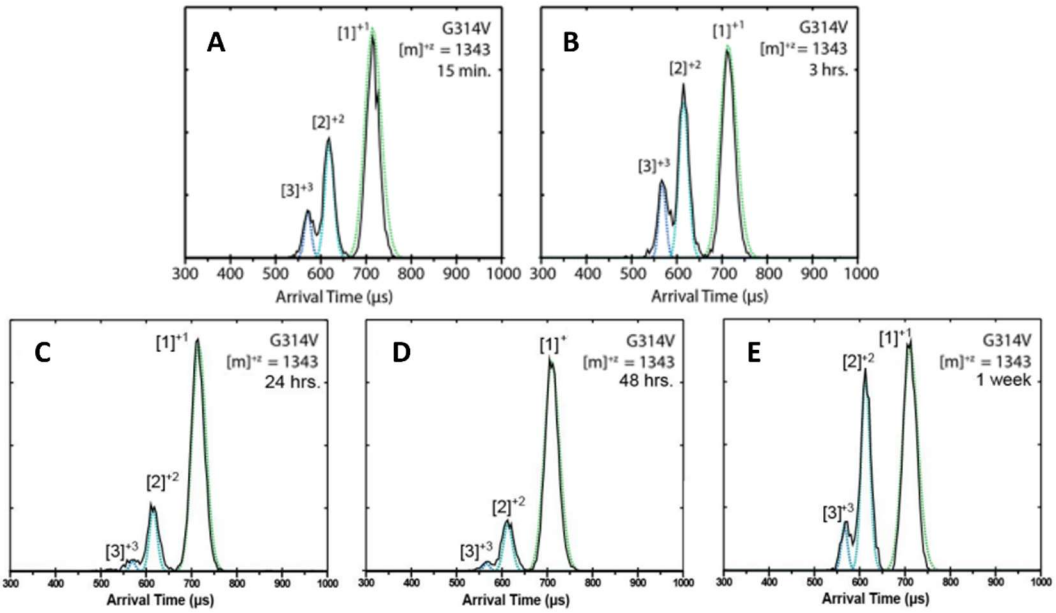

Figure 3.3 ATD of G314V at (A) 15 minutes, (b) 3 hours, (c) 24 hours, (D) 48 hours, and (E) 1 week. All ATDs demonstrate monomer, dimer, and trimer peaks in decreasing intensities. No major shift in oligomeric populations was observed. Experiments performed by Dr. Veronica Laos.[28]

3.3B Bulk Secondary Structure Characterization

Bulk secondary structure characterization was conducted using thioflavin-T (ThT) fluorescence assay and circular dichroism (CD) to monitor the overall level of aggregation of WT and ALS related mutations. The ThT fluorescence assay revealed WT, A315E, and A315T all showed significant increases in fluorescence, indicating β-sheet formation and the presence of fibrils (**Figure 3.4**). The fluorescence of the WT increases throughout the

duration of the 10-hour study. A315E closely matches the fluorescence of the WT but begins to decrease at 2 hours. A315T exhibits a much more rapid increase in fluorescence at early time points but reaches a maximum around 1 hour, after which it slowly begins to decrease. The decrease in fluorescence observed in both mutations is a common phenomenon that may be caused by fibril sedimentation or the loss of ThT binding sites as fibrils mature.

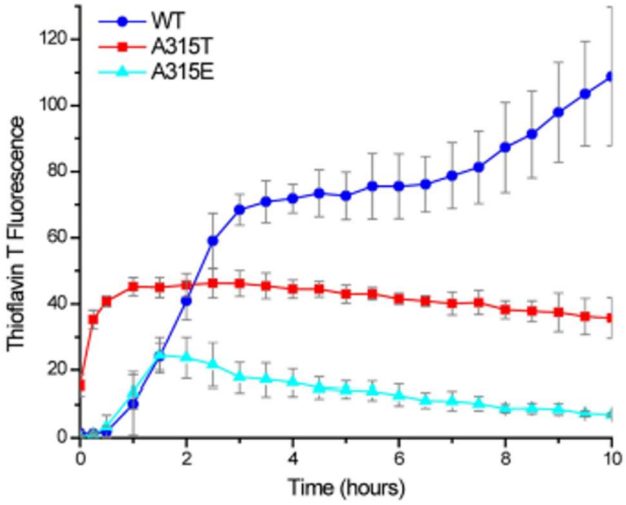

Figure 3.4 Thioflavin T fluorescence assay of WT TDP-43(307-319) (blue circles), A315T (red squares), and A315E (cyan triangles). All peptides express increases in fluorescence typically associated with fibril formation. A315T demonstrates a more rapid increase in fluorescence than the WT or A315E. A315T and A315E both experience a gradual decrease in fluorescence after reaching a peak around 2 hours. Experiments performed by Nicole M. Marsh, Brady Quon and Megan Fetters and overseen by Prof. Kristi Lazar Cantrell.[28]

Circular dichroism was used to monitor the relative quantity of beta sheet secondary structures in the bulk solutions. Beta sheets have a characteristic positive band at around 195 nm and negative band at around 216-218 nm. The growth of these bands signify significant structural changes typically associated with fibril formation. CD spectra show that WT,

A315T, and A315E all display significant increases in beta sheet proportions. WT displays a slight increase in beta sheet characteristics by 30 minutes of incubation, which grows to be more significant by 2 hours (**Figure 3.5A**). Beta sheet characteristics increase much more rapidly in A135T (**Figure 3.5B**). A315E demonstrates beta sheet growth slower than A315T but surpasses WT (**Figure 3.5C**). Together, ThT and CD suggest significant fibrilization for WT, A315T, and A315E. Both methods indicate the rapid aggregation propensity of A315T, which is in agreement with clinical results showing A315T is associated with more severe symptoms.

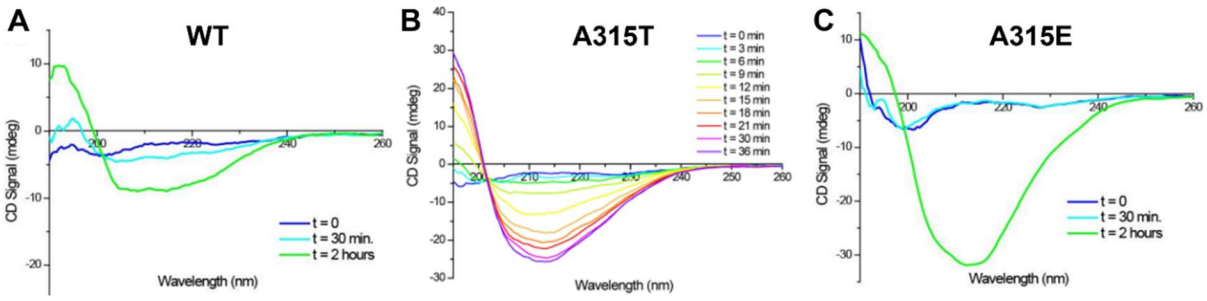

Figure 3.5 Far-UV circular dichroism spectra of (A) WT TDP-43(307-319), (B) A315T, and (C) A315E over their initial aggregation periods. All peptides demonstrate random coil characteristics at t=0. A positive band at 195 nm and a negative band at 216-218 nm is indicative of beta sheet formation and correlated with fibril formation. These bands were shown to grow over time for all peptides. A315T rapidly adopted beta sheet structures and was monitored more closely over a shorter time window. Experiments performed by Nicole M. Marsh, Brady Quon and Megan Fetters and overseen by Prof. Kristi Lazar Cantrell.[28]

3.3C Atomic Force Microscopy

TDP-43(307-319) peptides were also studied using AFM to correlate oligomer species with the formation of larger structures such as fibrils that are not observable with IM-

MS. WT TDP-43(307-319) and two ALS related mutant, A315T and A315E, were incubated at 100 μM in 10 mM ammonium acetate, pH 7.4, and 2% HFIP. Under the conditions of these experiments, the background of all AFM images is a peptide film. This film was sometimes shown to contain needle like features. These features were not consistently reproducible but were not observed to influence other the presence, frequency, or structure of other features.

The WT was observed to form fibril with a height of 2 nm by 15 minutes of incubation, notably before higher order oligomers were observable by IM-MS which suggests different aggregation pathways (**Figure 3.6A**). These fibrils can occasionally be seen to be undergoing a transition from protofibrils with an approximate height of 0.7 nm. This appears to be a conformational change, as multiple protofibrils were not observed to be associating to form a single fibril. By 3 hours and 8 hours, it is clear that fibrils are beginning to bundle together, a mechanism of growth typical for amyloid fibrils (**Figure 3.6B, C**). Height profiles show incremental heights of 2 nm and in many cases multiple fibrils can be observed converging into a larger fibrillar structure (**Figure 3.7A, B**). Fibril density begins to slightly decrease at 24 hours, likely as a result of decreased solubility following the association of several fibrils (**Figure 3.6D**). Fibrils are not observable at 48 hours, by which point it can be assumed sedimentation is complete.

Additionally, WT fibrils can occasionally be seen apparently growing out of loosely ordered peptide 'shards' with a highly regular height of 2 nm. **Figure 3.7** shows the clear phase distinction between the peptide background, peptide shards, protofibril tails, and fibrils. Shards have a lower phase than the underlying peptide film but a larger phase than fibrils, signifying the existence in a middle ground between disordered peptide film and

order, beta sheet-rich fibrils and protofibrils. Ultimately, these shards are inconsistently observed in experiments, so while interesting and potentially a future subject of study they cannot be considered necessary for fibril formation from these experiments.

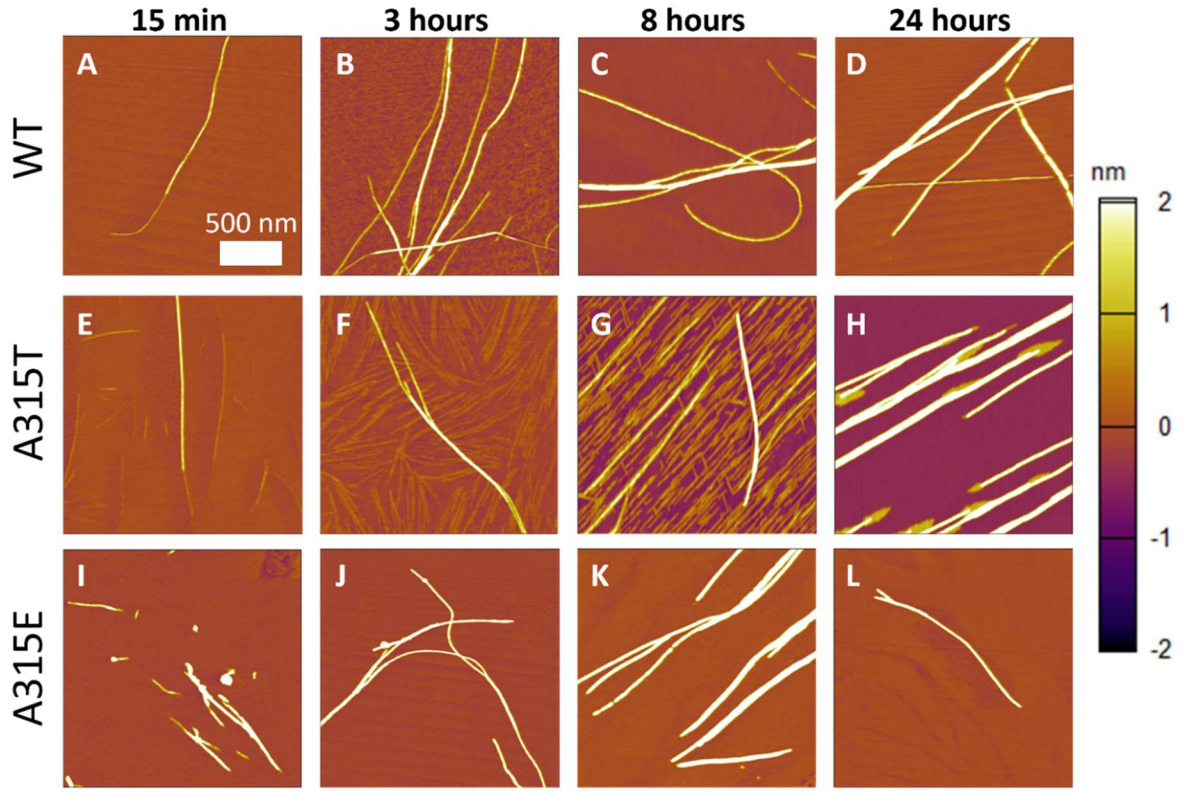

Figure 3.6 AFM investigation of (A-D) WT TDP-43(307-319), (E-H) A315T, and A315E (I-L) at 15 minutes, 3 hours, 8 hours, and 24 hours. Fibrils were observed at all time points for all peptides. Fibrils were observed to readily bundle together to produce larger fibrils. Fibrils are readily observable with protofibrillar tails. In A315T, a large quantity of isolated protofibrils are also observable.

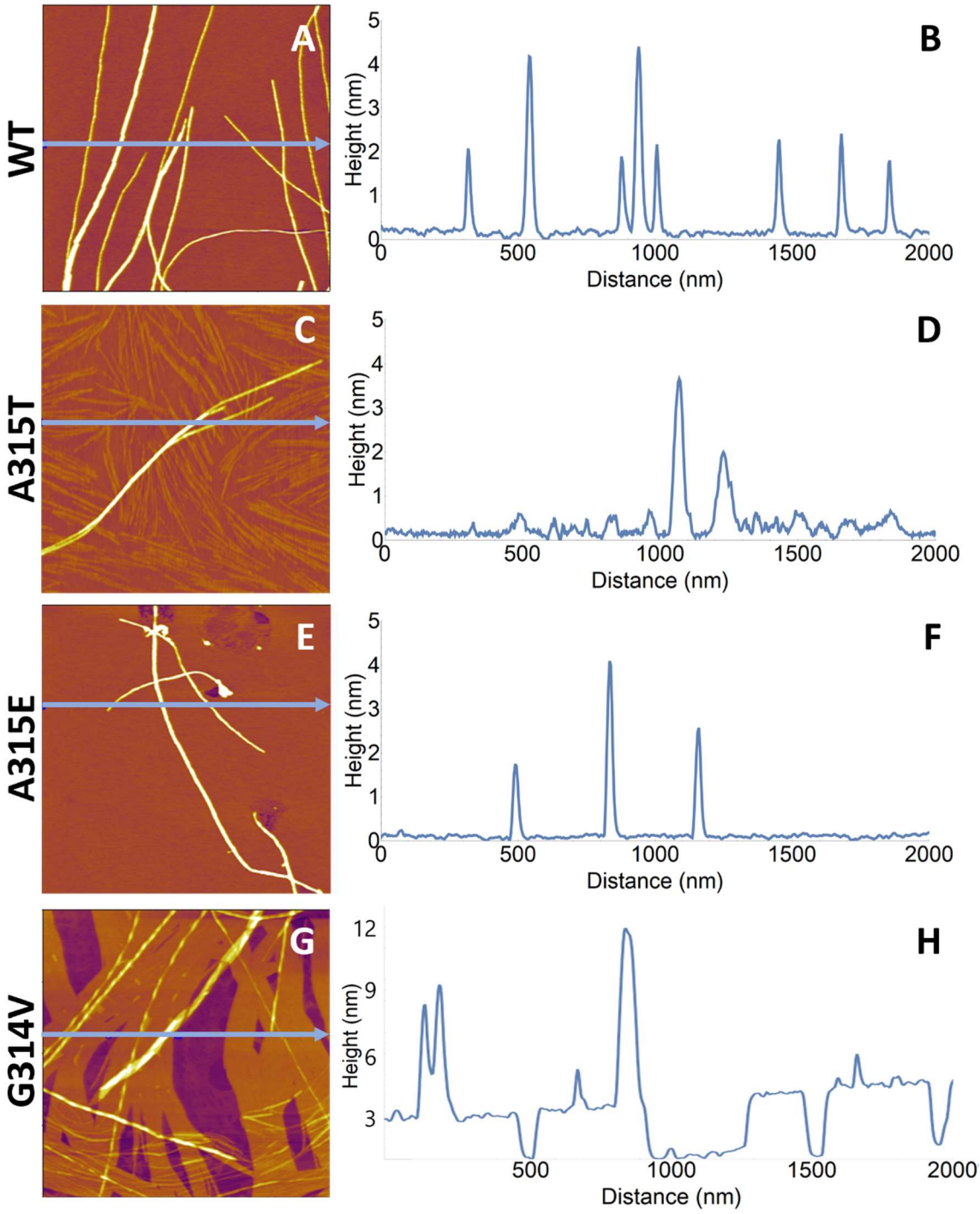

Figure 3.7 AFM height profile line cuts of fibrils presented in (A) WT TDP-43(307-319), (B) A315T, (C) A315E, and (D) G314V. WT, A315T, and A315E all demonstrate fibrils

with heights of approximately 2 nm intervals. G314V demonstrates fibrils with an irregular ribbon-like twist that also have heights of approximately 2 nm in flat regions.

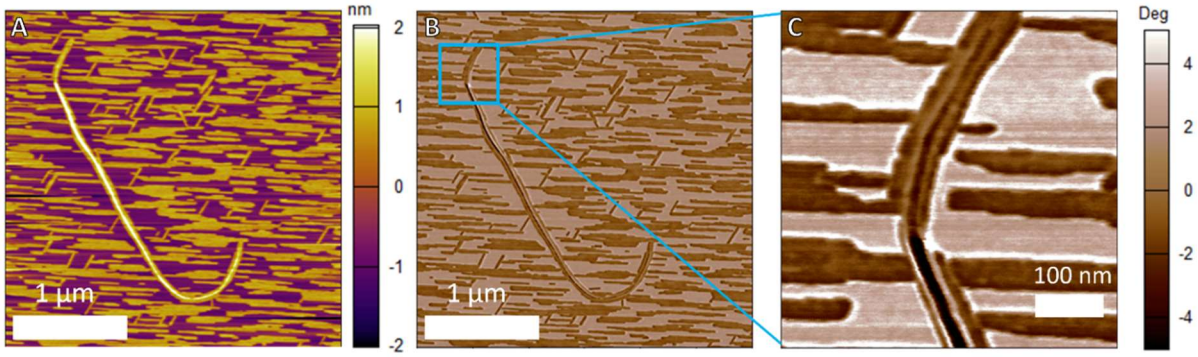

Figure 3.8 (A) AFM height image, (B) repulsive mode phase image and (C) zoomed-in phase image of WT TDP-43(307-319) fibril growing out of a peptide 'shard'. Lower phases are associated with harder features, while higher phases are associated with softer features. Phase images show a clear distinct phase for the underlaying peptide film, peptide shard, protofibril tail, and fibril, indicating these structures have increasing order associated with beta sheet formation.

The A315T mutation exhibits fibrils with similar height profiles to the WT, with a few notable deviations in the growth mechanism. Protofibril density is greatly increased at 15 minutes, with isolated protofibrils readily observable (**Figure 3.6E**). Additionally, pre-protofibrils observed both independently and as tails to protofibrils are observed with a height of ~0.2 nm, suggesting that there may be two distinct conformational changes on pathway to fibrils. Phase analysis of these protofibrils show a clear distinction in pre-protofibrils, protofibrils, and fibrils indicative of increased order and beta sheet stacking along this growth pathway (**Figure 3.8**). Fibrils themselves retain the 2 nm increment growth observed in the WT (**Figure 3.7 C, D**) Aggregation rich clumps composed largely of fibrils are also observable within the first hour of incubation (**Figure 3.9**). Given the size of these

features, it is likely that these undergo sedimentation, and they were not observed after 1 hour. Protofibrils and bundled fibrils continue to be observed through 8 hours (**Figure 3.6F, G**). Bundled fibrils are exclusively observed at 24 hours (**Figure 3.6H**).

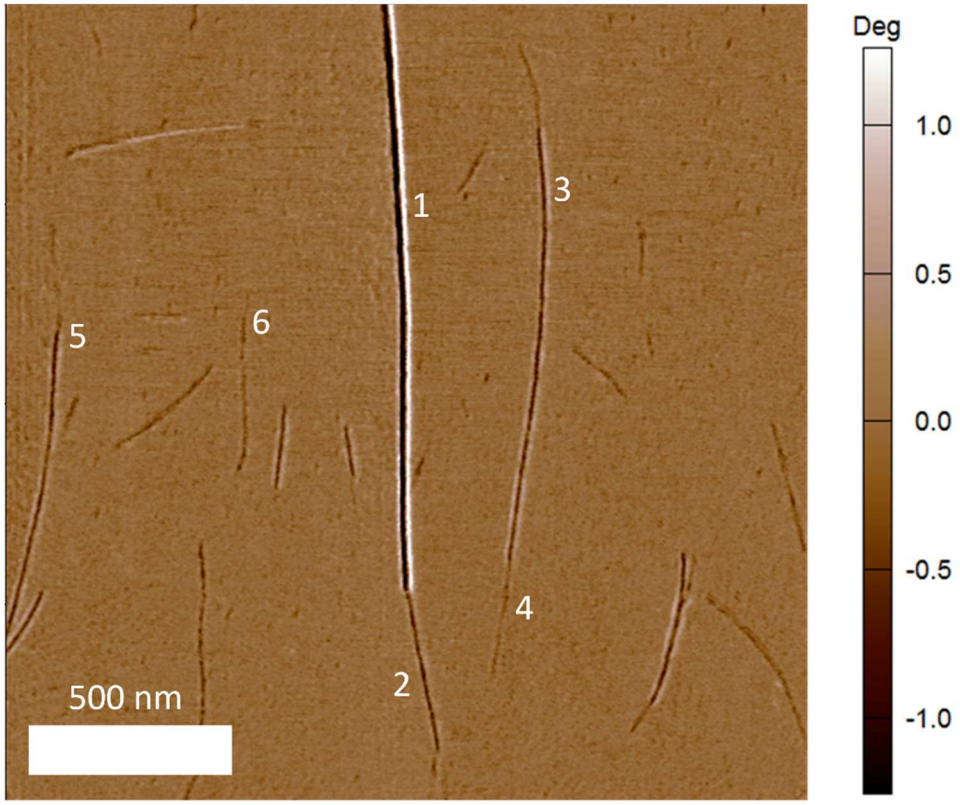

Figure 3.9 AFM repulsive mode phase image of TDP-43(307-319) A315T showing the distinct phases of the underlying peptide film, pre-protofibril, protofibril, and fibril. Lower phases are associated with harder features, while higher phases are associated with softer features. Markers indicate (1) a fibril with a (2) protofibril tail, (3) a protofibril with a (4) pre-protofibril tail, (5) an isolated protofibril, and (6) an isolated pre-protofibril.

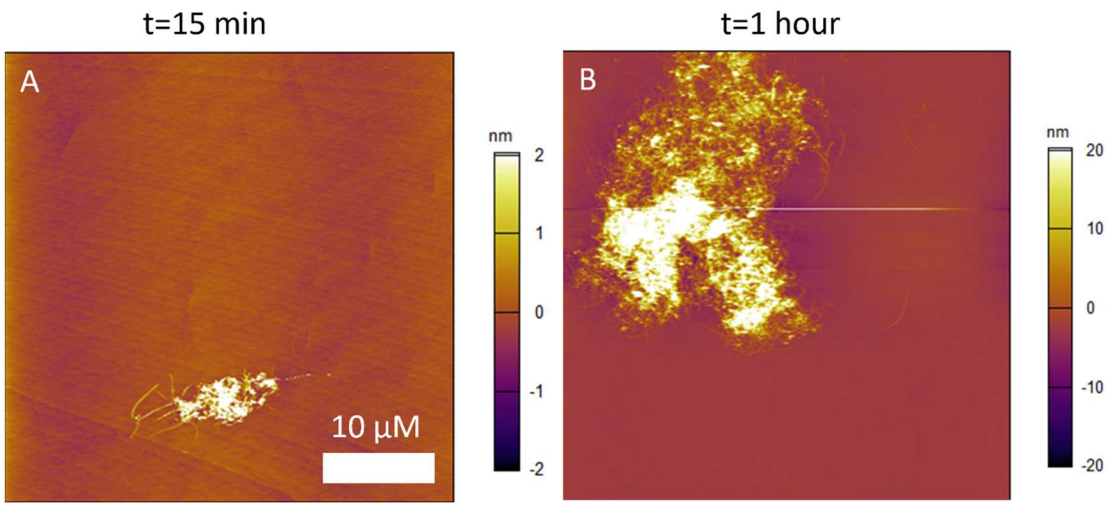

Figure 3.10 Fibrillar knots demonstrated by the aggregation enhancing mutation A315T at (A) 15 minutes and (B) 1 hour.

A315E also produces fibrils that have a similar height profile as both the WT and A315T. At 15 minutes these fibrils range from approximately 0.5-1 µm in length, while at this point both WT and A315T exhibited fibrils longer than 2 µm (**Figure 3.6I**). Despite the length difference, these fibrils also are shown to grow with 2 nm height increments (**Figure 3.7E, F**). Fibrils occasionally have protofibril tails, though like the fibrils themselves these tails are quite short. Bundling is observed to occur much earlier in the growth process and is readily observable at 15 minutes. By 3 hours and 8 hours, unbundled fibrils are the dominant feature (**Figure 3.6J, K**). This increased propensity to bundle may be associated with an increased rate of sedimentation, and fibril density is relatively low at 24 hours (**Figure 3.6L**).

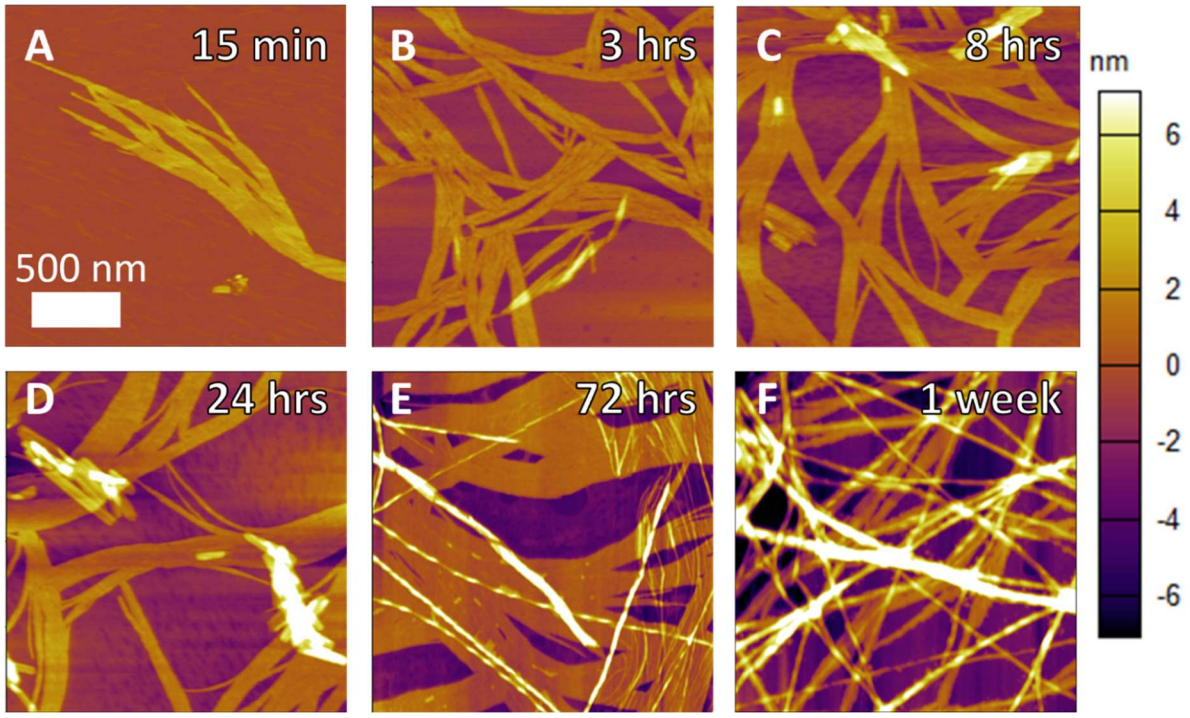

Figure 3.11 AFM investigation of G314V aggregation at (A) 15 minutes, (B) 3 hours, (C) 8 hours, (D) 24 hours, (E) 72 hours, and (F) 1 week. Over 24 hours G314V non-fibrillar features on top of a network of additional non-fibrillar features. By 72 hours, fibrils with a ribbon-like twist are observable. The density of these fibrils increases over 1 week.

The synthetic non-toxic mutant G314V was dissolved in a 50:50 mixture of 10 mM ammonium acetate, pH 7.4, and acetonitrile with 1% formic acid. Unlike the other peptides, G314V was not observed to form fibrils at 15 minutes (**Figure 3.11A**). Instead, a network of non-fibrillar features begins to form and is shown to persist for the duration. Non-fibrillar features were observed overlayed with this network starting at 3 hours (**Figure 3.11B**) and remain the only notable feature through 24 hours (**Figure 3.11 C, D**). These features were not observed to have a significantly different phase from the non-fibrillar network and are likely an extension of the network (**Figure 3.12A**). Fibrils are first observable after 72 hours

(**Figure 3.11E**), and fibril density is greatly increased at 1 week (**Figure 3.11F**). The fibrils are morphologically different, with a notable ribbon-like twist to them. Height analysis along one of these fibrils reveals a semi-regular variation in the height ranging from 2 to 6 nm (**Figure 3.13**). Fibrils do not appear to have a consistent pitch in the twist, and not all fibrils are observed to have a twist. Phase imaging of these fibrils confirms an increase in hardness typical of beta sheet-rich fibrils (**Figure 3.12B**). The presence of fibril in G314V, which does not form higher order oligomers, supports the notion that fibrils are off pathway from oligomerization.

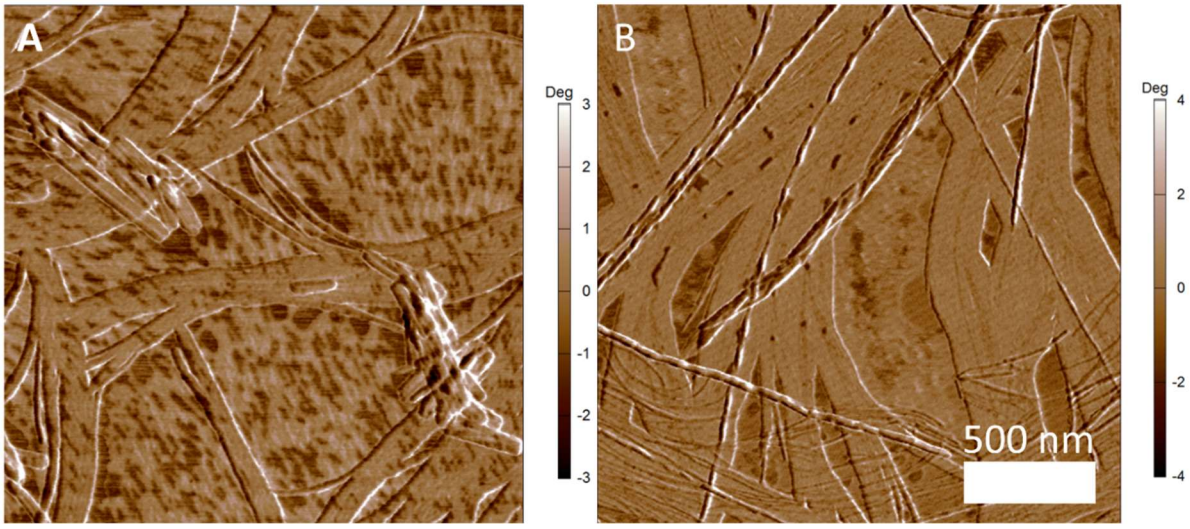

Figure 3.12 AFM repulsive mode phase image of TDP-43(307-319) G314V at (A) 24 hours and (B) 72 hours. Lower phases are associated with harder features, while higher phases are associated with softer features. The background at 24 hours shows phase hardening in some places that should not be conflated with the phase of features. Only non-fibrillar features are present at 24 hours, indicated by the lack of phase difference. By 72 hours, fibrils with distinct phase from the background can be observed.

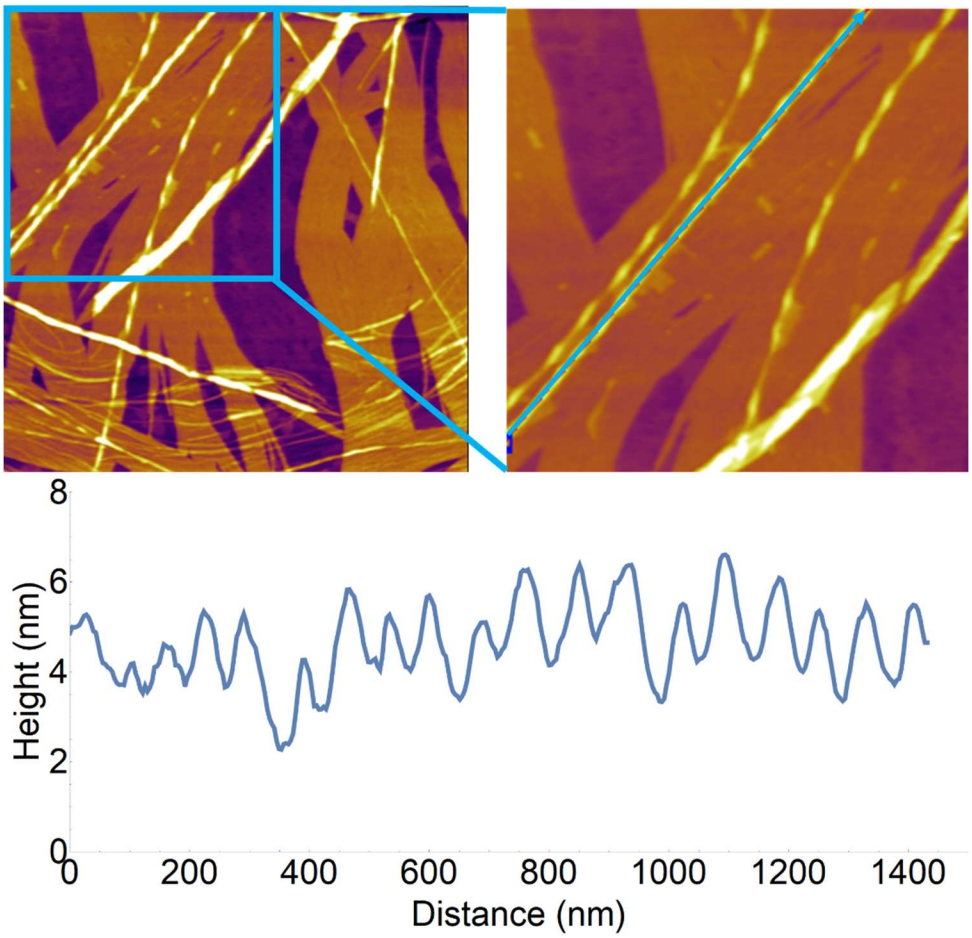

Figure 3.13 AFM height profile line cut of a ribbon-like twisted fibril formed by TDP-43(307-319) G314V. The pitch of the fibril is irregular and there is significant variation in the height for each twist. The fibril has a minimum height of 2 nm.

3.3D Atomic Force Microscopy: Low Concentration Studies

TDP-43(307-319) aggregation was also investigated under a variety of different incubation concentrations in an attempt to learn more about the aggregation mechanism. WT TDP-43(307-319) was incubated at a concentration of 5 μM in 10 mM ammonium acetate, pH 7.4, and 2% HFIP. Under these conditions the WT was not observed to form any notable discrete aggregates within 24 hours (**Figure 3.14**). This means that either fibrils are not being

formed at this low of a concentration or the rate of formation and the rate of sedimentation are such that fibrils never accumulate to observable quantities.

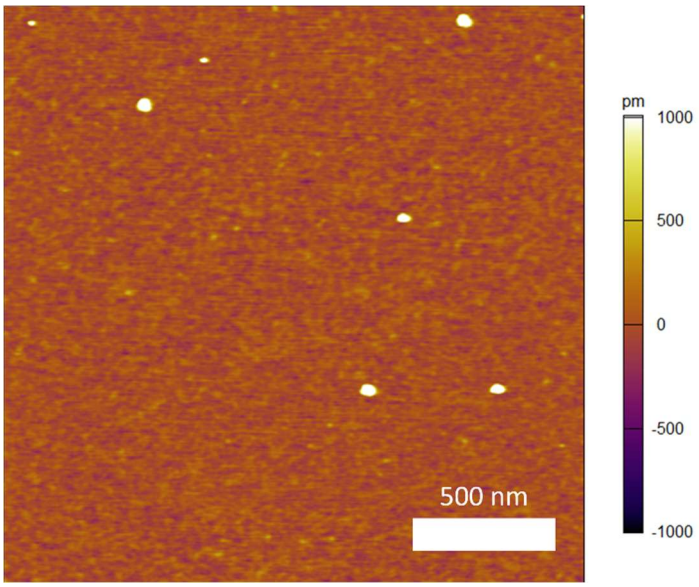

Figure 3.14 AFM image of WT TDP-43(307-319) incubated for 24 hours at a concentration of 5 µM in 10 mM ammonium acetate, pH 7.4, with 2% HFIP. No fibrilization was observable.

In order to test if sedimentation was occurring, 5 µM WT TDP-43 was incubated on top of the mica substrate for 3 days. By affixing a mica disc to an inverted vial with the top removed, fibrils undergoing sedimentation should be deposited onto the mica disc and observable using AFM. Following incubation, liquid on the mica was removed via shaking and any remaining liquid was dried using a vacuum desiccator as with the normal drying procedure. This procedure was successful in producing observable fibrils at a lower concentration than previous attempts and indicates that sedimentation is occurring (**Figure 3.15**).

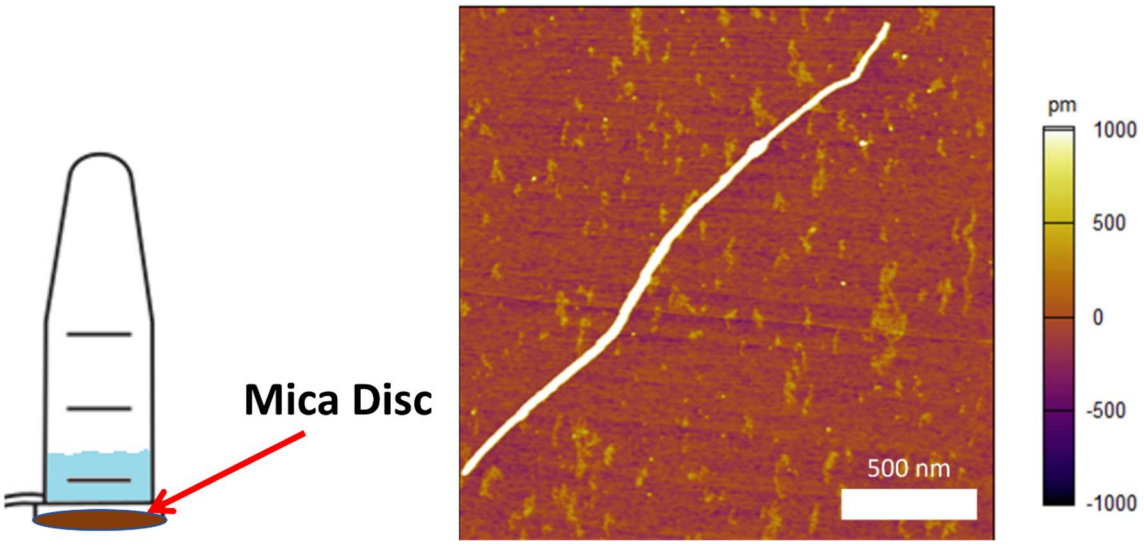

Figure 3.15 Cartoon of WT TDP-43(307-319) incubation on top of a mica disc and the corresponding AFM image showing a fibril having undergone sedimentation. WT TDP-43(307-319) was incubated at 5 µM in 10 mM ammonium acetate, pH 7.4, and 2% HFIP on top of a mica disc such that sedimented fibrils would be deposited onto the mica.

Attempts were also made to dilute TDP-43(307-319) in order to better visualize individual features. WT TDP-43(307-319) was incubated at 100 µM in 10 mM ammonium acetate, pH 7.4, and 2% HFIP. At desired intervals, aliquots of this solution were diluted into additional 10 mM ammonium acetate, pH 7.4, to create a 20 µM solution which was then deposited on mica and dried as normal using a vacuum desiccator. This procedure had the unexpected result of appearing to cause fibril dissociation (**Figure 3.16**). Full length fibrils were not observable at 1 hour of incubation, and instead what appear to be fibril fragments are seen. Because this procedure results in unwanted changes in features it was ultimately abandoned. However, this experiment demonstrates how rapid system changes can influence

assembly. Fibrils are formed as part of a complex equilibrium with oligomeric species. Decreasing the concentration of those oligomers can result in the dissociation of fibrils.

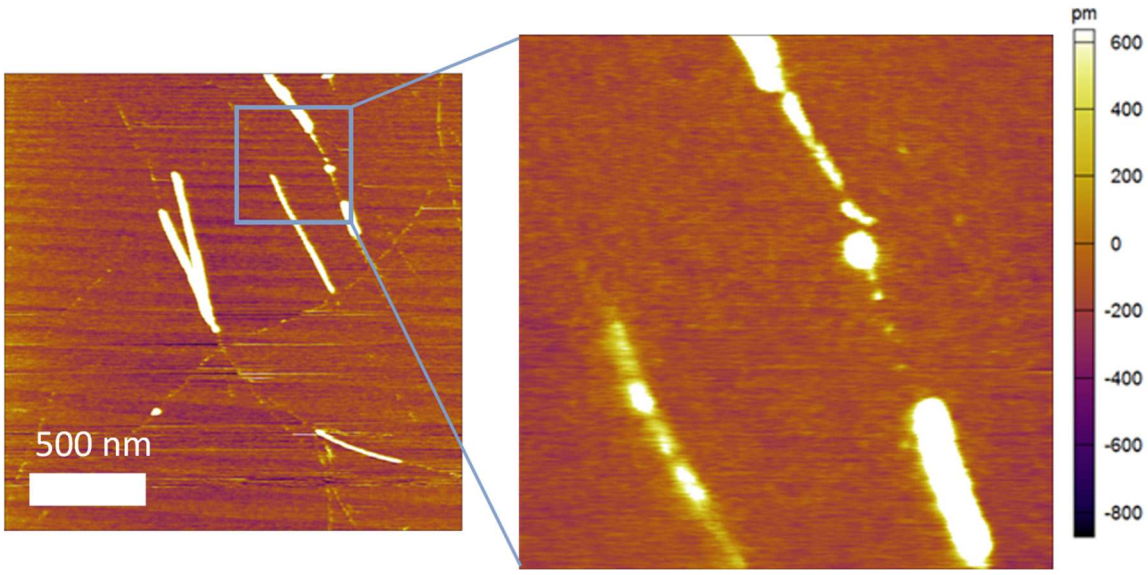

Figure 3.16 WT TDP-43(307-319) incubated for 1 hour at 100 µM in 10 mM ammonium acetate, pH 7.4, and 2% HFIP then diluted to 20 µM with additional ammonium acetate before imaging. Fibrils have begun to dissociate as a result of the rapid decrease in peptide concentration.

3.4 Conclusions

The amyloidogenic core region TDP-43(307-319) undergoes extensive aggregation that is suspected to be causative in ALS. Understanding this aggregation pathway is likely essential to developing effective treatment options for ALS. In this work, IM-MS was used to show extensive oligomerization of WT TDP-43(307-319) that is enhanced by the ALS related mutants A315T and A315E. The synthetic, non-toxic mutation G314V was shown to stifle oligomerization, preventing the formation of higher order oligomers. These results suggest that higher order oligomers are responsible for toxicity. As further evidence of this, recent MD work has also shown that the TDP-43(307-319) hexamers of the WT, A315T, and

A315E are all compatible with the cylindrin beta-barrel motif proposed as the toxic structure in several other disease-related peptides.[28]

Correlating AFM experiments with these results show that WT and A315E fibril formation begins early on in the aggregation pathway, notably before any higher order hexamers and octamer are observable. Due to rapid aggregation and the immediate formation of higher order oligomers, this conclusion cannot definitively be extended to A315T although lower concentration IM-MS and AFM studies may be able to provide additional insight. This leads to the conclusion that oligomerization and fibrilization occur via different pathways. In support of this, G314V was observed to form fibrils despite never forming higher order oligomers. Additionally, when describing the cylindrin Eisenberg et al note that because it contains out of register beta sheets that are atypical of fibrils, hydrogen bonds would have to break for the cylindrin to be incorporated into a fibril making it energetically unfavorable.[29] It should be noted that the formation of fibrils out of low order oligomers is notably a different mechanism than what was observed for amyloid beta 42, in which the toxic dodecamer species was observed to seed fibril formation.[38]

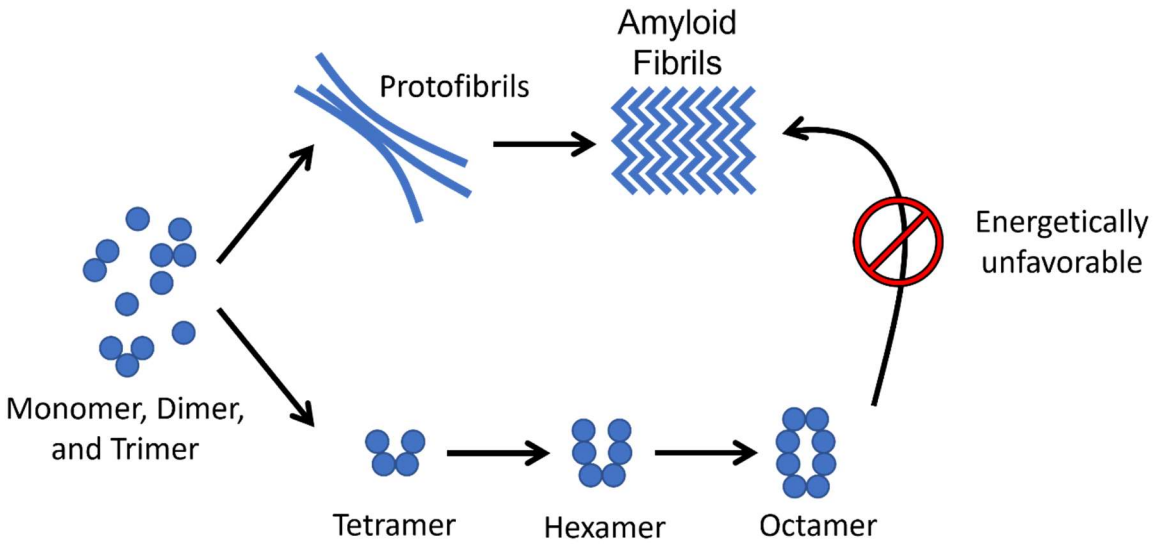

Figure 3.17 Cartoon demonstrating the bifurcated aggregation pathway of TDP-43(307319). Lower order oligomers were shown to be sufficient for fibril formation, indicating that oligomerization is off pathway. Additionally, if higher order oligomers adopt cylindrin-like structures hydrogen bond rearrangements would likely be necessary for them to be incorporated into fibrils, making the process energetically unfavorable.

In conclusion, we have elucidated a bifurcated aggregation pathway for oligomerization and fibrilization for TDP-43(307-319) (**Figure 3.17**). Low order oligomers are sufficient for fibril formation, and while it cannot be definitively concluded that higher order oligomers aren't involved later on, evidence exists suggesting its energetically unlikely. With this the self-aggregation properties ofTDP-43(307-319) established, future work can be done to study how it is modulated by potential therapeutic agents or disease-related aggregation enhancers.

3.5 References

1. Mehta, P.; Kaye, W.; Raymond, J. Punjani, R.; Larson, T.; Cohen, J.; Muravov, O.; Horton, K. Prevalence of Amyotophic Lateral Sclerosis – United States. Rep, 2015. *Morb Mortal Wkly Rep.* **2018**, *67* (46), 1285-9.
2. Mehta, P.; Raymond, J.; Punjani, R.; Han, M.; Larson, T.; Kaye, W.; Nelson, L. M.; Topol, B.; Muravov, O.; Genson, C.; Horton, K. Prevalence of amyotrophic lateral sclerosis in the United States Using Established and Novel Methodologies, 2017. *Amyotroph Lateral Scler Frontotemporal Degener* **2022,** Advanced online publication.
3. Millul, A.; Beghi, E.; Logroscino, G.; Micheli, A.; Vitelli, E.; Zardi, A. Survival of patients with amyotrophic lateral sclerosis in a population-based registry. *Neuroepidemiology* **2005**, *25* (3), 114-9.

4. Del Aguila, M. A.; Longstreth, W. T. Jr.; McGuire, V.; Koepsell, T. D.; van Belle, G. Prognosis in amyotrophic lateral sclerosis, a population-based study. *Neurology* **2003**,*60* (5), 813-9.
5. Byrne, S.; Walsh, C.; Lynch, C.; Bede, P. Elamin, M. Kenna, K. McLaughlin, R. Hardiman, O. Rate of familial amyotrophic lateral sclerosis: a systematic review and meta-analysis. *J. Neurol. Neurosurg. Psychiatry.* **2011**, *82*, 623-7.
6. Neumann M.; Sampathu D.M.; Kwong L.K.; Truax A.C.; Micsenyi M. C.;, Chou T.T.; Bruce J.; Schuck T.; Grossman M.; Clark C. M.; McCluskey L.F.; Miller B. L.; Masliah E.; Mackenzie I. R.; Feldman H.; Feiden W.; Kretzschmar H.A.; Trojanowski J.Q.; Lee V.M. Ubiquitinated TDP-43 in frontotemporal lobar degeneration and amyotrophic lateral sclerosis. *Science*. **2006,** *314* (5796), 130-3.
7. Arai T.; Hasegawa M.; Akiyama H,; Ikeda K.; Nonaka T.; Mori H.; Mann D.; Tsuchiya K.; Yoshida M.; Hashizume Y.; Oda T. TDP-43 is a component of ubiquitin-positive tau-negative inclusions in frontotemporal lobar degeneration and amyotrophic lateral sclerosis. *Biochem. Biophys. Res. Commun.* **2006,** *351* (3), 602-11.
8. Josephs, K. A.; Whitwell, J. L.; Weigand, S. D.; Murray, M. E.; Tosakulwong, N.; Liesinger, A. M.; Petrucelli, L.; Senjem, M. L.; Knopman, D. S.; Boeve, B. F.; Ivnik, R. J.; Smith, G. E.; Jack, C. R.; Parisi, J. E.; Petersen, R. C.; Dickson, D. W. TDP-43 is a key player in the clinical features associated with Alzheimer's disease. *Acta. Neuropathol.* **2014**, *127* (6), 811−824.
9. Josephs, K. A.; Murray, M. E.; Whitwell, J. L.; Parisi, J. E.; Petrucelli, L.; Jack, C. R.; Petersen, R. C.; Dickson, D. W. Staging TDP-43 pathology in Alzheimer's disease. *Acta. Neuropathol.* **2014**, *127* (3), 441−450.
10. Jo, M.; Lee, S.; Jean, Y.-M.; Kim, S.; Kwon, Y.; Kim, H.-J. The Role of TDP-43 propagation in neurodegenerative diseases: Integrating insights from clinical and experimental studies. *Exp. Mol. Med.* **2020**, *52*, 1652−1662.
11. Huang, W.; Zhou, Y.; Tu, L.; Ba, Z.; Huang, J.; Huang, N.; Luo, Y. TDP-43: From Alzheimer's disease to limbic-predominant age-related TDP-43 encephalopathy. *Front. Mol. Neurosci.* **2020**, *13*, 1−7.

12. Shih, Y.-S.; Tu, L.-H.; Chang, T.-Y.; Ganesan, K.; Chang, W.-W.; Chang, P.-S.; fang, Y.-S.; Lin, Y.-T.; Jin, L.-W.; Chen, Y.-R. TDP-43 interacts with amyloid-beta, inhibits fibrillization, and worsens pathology in a model of Alzheimer's disease. *Nat. Commun.* **2020**, *11*, 5950−5965.
13. de Boer E. M. J.; Orie,V. K.; Williams, T.; Baker, M. R.; De Oliveira, H. M.; Polvikoski, T.; Silsby, M.; Menon, P.; van den Bos, M.; Halliday, G. M.; van den Berg, L. H.; Van Den Bosch, L.; can Damme, P.; Kiernan, M.; van Es, M. A.; Vucic, S. TDP-43 proteinopathies: a new wave of neurodegenerative diseases. *J. Neurol. Neurosurg. Psychiatry.* **2021,** *92,* 86–95.
14. Tollervey, J.; Curk, T.; Rogelj, B.; Briese, M.; Cereda, M.; Kayikici, M.; Konig, J.; Hortobagyi, T.; Nishimura, A. L.; Zupenski, V.; Patani, R.; Chandran, S.; Rot, G.; Zupan, B.; Shaw, C. E.; Ule, J. Characterizing the RNA targets and position-dependent splicing regulation by TDP-43. *Nat. Neurosci.* **2011**, *14*, 452–458.
15. Suk, T.R., Rousseaux, M.W.C. The role of TDP-43 mislocalization in amyotrophic lateral sclerosis. *Mol. Neurodegeneration.* **2020**, *15*, 45**.**
16. Cohen, T. J., Lee, V. M., and Trojanowski, J. Q. TDP-43 functions and pathogenic mechanisms implicated in TDP-43 proteinopathies. *Trends Mol. Med.* **2011**, *17* (11), 659−67.
17. Pesiridis G. S.; Lee V. M.; Trojanowski J. Q. Mutations in TDP-43 link glycine-rich domain functions to amyotrophic lateral sclerosis. *Hum. Mol. Genet.* **2009,** *18* (R2), R156-62.
18. Zhu, L.; Xu, M.; Yang, M.; Yang, Y.; Li, Y.; Deng, J.; Ruan, L.; Liu, J.; Du, S.; Liu, X.; Feng, W.; Fushimi, K.; Bigio, E. H.; Mesulam, M.; Wang, C.; Wu, J. Y. An ALS-mutant TDP-43 neurotoxic peptide adopts an anti-parallel beta-structure and induces TDP-43 redistribution. *Hum. Mol. Genet.* **2014**, *23* (1), 6863−6877.
19. Gitcho, M. A.; Baloh, R. H.; Chakraverty, S.; Mayo, K.; Norton, J. B.; Levitch, D.; Hatanpaa, K. J.; White, C. L. 3rd; Bigio, E. H.; Caselli, R.; Baker, M.; Al-Lozi, M. T.; Morris, J. C.; Pestronk, A.; Rademakers, R.; Goate, A. M.; Cairns, N. J. TDP-43 A315T mutation in familial motor neuron disease. *Ann. Neurol.* **2008**, *63* (4), 535−8.

20. Fujita, Y.; Ikeda, M.; Yanagisawa, T.; Senoo, Y.; Okamoto, K. Different clinical and neuropathologic phenotypes of familial ALS with A315E TARDBP mutation. *Neurology.* **2011**, *77* (15), 1427−31.
21. Fang, Y.-S., Tsai, K.-J., Chang, Y.-J., Kao, P., Woods, R., Kuo, P.-H., Wu, C.-C., Liao, J.-Y., Chou, S.-C., Lin, V., Jin, L.-W., Yuan, H. S., Cheng, I. H., Tu, P.-H., and Chen, Y.-R. Full-length TDP-43 forms toxic amyloid oligomers that are present in frontotemporal lobar dementia-TDP patients. *Nat. Commun.* **2014**, *5*, 4824.
22. Glabe, C. G. Common mechanisms of amyloid oligomer pathogenesis in degenerative disease. *Neurobiol. Aging.* **2006,** *27*, 570−575.
23. Lesne, S. E.; Sherman, M. A.; Grant, M.; Kuskowski, M.; Schneider, J. A.; Bennett, D. A.; Ashe, K. Brain Amyloid-β oligomers in ageing and Alzheimer's disease. *Brain* **2013**, *136*, 1383−1398.
24. Sakono, M.; Zako, T. Amyloid oligomers: Formation and toxicity of Abeta oligomers. *FEBS J.* **2010**, *277*, 1348−1358.
25. Wyttenbach, T.; Kemper, P. R.; and Bowers, M. T. Design of a new electrospray ion mobility mass spectrometer. *Int. J. Mass Spectrom.* **2001,** *212* (1−3), 13−23.
26. Khurana, R.; Coleman, C.; Ionescu-Zanetti, C.; Carter, S. A.; Krishna, V.; Grover, R. K.; Roy, R.; Singh, S.; Mechanism of thioflavin T binding to amyloid fibrils. *J Struct Biol* **2005** *3* (141), 229-38.
27. Williams, A. T. R.; Winfield, S. A.; Miller, J. N. Relative Fluorescence Quantum Yields Using a Computer-controlled Luminescence Spectrometer. *Analyst* **1983** *108*, 1067-71.
28. Laos, V.; Do, T. D.; Bishop, D.; Jin, Y.; Marsh, N. M.; Quon, B.; Fetters, M.; Cantrell, K. L.; Buratto, S. K.; Bowers, M. T. Characterizing TDP-43(307-319) Oligomeric Assembly to Elucidate Mechanistic and Structural Implications Involved in the Etiology of ALS. *ACS Chem. Neurosci.* **2019**, *10* (9), 4112−4123.
29. Laganowsky, A.; Liu, C.; Sawaya, M. R.; Whitelegge, J. P.; Park, J.; Zhao, M.; Pensalfini, A.; Soriaga, A. B.; Landau, M.; Teng, P. K.; Cascio, D.; Glabe, C.; Eisenberg, D. Atomic view of a toxic amyloid small oligomer. *Science.* **2012**, *335* (6073), 1228−31.

30. Economou, N. J.; Giammona, M. J., Do, T. D.; Zheng, X.; Teplow, D. B.; Buratto, S. K.; Bowers, M. T. Amyloid β-Protein Assembly and Alzheimer's Disease: Dodecamers of Aβ42, but Not of Aβ40, Seed Fibril Formation. *J. Am. Chem. Soc.* **2016**, *138* (6), 1772-5.

IV. Modulating TDP-43 Aggregation with JPS Generated Inhibitors

4.1 Introduction

TAR DNA binding protein of 43 kDa (TDP-43) aggregation is associated with amyotrophic lateral sclerosis, tau- and alpha synuclein- negative frontotemporal lobar degeneration, and a subset of patients with Alzheimer's disease.[1-7] With no effective treatments, these and other neurodegenerative diseases are one of the major medical problems left unsolved to date. As such, they are attractive targets for the development of therapeutic agents. However, currently there are no proven disease-modifying drugs available for neurodegenerative diseases, and failed drugs have continued to accumulate. One significant problem with effective drug development is the selection of the right therapeutic target. Many early treatment attempts targeted the abnormal protein deposits characteristic of these diseases. However, recent research has implicated small soluble oligomers instead of insoluble fibrils that compose the protein deposits in many of these diseases. As such, modulating the oligomerization of disease-related proteins remains a hopeful avenue for drug development. 8,11

Current drug development primarily utilizes high throughput screening (HTS). HTS is an automated process that tests thousands of chemical compounds in order to identify potential hits with relevant biological activity.12 This process can be expensive, requiring a large library of chemical compounds to test from, and typically returns less than 0.1% hits. In order to address this, A. K. Singh et al developed the Joint Pharmacophore Space (JPS) as a novel method of pharmacophore analysis. From known information of thousands of

molecular assays, the geometric features of pharmacophores can be correlated with properties such as a compound's ability to bind with a target, permeate the blood-brain barrier, or cause toxicity. Using this information, a machine learning algorithm can design potential drug molecules based on desired attributes.[13-14] JPS was first used to develop the molecule AC0107 (**Figure 6.1C**), which was shown to modulate Aβ42 aggregation by reducing toxic oligomers to lower order, nontoxic oligomers.

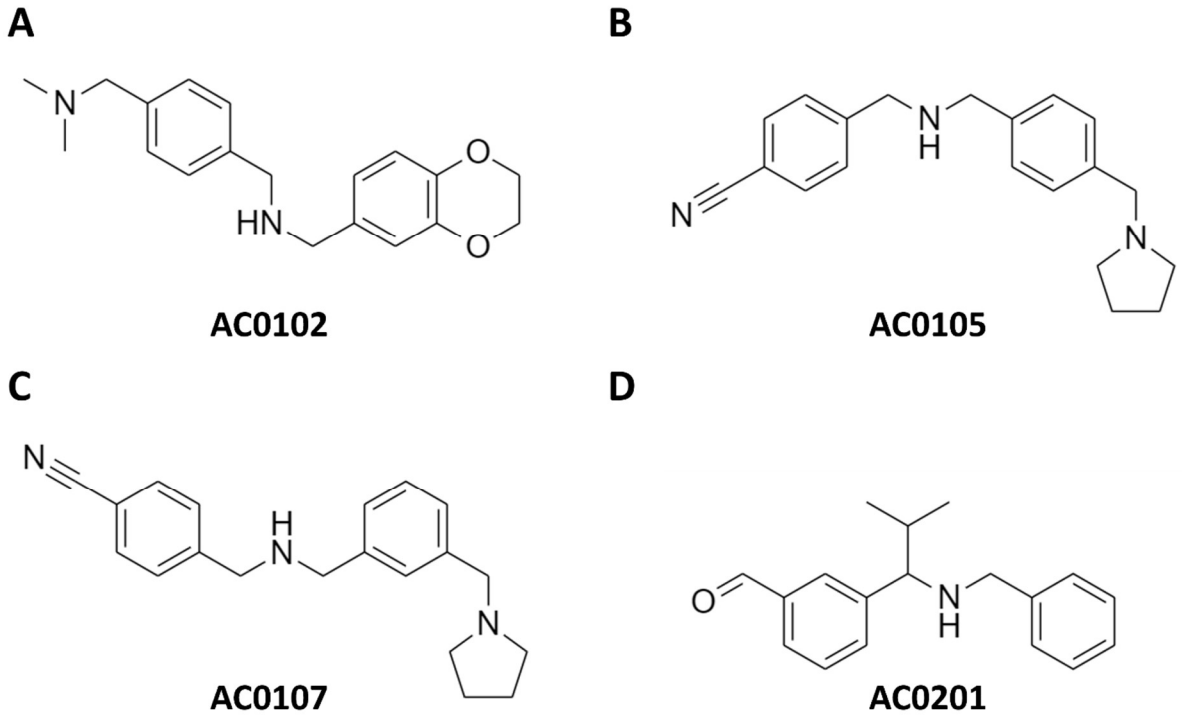

Figure 4.1 JPS generated inhibitor molecules. (A) AC0102, (B) AC0105, and (C) AC0107 are first-generation molecules, while (D) AC0201 is a second-generation molecule after the machine learning algorithm was retrained with results from AC0107.

Interest in these inhibitor molecules has extended to additional disease-related proteins because they are believed to cause toxicity via similar aggregation-based mechanisms. As discussed in Chapter 3, TDP-43 has an amylogenic core region in the C-

terminal region at residues 307-319 that has been shown to form fibrils and express neurotoxicity. [16] This region is believed to be the driving force behind aggregation observed in disease, and disrupting this aggregation may be essential in the development of therapeutics. Here, 3 first-generation molecules – AC0102, AC0105, and AC0107 (**Figure 6.1A-C**) – are examined for their effect on modulating the aggregation of TDP-43(307-319). The second-generation molecule AC0201 (**Figure 6.1D**), developed after the machine learning algorithm was retrained with the results from experiments between AC0107 and Aβ42, is also studied.

4.2 Materials and Methods

4.2A Protein Synthesis and Preparation

TDP-43(307−319) WT peptide 307[MGGGMNFGAFSIN]319 was synthesized using standard 9-fluorenylmethoxycarbonyl (Fmoc) chemistry using 2-(1H-benzotriazol-1-yl)-1,1,3,3-tetramethyluronium hexafluorophosphate/hydroxybenzotriazole (HBTU/HOBT) manual solid phase peptide synthesis. The peptide was amidated with an Fmoc-Rink Amide resin (Anaspec). The peptide was cleaved from the resin using 94% TFA, 5% triisopropylsilane, and 1% phenol for 2 h at 295 K. The crude peptide was purified by reverse phase high-performance liquid chromatography (RP-HPLC) on a semipreparative C18 column (Phenomenex) using gradients of water [0.1% (v/v) TFA] and acetonitrile [0.1% (v/v) TFA]. The peptide was dissolved in 6 M guanidine hydrochloride (GdnHCl) prior to injection due to its insolubility in water and acetonitrile. The peptide purity was >93% as determined by analytical RP-HPLC. The molecular mass of the peptide was verified by ESI mass spectrometry. Peptide synthesis was performed by Nicole M. Marsh, Brady Quon and Megan Fetters and oversaw by Kristi Lazar Cantrell (Westmont College, Santa Barbara, CA).

4.2B Joint Pharmacophore Space in Silico Modeling

Compounds studied in this work were generated by the JPS machine learning algorithm developed by Sayan Ranu and Ambuj K. Singh (University of California – Santa Barbara, Santa Barbara, CA). The JPS algorithm was trained using 30 known aggregation inhibitors of Aβ.[17-27] The ZINC data base[28] was then screened for target selectivity, blood-brain barrier permeability, and low adverse side effects. Compounds were generated using this information and underwent preliminary testing for BBB permeability and toxicity using the Caco-2 and hERG assays.[29-30] Promising compounds were tested using a sensitive tracking assay to evaluate their ability to inhibit membrane trafficking of Aβ. AC0107 was the first molecule experimentally examined using IM-MS for its ability to modulate Aβ aggregation.[15] Data from AC0107 was used to retrain the JPS algorithm to produce second-generation molecules.

4.2C Ion Mobility-Mass Spectrometry

Ion mobility-mass spectrometry (IM-MS) was used to study oligomerization in the presence of JPS small molecules. IM-MS separates species of a specific $[m]^{+z}$ (m = mass, z = charge) with different $[n]^{+z}$ (n = oligomer number) by measuring arrival time distributions (ATDs). Experiments were performed on a home-built ion mobility mass spectrometer consisting of a nano-electrospray ionization source, home-built ion funnel, 4.503 cm-long drift cell, quadrupole mass filter, and conversion dynode and electron multiplier detector. Ions are generated at the source, captured and stored in the ion funnel, and pulsed into the drift cell filled with approximately 3 Torr of helium gas. Ions exiting the drift cell are filtered by the quadrupole mass analyzer and finally reach the detector.[31] All ion mobility

experiments were performed by Dr. Veronica Laos (University of California – Santa Barbara, Santa Barbara, CA).

4.2D Atomic Force Microscopy

Atomic force microscopy (AFM) was used to study the effect of JPS small molecules on fibril morphology and assembly. Experiments were conducted using an MFP-3D AFM (Asylum Research, Goleta, CA) and Cantilever C on HQ:XSC11/Al BS AFM probes (NanoAndMore USA Corp, Watsonville, CA). Images were acquired in air using repulsive tapping mode. Samples were prepared for imaging by depositing 5 μL of solution on freshly cleaved V1-grade muscovite mica discs (Ted Pella, Edding, CA) and drying in a vacuum desiccator. Samples were visibly dry in approximately 5 minutes but were allowed to dry over-night.

4.3 Results and Discussion

4.3A Recovery

Recovery experiments were run on three first generation JPS generated molecules, AC0102, AC0105, and AC0107, and one second generation JPS generated molecule, AC0201, in order to test their ability to modulate pre-formed aggregates. Solutions containing 100 μM WT TDP-43 in 10 mM ammonium acetate buffer, pH 7.4, with 2% HFIP were allowed to incubate at room temperature for 4 hours to develop higher order oligomers. **Figure 4.2** details the aggregation state before the addition of the inhibitors. At 15 minutes, monomer, dimer, and a small trimer peak are present in the IM-MS ATD. Fibrils are also observable via AFM. By 4 hours, tetramer, hexamer, and octamer peaks have developed while fibril density significantly increases. Additional results and discussion concerning the self-aggregation of TDP-43 can be found in Chapter 3. Inhibitor molecules were then added

in a 1:1 mole ratio in order to monitor their effect on oligomerization and fibrilization and incubated at room temperature over 24 hours. For a direct comparison with AFM experiments, uninhibited WT TDP-43 was allowed to aggregate under the same conditions and imaged at the same time points using AFM (**Figure 4.3**). This was not done for IM-MS because continued aggregation results in poor signal at time points longer than 4 hours.

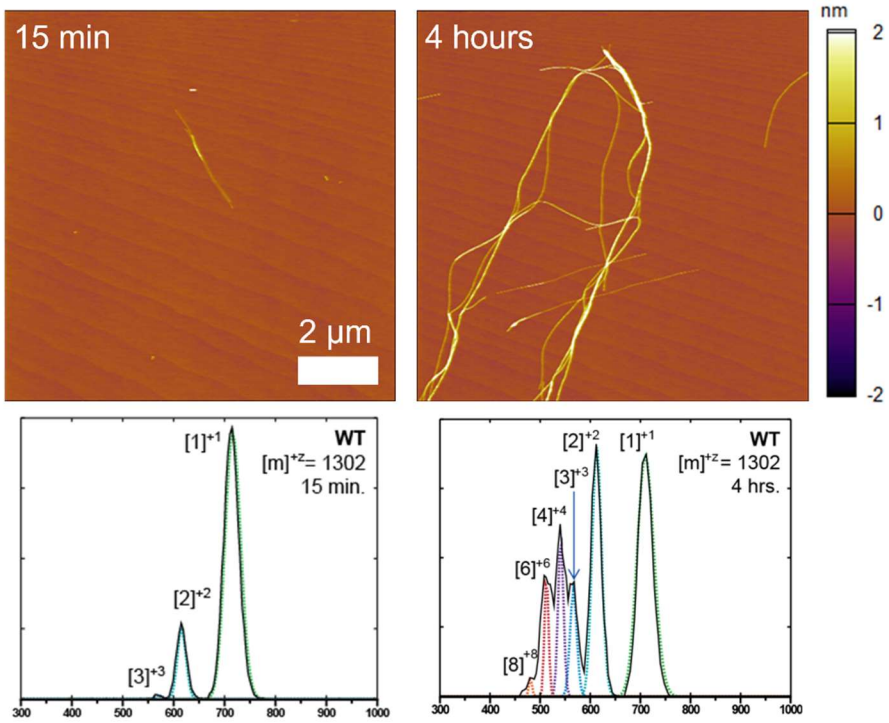

Figure 4.2 AFM images (top) and IM-MS ATDs (bottom) of the aggregation state of WT TDP-43 before addition of small molecule inhibitors. Fibrils are observable at 15 minutes, with a greatly increased fibril density at 4 hours. Monomer, dimer, and trimer peaks are observable in the 15-minute ATD. Tetramer, hexamer, and octamer peaks emerge by 4 hours. IM-MS experiments performed by Dr. Veronica Laos.[40]

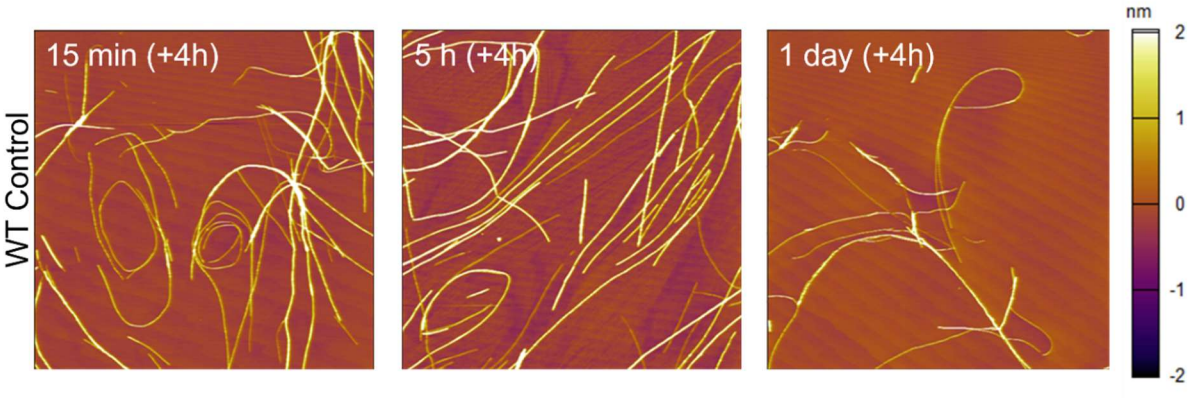

Figure 4.3 AFM control images of WT TDP-43 self-aggregation. Incubations times are given as additions to a normal 4-hour incubation time used in the inhibitor experiments. All time points demonstrate fibrils. Fibril density is slightly reduced at 1 day (+4 hours) due to sedimentation.

IM-MS reveals that all the inhibitor molecules had dramatic modulating effects of TDP-43 oligomerization. Introducing either AC0102 or AC0107 causes an initial uptick in higher order oligomers, with a significant increase in population of hexamer and octamer (**Figure 4.4A, G)**. At 3 hours, these populations are greatly reduced for AC0102 and completely absent for AC0107 (**Figure 4.4G, H**). AC0105 and AC0201 do not experience the same initial uptick in oligomerization, and disaggregation is largely complete by 3 hours (**Figure 4.4D, E, J, K**). By 24 hours, each molecule was successful in completely removing higher order oligomers and reducing TDP-43 to primarily its monomeric and dimeric state (**Figure 4.4C, F, I, L)**. Interestingly, none of the inhibitors were observed to form complexes with TDP-43, suggesting a short-lived, weak interaction.

AFM recovery experiments with AC0102 result in greatly reduced fibril density at all observed time points (**Figure 4.5A-C**). One explanation could be that AC0102 is actively breaking down fibrils. This seems unlikely, however, as the fibrils that remain have no

discernable change in morphology with remaining fibrils indicate no change in height relative to unmodulated TDP-43 self-aggregation (**Figure 4.6A-D**), and no fibril fragments are observable. More likely is that AC0102 is facilitating fibril sedimentation, although no direct evidence was observed to suggest a mechanism. The lack of observed inhibitor-TDP-43 complexes suggests that AC0102 is not directly binding to fibrils. One possibility is that AC0102 increases the association of fibrils, leading to larger structures with decreased solubility.

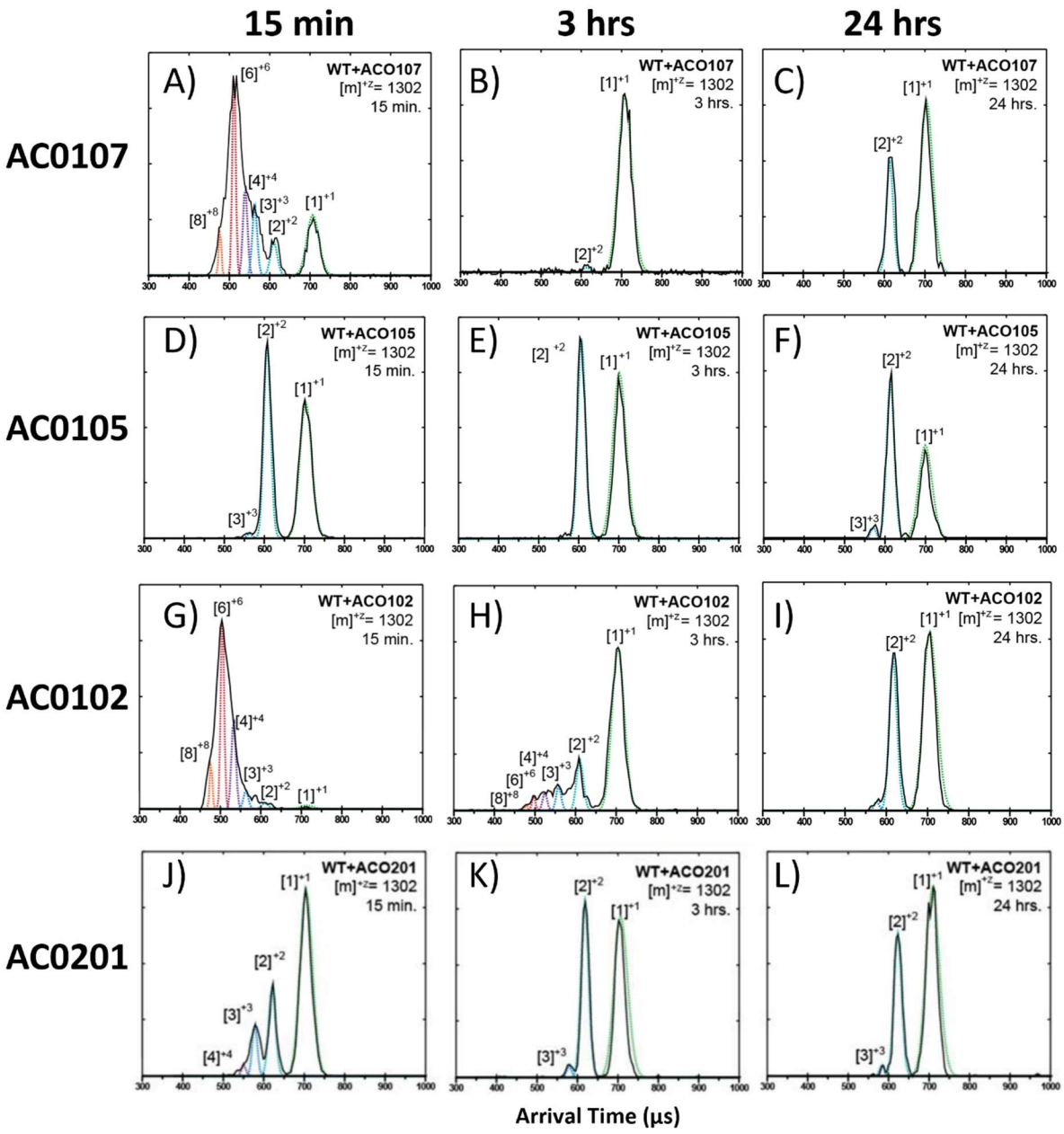

Figure 4.4 ATDs of the co-incubation of WT TDP-43 with the small molecule inhibitor AC0107 (A-C) AC0105 (D-F), AC0102 (G-I), and AC0201 (J-K). Both AC0107 and AC0102 exhibit an initial increase in oligomerization upon addition of the inhibitors. All inhibitors are observed to reduce TDP-43 to primarily monomer and dimer by 24 hours. All experiments performed by Dr. Veronica Laos.[40]

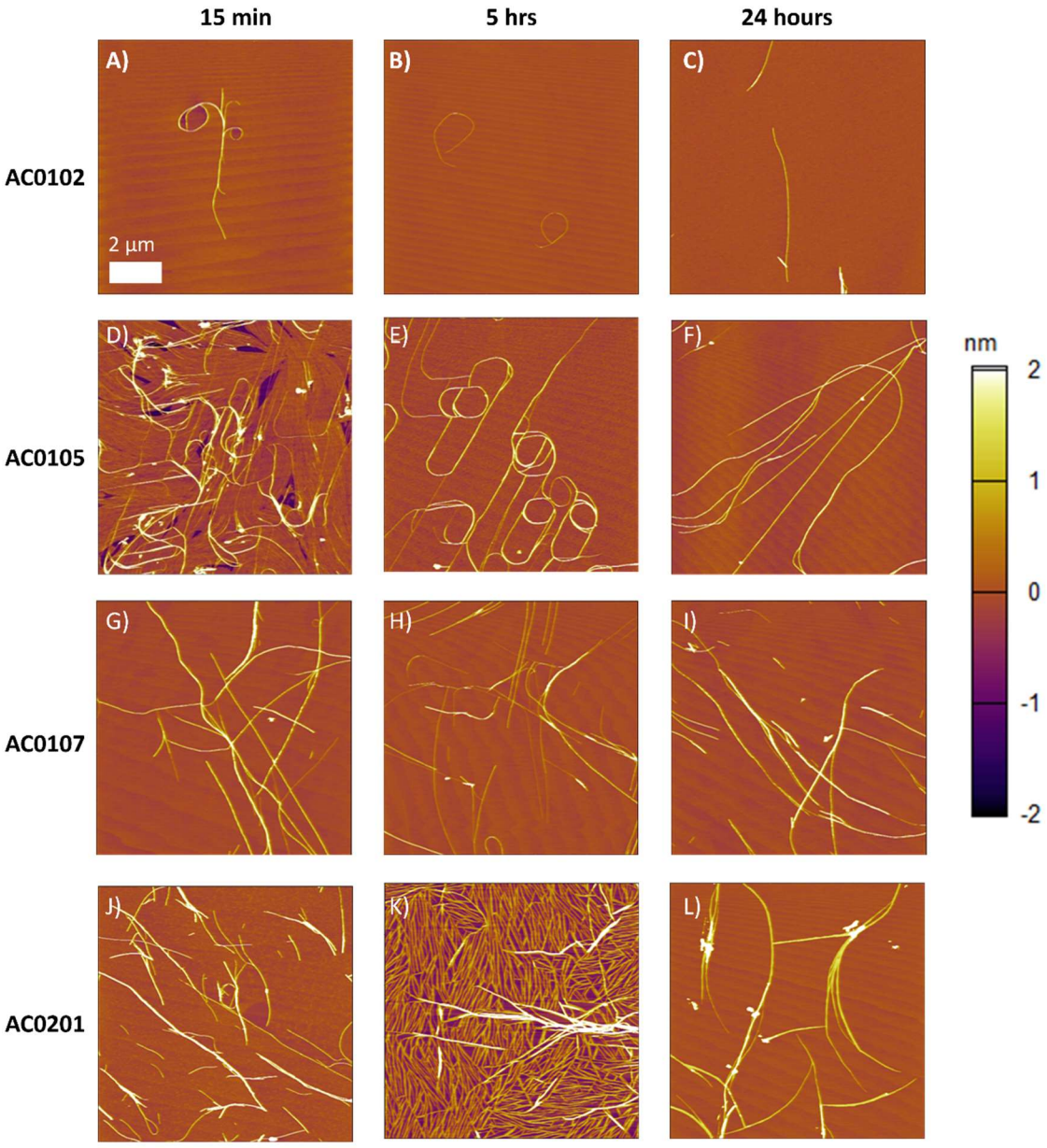

Figure 4.5 Aggregated WT TDP-43 modulated by JPS small molecule inhibitors. WT-TDP-43 was incubated for 4 hours to form high order oligomers, after which an inhibitor was added in a 1:1 mole ratio. AC0102 demonstrates reduced fibril density (A-C). AC0105 (D-F) and AC0107 (G-H) are not significantly different from unmodulated aggregation. AC0201 is largely similar to unmodulated aggregation but demonstrates a change in the background peptide film at 5 hours (J-L).

AC0105, AC0107, and AC0201 were not observed to significantly reduce fibril density over the course of 24 hours in recovery experiments (**Figure 4.5D-L**). Additionally, fibrils in all experiments have consistent height profiles of 2 nm increments consistent with unmodulated TDP-43 self-aggregation (**Figure 4.6C-J**) and no morphological changes were observed. This is not necessarily a surprising result, as previous work with TDP-43 indicated that higher order oligomers are off pathway from fibril formation. This indicates some level of specificity in the protein-protein interactions that the inhibitors disrupt. AC0105 and AC0107 did not have a noticeable effect on observed aggregation (**Figure 4.5D-I**). AC0201 displays a transient change in the background peptide film (**Figure 4.5K**), but fibril density appears unchanged (**Figure 4.5J-L**). While it should be cautioned that variations of the peptide film can occasionally be observed in WT TDP-43 self-aggregation, it is possible that the rapid disaggregation of higher order oligomers facilitates organization into larger structures as a result of an increased concentration of lower order oligomers.

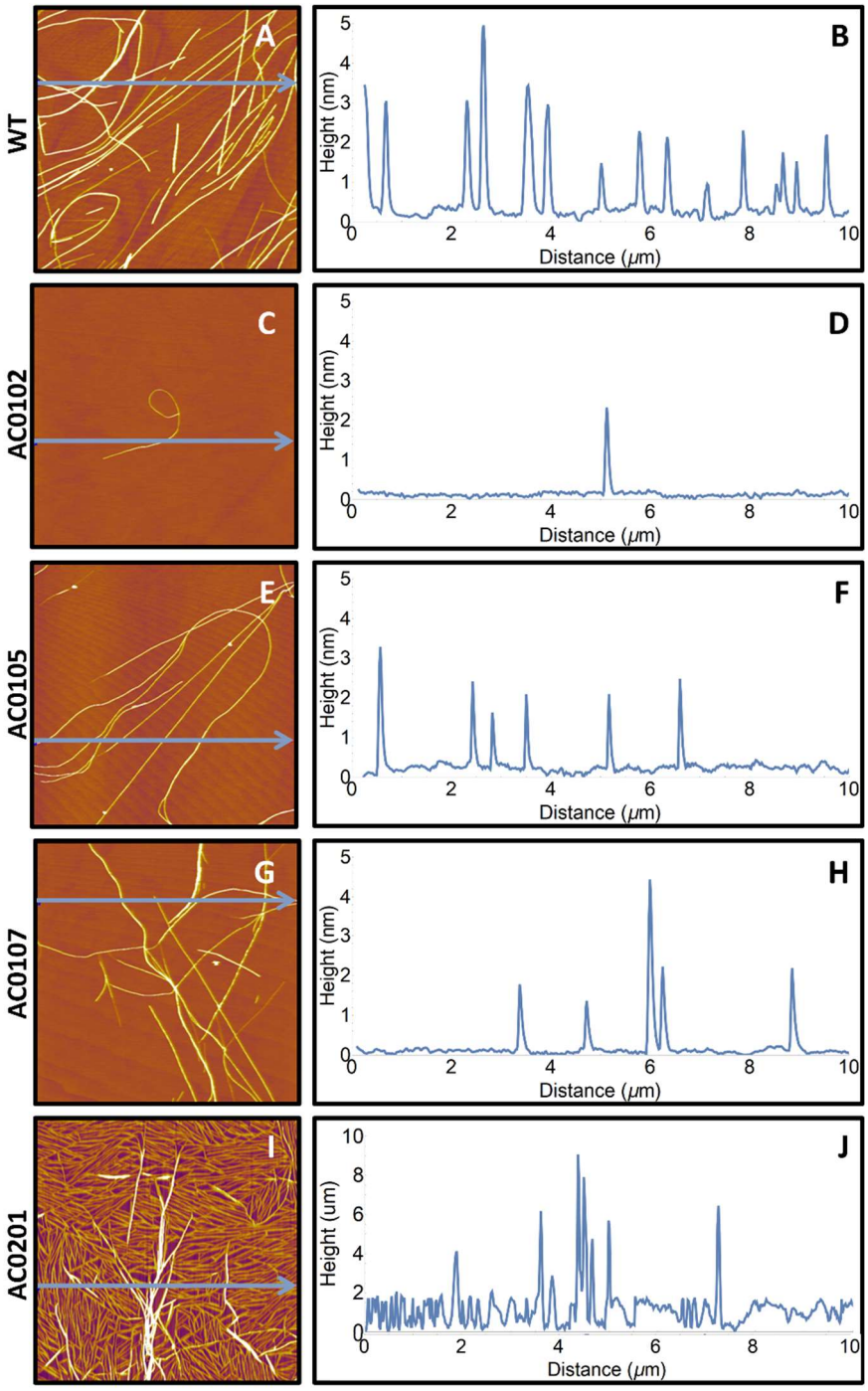

Figure 4.6 Line cuts of (A, B) WT TDP-43 and recovery experiments with WT TDP-43 and (C, D) AC0102, AC0105, AC0107, and AC0201. WT TDP-43 was incubated for 4 hours before adding inhibitor molecules. All line cuts show fibrils with heights in approximately 2 nm increments.

4.3B Coincubation

In addition to recovery experiments, AC0107 was also co-incubated with TDP-43. TDP-43 was allowed to fully dissolve in ammonium acetate, pH7.4, with 2% HFIP over 15 minutes, after which a 1:1 ratio of AC0107 was added to the solution. Upon initial addition of AC0107, IM-MS ATDs demonstrate a notable increase in higher order oligomers after 15 minutes, with both the octamer and hexamer presenting before they did in the control experiment. The distribution has begun to shift back toward lower order oligomers by 1 hour with the depletion of the octamer peak, and by two hours only monomer and dimer are present in solution. The ratio of dimer to monomer continues to decrease through 4 hours (**Figure 4.7**).

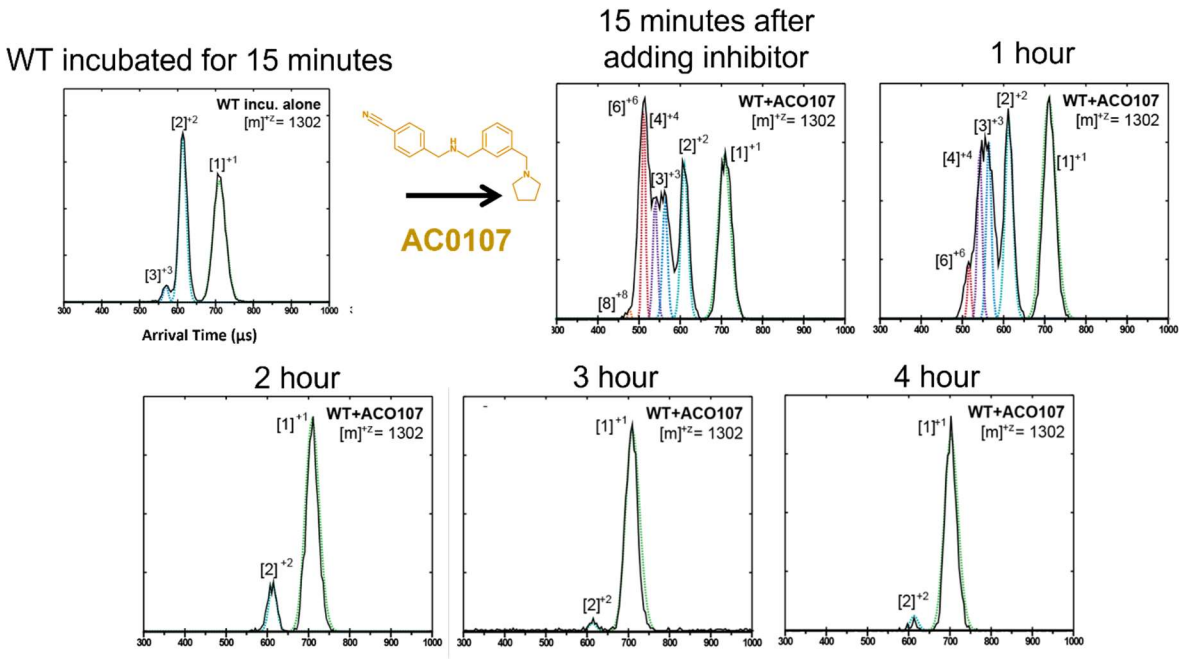

Figure 4.7 IM-MS ATDs of WT TDP-43 co-incubated with AC0107. 15 minutes adding AC0107 shows an increase in higher order oligomers, including the hexamer and octamer. The populations of these species begin to fall at 1 hour. By 2 hours only dimer

and monomer remain, and the dimer peak continues to shrink through 4 hours. All experiments performed by Dr. Veronica Laos.[40]

AFM imaging shows that through 1 hour after adding AC0107 fibril density remains considerably lower than the control experiment. Interestingly, this coincides with the presence of higher order oligomers, and may be a result of oligomerization that is off pathway from fibril formation. By 3 hours, fibril density has begun to increase, correlating with the depletion of higher order oligomers. By 5 hours, significant fibrilization is observed, far surpassing what is typically observed in control experiments. Concurring with this observation, observed fibril density after 24 hours is greatly decrease (**Figure 4.8**). This would be the expected result under the accelerated rates of sedimentation which would be expected under accelerated rates of fibril formation.

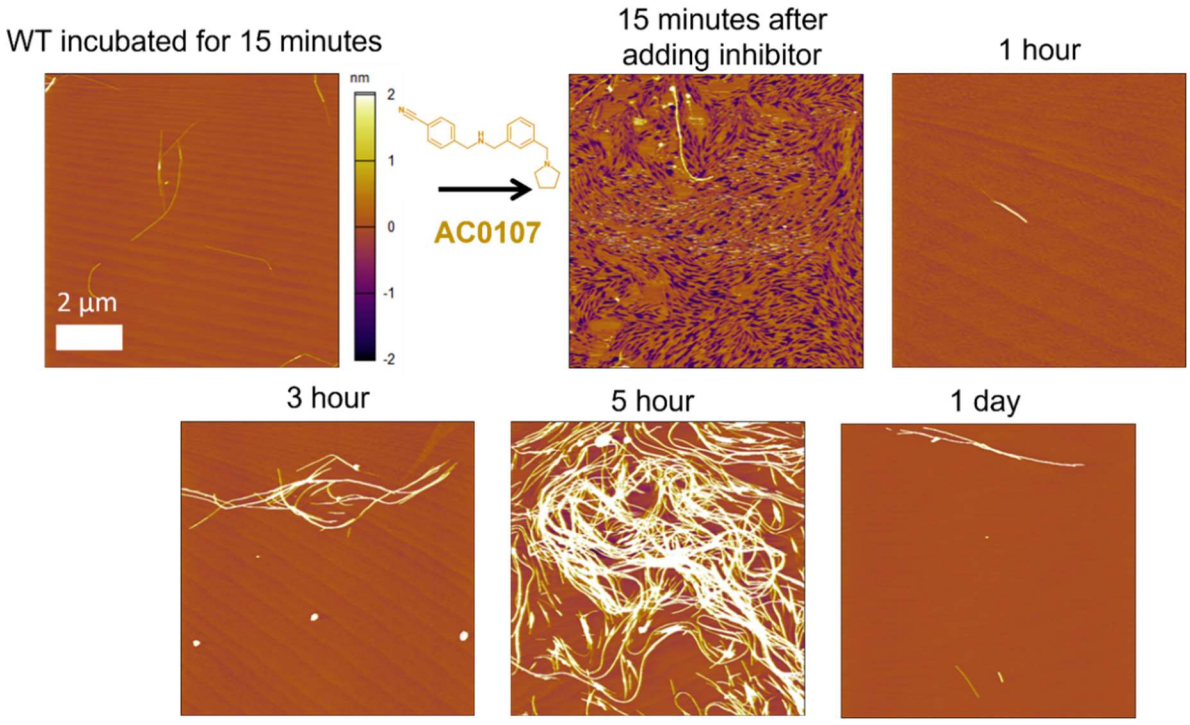

Figure 4.8 AFM height images of WT TDP-43 co-incubated with AC0107. 15 minutes and 1 hour after adding AC0107 demonstrate reduced fibril formation compared with

WT TDP-43 self-aggregation. Fibril density begins to increase at 3 hours and is significantly higher than WT TDP-43 self-aggregation at 5 hours. By 1 day fibril dentistry is greatly reduced due to sedimentation.

While AC0107 was quite effective at reducing TDP-43 to its monomeric state after an initial increase in higher order oligomers, it appears to have the opposite effect on fibrils. This may not be a direct effect of the inhibitor. Rather, this can be explained under the mechanistic assumption that monomeric TDP-43 is necessary for the formation of fibrils. By disrupting the formation of higher order oligomers, the population of monomers is significantly higher than would be observed in the control experiment. As there is no longer a bifurcated aggregation pathway depleting monomers, fibrilization is greatly enhanced.

4.4 Conclusion

Four JPS generated inhibitor molecules, AC0102, AC0105, AC0107, and AC0201, were shown to significantly modulate the oligomerization of TDP-43 without having a clear impact on fibrilization. All inhibitors were shown to eliminate higher order oligomers believed to be disease-related in recovery experiments, with AC0105 and AC0201 doing so on the shortest time scale. Interestingly, no inhibitor was shown to affect fibril morphology, and coincubation experiments show that AC0107 does not prevent fibril formation. This supports the previous conclusion that fibril formation is off-pathway from oligomerization. Additionally, a failure to impact fibril structures may not reduce these inhibitors' therapeutic appeal. Research strongly suggests that oligomers are the toxic agent in neurodegenerative diseases such as those associated with TDP-43, and fibrils are relatively nontoxic.[8-11]

One potential inference from these results is that the intermolecular interactions between individual TDP-43 peptides are different for oligomers and fibrils. In their work

describing the cylindrin, Eisenberg et al note that the cylindrin is constructed of out-of-register beta sheets which are atypical of fibrils, making conversion between the two structures energetically unfavorable.[33] As the hexamer of TDP-43 has been shown to be compatible with the cylindrin beta barrel motif,[34] one possible explanation for the selectivity of the inhibitors studied here is that they are interacting with out-of-register beta sheets. Another possibility is that oligomers and fibrils may differ between parallel or antiparallel beta sheets.

While the exact reason these inhibitors modulate oligomers while fibrils are unchanged remains to be elucidated, these experiments suggest that the inhibitors act with some measure of selectivity. While the inhibitors have been shown to act on several different disease-related proteins, it is important that they don't interfere with all forms of oligomerization. Many proteins exist as oligomers in their native state and disrupting functional complexes could have negative effects that outweigh therapeutic benefits. These experiments indicate that the inhibitors do not disrupt all forms of aggregation.

In summary, the work here demonstrates that the JSP machine learning algorithm has generated four inhibitor molecules that selectively disrupt the higher order oligomerization of TDP-43 without interfering with fibrilization. Further work including in vivo studies must be done to determine the full efficacy and safety of these and other JPS inhibitors, but the JPS methodology promises to be an exciting new development in the search for therapeutic agents targeting neurodegenerative diseases and beyond.

4.5 References

1. Neumann M.; Sampathu D.M.; Kwong L.K.; Truax A.C.; Micsenyi M. C.;, Chou T.T.; Bruce J.; Schuck T.; Grossman M.; Clark C. M.; McCluskey L.F.; Miller B. L.; Masliah E.; Mackenzie I. R.; Feldman H.; Feiden W.; Kretzschmar H.A.;

Trojanowski J.Q.; Lee V.M. Ubiquitinated TDP-43 in frontotemporal lobar degeneration and amyotrophic lateral sclerosis. *Science*. **2006,** *314* (5796), 130-3.

2. Arai T.; Hasegawa M.; Akiyama H,; Ikeda K.; Nonaka T.; Mori H.; Mann D.; Tsuchiya K.; Yoshida M.; Hashizume Y.; Oda T. TDP-43 is a component of ubiquitin-positive tau-negative inclusions in frontotemporal lobar degeneration and amyotrophic lateral sclerosis. *Biochem. Biophys. Res. Commun.* **2006,** *351* (3), 602-11.
3. Josephs, K. A.; Whitwell, J. L.; Weigand, S. D.; Murray, M. E.; Tosakulwong, N.; Liesinger, A. M.; Petrucelli, L.; Senjem, M. L.; Knopman, D. S.; Boeve, B. F.; Ivnik, R. J.; Smith, G. E.; Jack, C. R.; Parisi, J. E.; Petersen, R. C.; Dickson, D. W. TDP-43 is a key player in the clinical features associated with Alzheimer's disease. *Acta. Neuropathol.* **2014**, *127* (6), 811−824.
4. Josephs, K. A.; Murray, M. E.; Whitwell, J. L.; Parisi, J. E.; Petrucelli, L.; Jack, C. R.; Petersen, R. C.; Dickson, D. W. Staging TDP-43 pathology in Alzheimer's disease. *Acta. Neuropathol.* **2014**, *127* (3), 441−450.
5. Jo, M.; Lee, S.; Jean, Y.-M.; Kim, S.; Kwon, Y.; Kim, H.-J. The Role of TDP-43 propagation in neurodegenerative diseases: Integrating insights from clinical and experimental studies. *Exp. Mol. Med.* **2020**, *52*, 1652−1662.
6. Huang, W.; Zhou, Y.; Tu, L.; Ba, Z.; Huang, J.; Huang, N.; Luo, Y. TDP-43: From Alzheimer's disease to limbic-predominant age-related TDP-43 encephalopathy. *Front. Mol. Neurosci.* **2020**, *13*, 1−7.
7. Shih, Y.-S.; Tu, L.-H.; Chang, T.-Y.; Ganesan, K.; Chang, W.-W.; Chang, P.-S.; fang, Y.-S.; Lin, Y.-T.; Jin, L.-W.; Chen, Y.-R. TDP-43 interacts with amyloid-beta, inhibits fibrillization, and worsens pathology in a model of Alzheimer's disease. *Nat. Commun.* **2020**, *11*, 5950−5965.
8. Fang, Y.-S., Tsai, K.-J., Chang, Y.-J., Kao, P., Woods, R., Kuo, P.-H., Wu, C.-C., Liao, J.-Y., Chou, S.-C., Lin, V., Jin, L.-W., Yuan, H. S., Cheng, I. H., Tu, P.-H., and Chen, Y.-R. Full-length TDP-43 forms toxic amyloid oligomers that are present in frontotemporal lobar dementia-TDP patients. *Nat. Commun.* **2014**, *5*, 4824.
9. Glabe, C. G. Common mechanisms of amyloid oligomer pathogenesis in degenerative disease. *Neurobiol. Aging.* **2006,** *27*, 570−575.

10. Lesne, S. E.; Sherman, M. A.; Grant, M.; Kuskowski, M.; Schneider, J. A.; Bennett, D. A.; Ashe, K. Brain Amyloid-β oligomers in ageing and Alzheimer's disease. *Brain* **2013**, *136*, 1383−1398.
11. Sakono, M.; Zako, T. Amyloid oligomers: Formation and toxicity of Abeta oligomers. *FEBS J.* **2010**, *277*, 1348−1358.
12. Pereira, D. A.; Williams, J. A. Origin and Evolution of High Throughput Screening. *Br. J. Pharmacol.* **2007**, *152*, 53-61.
13. Ranu, S.; Singh, A. K. Novel Method for Pharmacophore Analysis by Examining the Joint Pharmacophore Space. *J. Chem. Inf. Model.* **2011**, *51* (5), 1106-1121.
14. Lang, C. A.; Ray, S. S.; Liu, M.; Singh, A. K.; and Cuny, G. D. Discovery of LRRK2 Inhibitors Using Sequential in Silico Joint Pharmacophore Space (JPS) and Ensemble Docking. *Bioorg. Med. Chem. Lett.* **2015**, *25* (13), 2713−2719.
15. Downey, M. A.; Giammona, M. J.; Lang, C. A.; Buratto, S. K.; Singh, A.; Bowers, M. T. Inhibiting and Remodeling Toxic Amyloid-Beta Oligomer Formation Using a Computationally Designed Drug Molecule That Targets Alzheimer's Disease. *J. Am. Soc. Mass Spectrom.* **2019**, *30* (1), 85−93.
16. Zhu, L.; Xu, M.; Yang, M.; Yang, Y.; Li, Y.; Deng, J.; Ruan, L.; Liu, J.; Du, S.; Liu, X.; Feng, W.; Fushimi, K.; Bigio, E. H.; Mesulam, M.; Wang, C.; Wu, J. Y. An ALS-mutant TDP-43 neurotoxic peptide adopts an anti-parallel beta-structure and induces TDP-43 redistribution. *Hum. Mol. Genet.* **2014**, *23* (1), 6863−6877.
17. (49) Ryan, T. M., Roberts, B. R., McColl, G., Hare, D. J., Doble, P. A., Li, Q.- X., Lind, M., Roberts, A. M., Mertens, H. D. T., Kirby, N., Pham, C. L. L., Hinds, M. G., Adlard, P. A., Barnham, K. J., Curtain, C. C., and Masters, C. L. (2015) Stabilization of Nontoxic Aβoligomers: Insights into the Mechanism of Action of Hydroxyquinolines in Alzheimer's Disease. J. Neurosci. 35 (7), 2871−2884.
18. Zheng, X.; Liu, D.; Klarner, F.-G.; Schrader, T.; Bitan, G.; and¨Bowers, M. T. Amyloid β Protein Assembly: the Effect of Molecular Tweezers CLR01 and CLR03. *J. Phys. Chem. B*. **2015,** *119* (14), 4831−4841.
19. Lee, S.; Zheng, X.; Krishnamoorthy, J.; Savelieff, M. G.; Park, H. M.; Brender, J. R.; Kim, J. H.; Derrick, J. S.; Kochi, A.; Lee, H. J.; Kim, C.; Ramamoorthy, A.; Bowers, M. T.; and Lim, M. H. Rational Design of a Structural Framework with Potential Use

to Develop Chemical Reagents that Target and Modulate Multiple Facets of Alzheimer's Disease. *J. Am. Chem. Soc.* **2014,** *136* (1), 299−310.

20. Zheng, X.; Gessel, M. M.; Wisniewski, M. L.; Viswanathan, K.; Wright, D. L.; Bahr, B. A.; and Bowers, M. T. Z-Phe-aladiazomethylketone (PADK) Disrupts and Remodels Early Oligomer States of the Alzheimer Disease Aβ42 Protein. *J. Biol. Chem.* **2012,***287* (9), 6084−6088.
21. LeVine, H.; Ding, Q.; Walker, J. A.; Voss, R. S.; and AugelliSzafran, C. E. Clioquinol and other Hydroxyquinoline Derivatives Inhibit Aβ(1−42) Oligomer Assembly. *Neurosci. Lett.* **2009,** *465* (1), 99−103.
22. Rammes, G.; Gravius, A.; Ruitenberg, M.; Wegener, N.; Chambon, C.; Sroka-Saidi, K.; Jeggo, R.; Staniaszek, L.; Spanswick, D.; O'Hare, E.; Palmer, P.; Kim, E. M.; Bywalez, W.; Egger, V.; and Parsons, C. G. MRZ99030- A Novel Modulator of Aβ Aggregation: II- Reversal of Aβ Oligomer-induced Deficits in Long-term Potentiation (LTP) and Cognitive Performance in Rats and Mice. *Neuropharmacology*. **2015**, *92*, 170 −182.
23. Arai, T.; Sasaki, D.; Araya, T.; Sato, T.; Sohma, Y.; and Kanai, M. A. Cyclic KLVFF-derived Peptide Aggregation Inhibitor Induces the Formation of Less-toxic Off-pathway Amyloidβ Oligomers. *ChemBioChem*. **2014**, *15* (17), 2577 −2583.
24. Hayden, E. Y.; Yamin, G.; Beroukhim, S.; Chen, B.; Kibalchenko, M.; Jiang, L.; Ho, L.; Wang, J.; Pasinetti, G. M.; and Teplow, D. B. Inhibiting Amyloid β-protein Assembly: Sizeactivity Relationships Among Grape Seed-derived Polyphenols. *J. Neurochem*. **2015,** *135* (2), 416 −430.
25. Taylor, M.; Moore, S.; Mayes, J.; Parkin, E.; Beeg, M.; Canovi, M.; Gobbi, M.; Mann, D. M.; and Allsop, D. Development of a Proteolytically Stable Retro-inverso Peptide Inhibitor of β-amyloid Oligomerization as a Potential Novel Treatment for Alzheimer's Disease. *Biochemistry.* **2010,** *49* (15), 3261 −3272.
26. Yamin, G.; Ruchala, P.; and Teplow, D. B. A Peptide Hairpin Inhibitor of Amyloid β-protein Oligomerization and Fibrillogenesis. *Biochemistry*. **2009,** *48* (48), 11329−11331.
27. Yang, F.; Lim, G. P.; Begum, A. N.; Ubeda, O. J.; Simmons, M. R.; Ambegaokar, S. S.; Chen, P. P.; Kayed, R.; Glabe, C. G.; Frautschy, S. A.; and Cole, G. M. Curcumin

Inhibits Formation of Amyloid β Oligomers and Fibrils, Binds Plaques, and Reduces Amyloid in vivo. *J. Biol. Chem.* **2005,** *280* (7), 5892 −5901.

28. Irwin, J. J.; and Shoichet, B. K. ZINC- A Free Database of Commercially Available Compounds for Virtual Screening. *J. Chem. Inf. Model.* **2005**, *45* (1), 177 −182.
29. Izzo, N. J.; Staniszewski, A.; To, L.; Fa, M.; Teich, A. F.; Saeed, F.; Wostein, H.; Walko, T., III; Vaswani, A.; Wardius, M.; Syed, Z.; Ravenscroft, J.; Mozzoni, K.; Silky, C.; Rehak, C.; Yurko, R.; Finn, P.; Look, G.; Rishton, G.; Safferstein, H.; Miller, M.; Johanson, C.; Stopa, E.; Windisch, M.; Hutter-Paier, B.; Shamloo, M.; Arancio, O.; LeVine, H., III; and Catalano, S. M. Alzheimer 's Therapeutics Targeting Amyloid Beta 1 −42 Oligomers I: Abeta 42 Oligomer Binding to Specific Neuronal Receptors is Displaced by Drug Candidates That Improve Cognitive Deficits. *PLoS One*. **2014,** *9* (11), No. e111898.
30. Izzo, N. J.; Xu, J.; Zeng, C.; Kirk, M. J.; Mozzoni, K.; Silky, C.; Rehak, C.; Yurko, R.; Look, G.; Rishton, G.; Safferstein, H.; Cruchaga, C.; Goate, A.; Cahill, M. A.; Arancio, O.; Mach, R. H.; Craven, R.; Head, E.; LeVine, H., III; Spires-Jones, T. L.; and Catalano, S. M. Alzheimer 's Therapeutics Targeting Amyloid Beta 1 −42 oligomers II: Sigma-2/PGRMC1 Receptors Mediate Abeta 42 Oligomer Binding and Synaptotoxicity. *PLoS One.* **2014,** *9* (11), No. e111899
31. Wyttenbach, T.; Kemper, P. R.; and Bowers, M. T. Design of a new electrospray ion mobility mass spectrometer. *Int. J. Mass Spectrom.* **2001,** *212* (1−3), 13−23.
32. Laos, V.; Bishop, D.; Lang, A. C.; Marsh, N. M.; Cantrell, K. L.; Buratto, S. K.; Singh, A. K.; Bowers, M. T. Modulating ALS-Related Amyloidogenic TDP-43$_{307-319}$ Oligomeric Aggregation with Computationally Derived Therapeutic Molecules. *Biochemistry*. **2020**, *59* (4), 499-508.
33. Laganowsky, A.; Liu, C.; Sawaya, M. R.; Whitelegge, J. P.; Park, J.; Zhao, M.; Pensalfini, A.; Soriaga, A. B.; Landau, M.; Teng, P. K.; Cascio, D.; Glabe, C.; Eisenberg, D. Atomic view of a toxic amyloid small oligomer. *Science.* **2012**, *335* (6073), 1228−31.
34. Laos, V.; Do, T. D.; Bishop, D.; Jin, Y.; Marsh, N. M.; Quon, B.; Fetters, M.; Cantrell, K. L.; Buratto, S. K.; Bowers, M. T. Characterizing TDP-43(307-319)

Oligomeric Assembly to Elucidate Mechanistic and Structural Implications Involved in the Etiology of ALS. *ACS Chem. Neurosci.* **2019**, *10* (9), 4112−4123.

V. Co-aggregation of TDP-43 and AD-Related Amyloid Beta

5.1 Introduction

Alzheimer's disease (AD) is a neurodegenerative disease and the most common cause of dementia. An estimated 50 million people worldwide have AD, including 6 million in the United States where it is the 7th leading cause of death. Like other neurodegenerative disease, no cure or disease modifying drugs currently exist. AD typically has an onset of at least 65 years of age, with increased age positively correlated with an increased likelihood of developing the disease. Due to an aging population, AD cases are predicted to balloon to 13 million in the United States by the year 2050 absent the advent of effective intervention.[1-3] In addition to the cost of life, AD and other forms of dementia impose a significant financial burden, totaling $321 billion in 2022 in the United States.[4]

Amyloid beta (Aβ) and tau protein aggregates have been the pathological hallmark of AD since its initial characterization. In AD, these proteins are observed to misfold and aggregate into oligomers and fibrils. Large, fibril-rich amyloid plaques and neurofibrillary tangles comprised primarily of Aβ and tau aggregates respectively and were attractive early therapeutic targets for their clear aberrant nature.[5,6] More recent research, however, has shown that these larger structures are not necessarily correlated with AD prognosis.[7] In several systems fibrils have been observed to be relatively non-toxic and instead small soluble oligomers are implicated in disease progression.[21,24] This revelation, however, has thus far been ineffective at inspiring effective drug development.

An interesting new development in the study of AD is that the presence of TAR DNA binding protein of 43 kDa (TDP-43) aggregates is associated with increased cognitive impairment.[8,15] As discussed in previous chapters, TDP-43 is clinically important for its role in amyotrophic lateral sclerosis (ALS) and tau- and alpha synuclein-negative frontotemporal lobar degeneration (FTD-TDP) that are both similarly caused by protein misfolding. [6-7] A recent mouse model study shows that TDP-43 can significantly advance AD pathology by interacting with Aβ. Understanding these interactions may be essential in the development of AD therapeutics.[12]

As discussed in previous chapters, TDP-43(307-319) was identified as the amyloidogenic core or the protein and is both toxic and capable of forming fibrils.[18] It is also located near the C-terminus, and C-terminal fragments are observed to be the main component of TDP-43 aggregates.[17-13] The G314V mutation of this fragment has been shown to be non-toxic and is associated with reduced oligomerization and delayed fibrilization. Aβ(25-35) has similarly been shown to be toxic and aggregate, and is physiologically observable.[22-24] Primary peptide sequences are given in **Table 6.1**.

Peptide	Primary Structure
Aβ	25 G S N K G A I I G L M 35
TDP-43	307 M G G G M N F G A F S I N 319
G314V	307 M G G G M N F V A F S I N 319

Table 5.1 Primary sequences of Aβ(25-35), WT TDP-43(307-319), and TDP-43(307-319) G314V. Hydrophobic residues are highlighted in beige, polar residues are highlighted in green, and positively charged residues are highlighted in grey. Residues that are

shared between the peptides are in red lettering. The G314V mutation at the central glycine (bold lettering) is in magenta lettering.

In this work, atomic force microscopy (AFM) will be used to investigate the impact of co-aggregating TDP-43(307-319) and Aβ(25-35) on early-stage fibril formation and correlated to oligomeric data revealed by ion mobility-mass spectrometry (IM-MS). Studies of WT TDP-43(307-319) reveal significant oligomeric interaction resulting between the two proteins resulting in a rapid increase in toxic species with minimal changes in fibrilization. The G314V mutation of TDP-43(307-319) prevents enhanced oligomerization in co-aggregation but was observed to undergo accelerate fibrilization.

5.2 Experimental Methods

5.2A Peptide Synthesis and Purification

TDP-43(307−319) WT peptide 307[MGGGMNFGAFSIN]319 was synthesized using standard 9-fluorenylmethoxycarbonyl (Fmoc) chemistry using 2-(1H-benzotriazol-1-yl)-1,1,3,3-tetramethyluronium hexafluorophosphate/hydroxybenzotriazole (HBTU/HOBT) manual solid phase peptide synthesis. The peptide was amidated with an Fmoc-Rink Amide resin (Anaspec). The peptide was cleaved from the resin using 94% TFA, 5% triisopropylsilane, and 1% phenol for 2 h at 295 K. The crude peptide was purified by reverse phase high-performance liquid chromatography (RP-HPLC) on a semipreparative C18 column (Phenomenex) using gradients of water [0.1% (v/v) TFA] and acetonitrile [0.1% (v/v) TFA]. The peptide was dissolved in 6 M guanidine hydrochloride (GdnHCl) prior to injection due to its insolubility in water and acetonitrile. The peptide purity was >93% as determined by analytical RP-HPLC. The molecular mass of the peptide was verified by ESI mass spectrometry. Peptide synthesis was performed by Nicole M. Marsh, Brady Quon and

Megan Fetters and overseen by Prof. Kristi Lazar Cantrell (Westmont College, Santa Barbara, CA).

5.2B Ion Mobility-Mass Spectrometry

Ion mobility-mass spectrometry (IM-MS) was used to study oligomerization of TDP-43(307-319) peptides. IM-MS separates species of a specific $[m]^{+z}$ (m = mass, z = charge) with different $[n]^{+z}$ (n = oligomer number) by measuring arrival time distributions (ATDs). Experiments were performed on a home-built ion mobility mass spectrometer consisting of a nano-electrospray ionization source, home-built ion funnel, 4.503 cm-long drift cell, quadrupole mass filter, and conversion dynode and electron multiplier detector. Ions are generated at the source, captured and stored in the ion funnel, and pulsed into the drift cell filled with approximately 3 Torr of helium gas. Ions exiting the drift cell are filtered by the quadrupole mass analyzer and finally reach the detector.[25] All ion mobility experiments were performed by Dr. Veronica Laos (University of California – Santa Barbara, Santa Barbara, CA).

5.2C Atomic Force Microscopy

Atomic force microscopy (AFM) was used to characterize TDP-43(307-319) fibril growth and morphology, and correlate these with oligomeric assembly. Experiments were conducted using an MFP-3D AFM (Asylum Research, Goleta, CA) and Cantilever C on HQ:XSC11/Al BS AFM probes (NanoAndMore USA Corp, Watsonville, CA). Images were acquired in air using repulsive tapping mode. Samples were prepared for imaging by depositing 5 µL of solution on freshly cleaved V1-grade muscovite mica discs (Ted Pella, Edding, CA) and drying in a vacuum desiccator. Samples were visibly dry in approximately 5 minutes but were allowed to dry over-night.

5.3 Results and Discussion

5.3A Ion Mobility-Mass Spectrometry

Ion mobility-mass spectrometry (IM-MS) is a powerful technique for evaluating the soluble phase oligomerization of disease-causing peptides. To prepare WT TDP-43 for coincubation with Aβ(25-35), both peptides were prepared at 100 μM concentrations in 10 mM ammonium acetate, pH 7.4, with 2% HFIP. Peptides were then allowed to incubate for a set amount of time; WT TDP-43 was incubated for 15 minutes and 4 hours to create fresh and aggregated WT TDP-43 respectively, and Aβ(25-35) was incubated for 15 minutes and 1 week to create fresh and aggregated Aβ(25-35) respectively. Mixtures were prepared of fresh WT TDP-43 + fresh Aβ(25-35), fresh WT TDP-43 + aggregated Aβ(25-35), and aggregated WT TDP-43 + fresh Aβ(25-35) by creating a 50:50 mixture of the two corresponding solutions. Final solutions had a total peptide concentration of 100 μM.

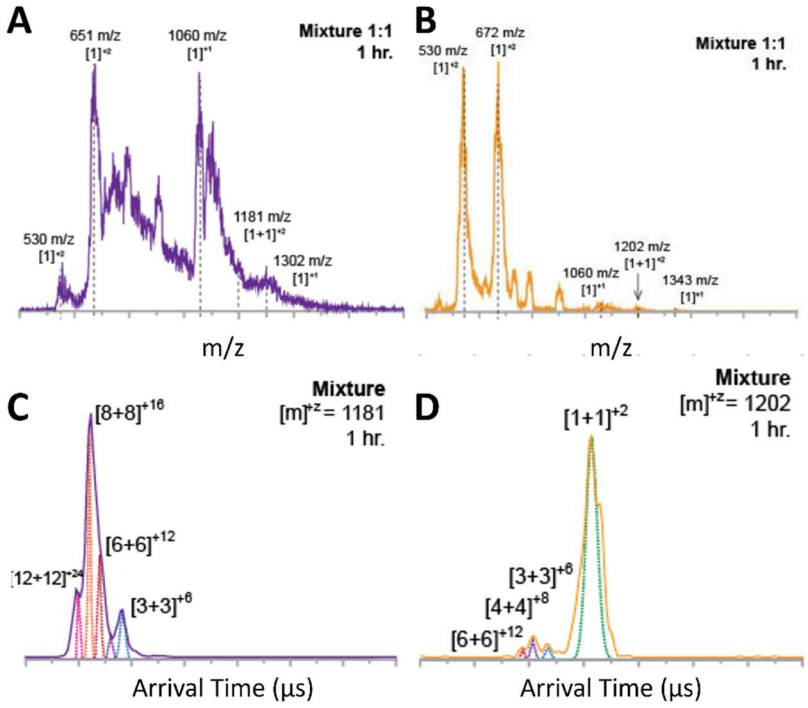

Figure 5.1 Mass spectra and arrival time distributions of TDP-43 and Aβ mixtures. Mass spectra of (A) fresh WT TDP-43(307-319) + fresh Aβ(25-35) and (B) TDP-43(307-319) G314V + fresh Aβ(25-35) at 1 hour. Both mass spectra demonstrate a minor hetero-dimer peak. Arrival time distribution of the heterodimer [1+1]+2 peak of (C) fresh WT TDP-43(307-319) + fresh Aβ(25-35) and (D) TDP-43(307-319) G314V + fresh Aβ(25-35) at 1 hour demonstrate oligomerization. All experiments performed by Dr. Veronica Laos. [26]

MS reveals a hetero-dimer $[1+1]^{+2}$ peak for WT TDP-43(307-319) and Aβ(25-35) (**Figure 6.1A**) with extensive oligomerization observed in the ATD (**Figure 5.1C**). Analysis of the $[1]^{+1}$ peaks of both WT TDP-43(307-319) and Aβ(25-35) also reveals significant changes in oligomer distributions. Following mixing of fresh WT TDP-43(307-319) + fresh Aβ(25-35), both peptides underwent a dramatic shift in population towards higher order oligomers in a short time frame (**Figure 5.2**). Monomer peak intensity falls significantly compared to self-aggregation, indicative of rapid aggregation. Similar results are observed in the co-aggregation of fresh WT TDP-43(307-319) + aggregated Aβ(25-35) (**Figure 5.3**). In self-aggregated Aβ(25-35), the monomer peak remains dominant through 1 week. However, with the addition of TDP-43(307-319) this population is almost completely eliminated. Both these experiments indicate significant transient interactions between WT TDP-43(307-319) and Aβ(25-35) that promote self-aggregation. Interestingly, co-aggregation of aggregated WT TDP-43(307-319) + fresh Aβ(25-35) results in no significant increase in aggregation for Aβ(25-35) and an elimination of higher order oligomers for WT TDP-43(307-319) (**Figure 5.4**). This is likely a result of sequestering WT TDP-43(307-319) in insoluble structures

followed by the two-fold decrease in concentration prescribed by the mixing procedure resulting in a significantly reduced concentration, reducing all forms of aggregation.

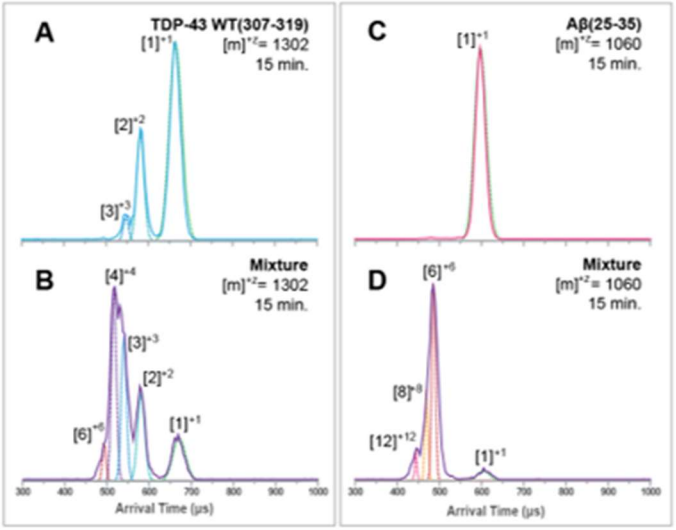

Figure 5.2 ATDs of (A) the $[1]^{+1}$ peak of fresh WT TDP-43(307-319), (B) the $[1]^{+1}$ peak of fresh Aβ(25-35), (C) the $[1]^{+1}$ peak of WT TDP-43 in the 1:1 mixture after 15 minutes, and (D) the $[1]^{+1}$ peak of Aβ(25-35) in the mixture after 15 minutes. The mixture accelerates aggregation for both WT TDP-43(307-319) and Aβ(25-35). All experiments performed by Dr. Veronica Laos. [26]

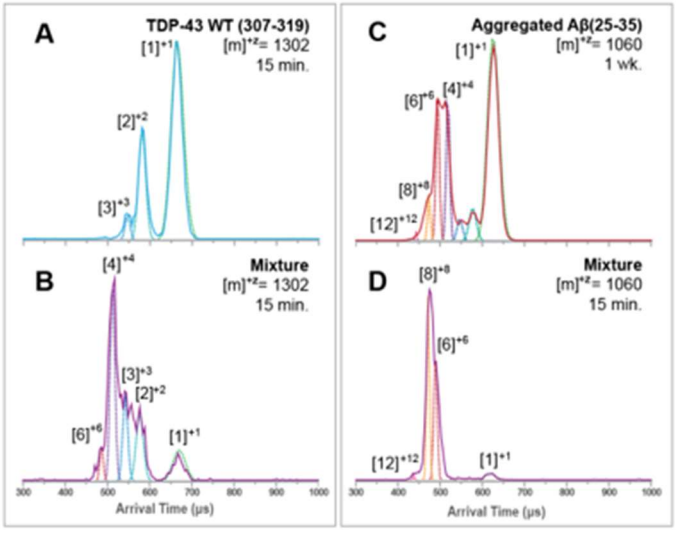

Figure 5.3 ATDs of (A) the $[1]^{+1}$ peak of fresh WT TDP-43(307-319), (B) the $[1]^{+1}$ peak of aggregated Aβ(25-35), (C) the $[1]^{+1}$ peak of TDP-43 in the 1:1 mixture after 15 minutes, and (D) the $[1]^{+1}$ peak of Aβ(25-35) in the mixture after 15 minutes. The mixture accelerates aggregation for WT TDP-43(307-319). All experiments performed by Dr. Veronica Laos.[26]

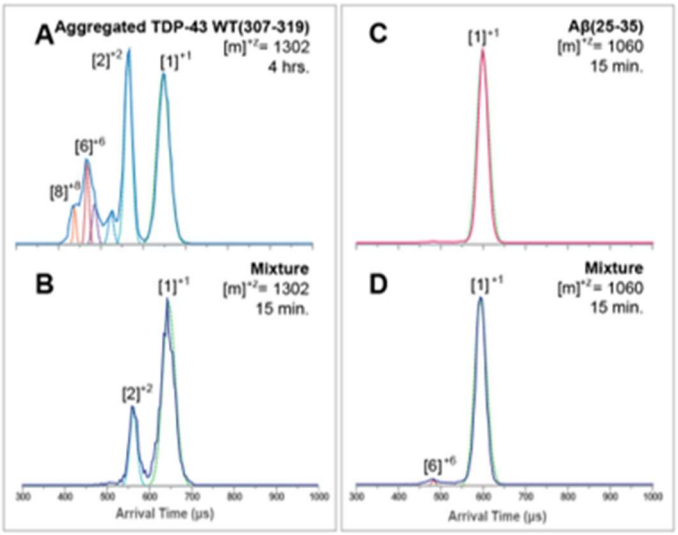

Figure 5.4 ATDs of (A) the $[1]^{+1}$ peak of aggregated WT TDP-43(307-319), (B) the $[1]^{+1}$ peak of fresh Aβ(25-35), (C) the $[1]^{+1}$ peak of WT TDP-43 in the 1:1 mixture after 15 minutes, and (D) the $[1]^{+1}$ peak of Aβ(25-35) in the mixture after 15 minutes. The mixture demonstrates reduced aggregation for WT TDP-43(307-319) and has minimal effect on Aβ(25-35). All experiments performed by Dr. Veronica Laos. [26]

TDP-43 G314V was also co-aggregated with Aβ(25-35). G314V was prepared at 100 μM in a 50:50 mixture of acetonitrile and 10 mM ammonium acetate, pH 7.4, with 1% formic acid. Because G314V never forms higher order oligomers, it was only prepared fresh. Aβ(25-35) was prepared at 100 μM in the same manner as above. Mixtures were prepared of TDP-43 G314V + fresh Aβ(25-35) and TDP-43 G314V + aggregated Aβ(25-35). TDP-43

G314V and Aβ(25-35) were also observed to form a hetero-dimer $[1+1]^{+2}$ MS peak (**Figure 5.1 B**). ATDs show that the G314V mutation significantly reduced but does not completely eliminate oligomerization of the heterodimer (**Figure 5.1 D**). Co-aggregation of TDP-43 G314V + fresh Aβ(25-35) yields similar results to the self-aggregation of these peptides, suggesting minimal interaction between the two peptides (**Figure 5.5**). Similarly, only a moderate shift of Aβ(25-35) away from higher order oligomers is observed in the fresh TDP-43 G314V + aggregated Aβ(25-35) mixture (**Figure 5.6**). This is likely attributable to the two-fold dilution implicit to these experiments. Overall, the G314V mutation was observed to limit oligomeric interaction between TDP-43(307-319) and Aβ(25-35).

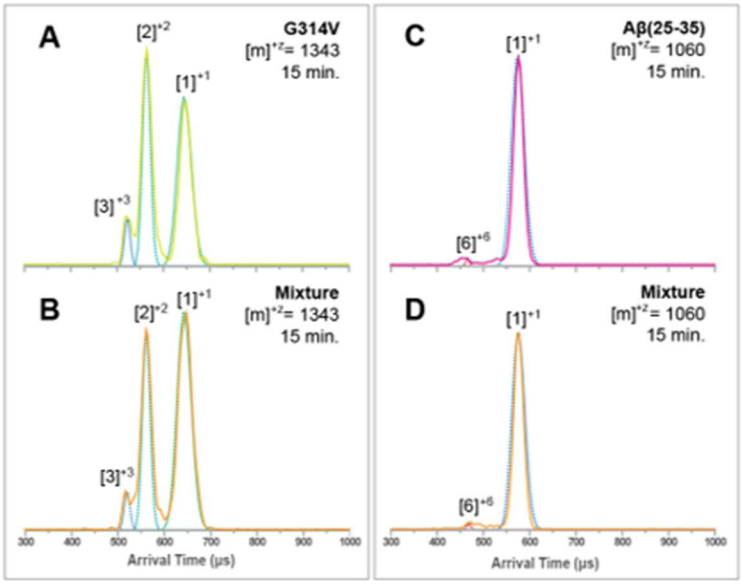

Figure 5.5 ATDs of (A) the $[1]^{+1}$ peak of G314V TDP-43(307-319), (B) the $[1]^{+1}$ peak of fresh Aβ(25-35), (C) the $[1]^{+1}$ peak of WT TDP-43 in the 1:1 mixture after 15 minutes, and (D) the $[1]^{+1}$ peak of Aβ(25-35) in the mixture after 15 minutes. The mixture has a negligible effect on aggregation. All experiments performed by Dr. Veronica Laos. [26]

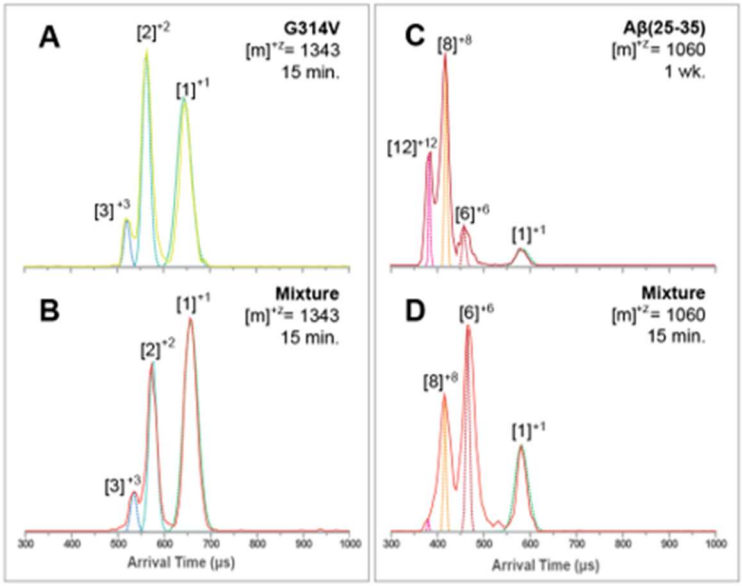

Figure 5.6 ATDs of (A) the $[1]^{+1}$ peak of G314V TDP-43(307-319), (B) the $[1]^{+1}$ peak of aggregated Aβ(25-35), (C) the $[1]^{+1}$ peak of WT TDP-43 in the 1:1 mixture after 15 minutes, and (D) the $[1]^{+1}$ peak of Aβ(25-35) in the mixture after 15 minutes. The mixture has a negligible effect on aggregation. All experiments performed by Dr. Veronica Laos. [26]

5.3B Atomic Force Microscopy

Atomic force microscopy (AFM) complements IM-MS by allowing the presence of soluble oligomers to be correlated with larger insoluble structures such as fibrils. In order to study the co-aggregation of WT TDP-43 and G314V with Aβ(25-35), peptides were first studied independently. The self-aggregation properties of WT TDP-43 and G314V were previously discussed in detail in Chapter 3. WT-TDP-43 was prepared at 100 μM in 10 mM ammonium acetate, pH 7.4, with 2% HFIP and rapidly forms fibrils within 15 minutes of incubation and are observable through 24 hours (**Figure 5.7A, B**). The non-toxic mutant

G314V was prepared at 100 μM in a 50:50 mixture of acetonitrile and 10 mM ammonium acetate, pH 7.4, and 1% formic acid. This mutation is associated with attenuated aggregation that forms fibrils only after several days (**Figure 5.7C-E**). Aβ(25-35) was also prepared at 100 in 10 mM ammonium acetate, pH 7.4, and 2% HFIP and displays less fibrillization than TDP-43. Over 1 week only pre-protofibrillar features are observable with height of approximately 0.2 nm and typically extending no more than 500 nm in length (**Figure 5.7F-H**).

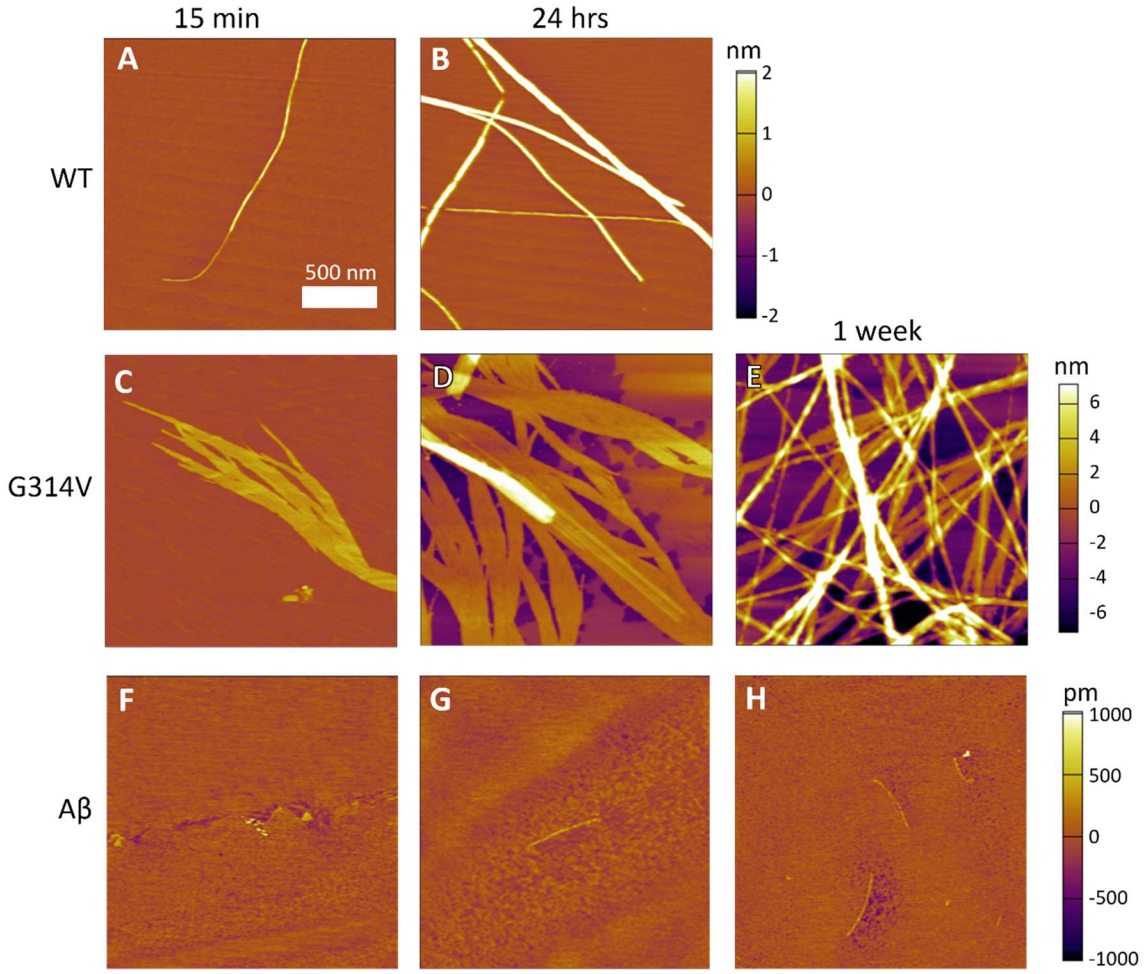

Figure 5.7 Self-aggregation of (A, B) WT TDP-43(307-319), (C-E) TDP-43(307-319) G314V, and (F-H) Aβ(25-35) over the course of 1 week. WT TDP-43(307-319) rapidly

undergoes fibril formation. The G314V mutation inhibits aggregation, delaying the onset of fibril formation. Aβ(25-35) is only ever observed to form short protofibrils. WT TDP-43 is not shown at 1 week because it undergoes extensive sedimentation, such that fibrils are not observable after 48 hours.

Co-aggregation mixtures of TDP-43 and Aβ(25-35) were prepared in the same manner described in the previous section. Mixtures of both fresh WT TDP-43 + fresh Aβ(25-35) and fresh WT TDP-43 + aggregated Aβ(25-35) produced very similar results. Fibril formation is in its early stages 15 minutes after mixing (**Figure 5.8A, D**) and fully formed fibrils are observable at 3 hours (**Figure 5.8B, E**) and 24 hours (**Figure 5.8C, F**). These fibrils appear morphologically consistent with WT TDP-43 self-aggregation. This fibril formation occurs despite a relatively low population of monomers. Given the bifurcated pathway between oligomerization and fibrilization, it's possible that Aβ(25-35) is also facilitating fibril formation in some capacity. The initial aggregation state of Aβ(25-35) did not have a noticeable effect on observable features. Considering fresh WT TDP-43(307-319) induces rapid aggregation on Aβ(25-35), it is not surprising that these two experiments yielded similar results.

The mixture of aggregated WT TDP-43 + fresh Aβ(25-35) yielded low fibril densities at 15 minutes and 3 hours (**Figure 5.8G, H**), while no fibrils were observable at 24 hours (**Figure 5.8I**). This is likely due to a reduced effective concentration of WT TDP-43. It has been established in self-aggregation experiments that TDP-43 undergoes sedimentation, to the point where after 48 hours fibrils are not readily observable. This should mean that at some concentration fibrilization is not occurring at an observable rate. Excluding the effect of Aβ(25-35) on aggregation, then the mixture is essentially a twofold dilution of TDP-43 that

has been aggregated for 4 hours over which sedimentation has been occurring. The concentration of WT TDP-43 in solution would then be lower than the advertised 50 μM.

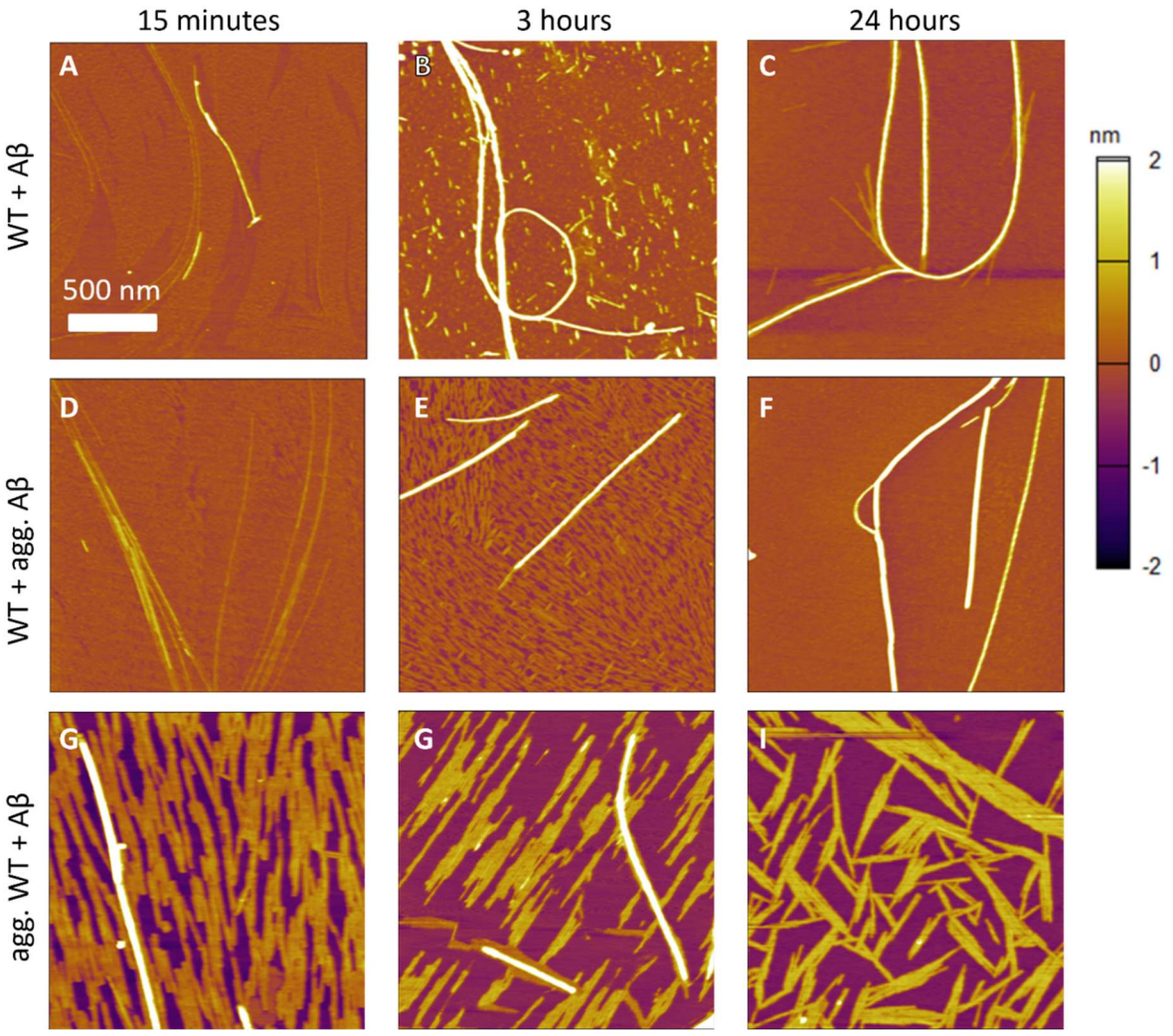

Figure 5.8 AFM co-aggregation experiments between (A-C) fresh WT TDP-43(307-319) + fresh Aβ(25-35) (D-F) fresh WT TDP-43(307-319) + aggregated Aβ(25-35), and (G-I) aggregated WT TDP-43(307-319) + fresh Aβ(25-35). Mixing fresh WT TDP-43(307-319) with either aggregated or fresh Aβ(25-35) results in minimal differences from WT TDP-

43(307-319) self-aggregation. The aggregated WT TDP-43(307-319) + fresh Aβ(25-35) mixture returns reduced fibril density.

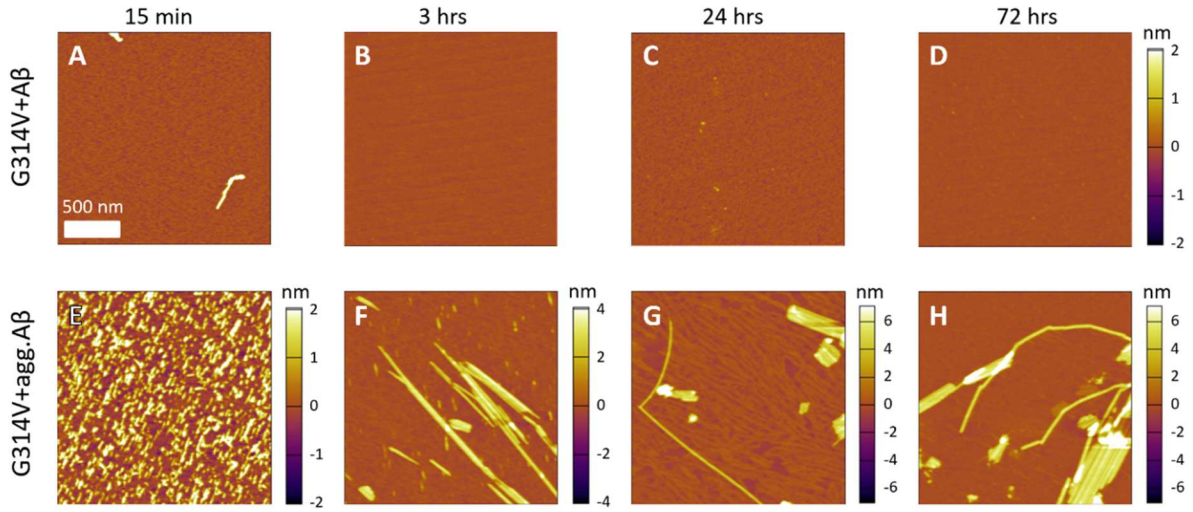

Figure 5.9 AFM co-aggregation experiments between (A-D) TDP-43(307-319) G314V+ fresh Aβ(25-35) and (E-H) TDP-43(307-319) G314V + aggregated Aβ(25-35. Mixing TDP-43(307-319) G314V with fresh Aβ(25-35) does not result in observable features, while TDP-43(307-319) G314V with aggregated Aβ(25-35) results in an increased rate of fibril formation.

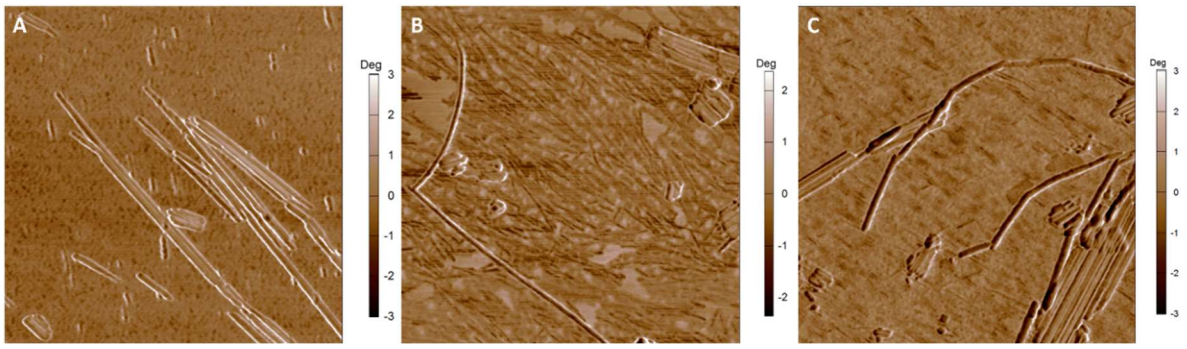

Figure 5.10 AFM repulsive mode phase images of TDP-43(307-319) G314V co-aggregated with aggregated Aβ(25-35) after (A) 3 hours, (B) 24 hours, and (c) 72 hours. Lower phases are associated with harder features, while higher phases are associated with softer features. Early features have a similar phase as the background peptide film, suggesting non-fibrillar features. Fibrils observed at 24 and 72 hours both have a lower phase than the background, indicative of beta sheet formation.

Co-aggregation of TDP-43(307-319) G314V + fresh Aβ(25-35) yielded no observable aggregation over the course of 72 hours (**Figure 5.9A-D**). Considering the decrease in concentration relative to self-aggregation studies, this is consistent with monomeric Aβ(25-35) having no effect on TDP-43(307-319) G314V aggregation. In stark contrast, several types of features were observable in the co-aggregation of TDP-43(307-319) G314V + aggregated Aβ(25-35). Non-discreet, amorphous aggregates are primarily observed at early time points (**Figure 5.9E**). By three hours, non-fibrillar aggregates have formed (**Figure 5.9F**). Phase analysis shows that these aggregates have a similar hardness to the background peptide film, suggesting minimal beta sheet formation (**Figure 5.10A**). By comparison, additional features observed at 24 hours and 72 hours appear to be fibrillar in nature (**Figure 5.9G, H**). The phase of these features is notably lower than both the background and non-fibrillar features, indicative of beta sheet-rich fibrils (**Figure 5.10B, C**). Interestingly, these fibrils were observed at earlier time points than TDP-43(307-319) G314V fibrils were observed in self-aggregation and lack the characteristic ribbon twist. This suggests that Aβ(25-35) is both promoting and modulating TDP-43(307-319) G314V fibrilization. The alternative that TDP-43(307-319) G314V is inducing fibril formation in

Aβ(25-35) is unlikely given that it was never observed to form large fibrils in self-aggregation experiments.

5.4 Conclusion

Abnormal TDP-43 aggregation has been associated with more sever cognitive decline in AD, a disease typically associated with Aβ aggregation.[8-15,12] The presented work uses IM-MS and AFM to demonstrates that these proteins interact on a molecular level. WT TDP-43(307-319) and Aβ(25-35) can promote rapid oligomerization in one another and form hetero-oligomers. Monomeric species were sufficient for this be observed in co-aggregation, and the initial aggregation state of Aβ(25-35) did not have an effect. Pre-aggregated WT TDP-43(307-31) was shown not to promote aggregation in Aβ(25-35) and was itself reduced to lower order oligomers upon co-aggregation. This is likely an effect of WT TDP-43(307-31) forming insoluble aggregates such as fibrils that reduce the effective concentration in solution that can interact with Aβ(25-35).

Fibril formation in the co-aggregation of WT TDP-43(307-319) and Aβ(25-35) was consistent with WT TDP-43(307-319) self-aggregation. There was insufficient evidence to conclusively say that Aβ(25-35) significantly alters the fibrilization process for WT TDP-43(307-319). Interestingly, however, aggregated Aβ(25-35) promoted fibrilization when co-aggregated with TDP-43(307-319) G314V without noticeably effecting the oligomer distribution. This observation suggests that Aβ(25-35) may have an impact on WT TDP-43(307-319) fibrilization that was not observable under the utilized experimental conditions. Because the G314V mutation significantly retards fibrilization, changes in the onset of fibril formation are relatively easy to observe. WT TDP-43(307-319) aggregates much more rapidly, and as such variations may not have been captured in these experiments. More

quantitative secondary structure analysis could be useful in elucidating potential changes in fibril density.

In summary, TDP-43 and Aβ were observed to significantly upregulate each other's aggregation. This implies such cross talk may play an important role in AD progression. Given the similar mechanisms of many neurodegenerative diseases, this also suggests that this type of protein-protein interaction may be more widespread. Consideration must be given to these interactions in the development of potential therapeutic agents. The inhibitor molecules addressed in Chapter 4 will require additional study to prove they can compete with aggregation inducing Aβ.

5.5 References

1. Alzheimer's Disease International. 2018. *World Alzheimer's Report 2018 – The state of the art dementia research: New Frontiers*. London: Alzheimer's Disease International.
2. World Health Organization. *Fact Sheets: Dementia*. World Health Organization, September 2021. ://www.who.int/en/news-room/fact-sheets/detail/dementia. (Accessed 2022-09-07).
3. Murphy, S. L.; Kochanek, K.D.; Xu, J. Q.; Arias, E. *Mortality in the United States, 2020.* NCHS Data Brief, no 427. Hyattsville, MD: National Center for Health Statistics. 2021.
4. Alzheimer's Association Report. 2020 Alzheimer's disease facts and figures. *Alzheimers Dement.* **2020**, 16, 391-460.
5. Trejo-Lopez, J. A.; Yachnis, A. T.; Prokop, S. Neuropathology of Alzheimer's Disease. *Neurotherapeutics.* **2022**, *19*, 173–185.
6. Ittner, L. M.; Gotz, J. Amyloid-β and tau – a toxic *pas de deux* in Alzheimer's disease. *Nat. Rev. Neurosci.* **2011**, *12*, 67-72.

7. Tiraboschi, P.; Sabbagh, M. N.; Hansen, L. A.; Salmon, D. P.; Merdes, A.; Gamst, A.; Masliah, E.; Alford, M.; Thal, L. J.; Corey-Bloom, J. *Neurology*. **2004**, *62* (7), 1141-1147.
8. Fang, Y.-S., Tsai, K.-J., Chang, Y.-J., Kao, P., Woods, R., Kuo, P.-H., Wu, C.-C., Liao, J.-Y., Chou, S.-C., Lin, V., Jin, L.-W., Yuan, H. S., Cheng, I. H., Tu, P.-H., and Chen, Y.-R. Full-length TDP-43 forms toxic amyloid oligomers that are present in frontotemporal lobar dementia-TDP patients. *Nat. Commun.* **2014**, *5*, 4824.
9. Glabe, C. G. Common mechanisms of amyloid oligomer pathogenesis in degenerative disease. *Neurobiol. Aging.* **2006,** *27*, 570−575.
10. Lesne, S. E.; Sherman, M. A.; Grant, M.; Kuskowski, M.; Schneider, J. A.; Bennett, D. A.; Ashe, K. Brain Amyloid-β oligomers in ageing and Alzheimer's disease. *Brain* **2013**, *136*, 1383−1398.
11. Sakono, M.; Zako, T. Amyloid oligomers: Formation and toxicity of Abeta oligomers. *FEBS J.* **2010**, *277*, 1348−1358.
12. Josephs, K. A.; Whitwell, J. L.; Weigand, S. D.; Murray, M. E.; Tosakulwong, N.; Liesinger, A. M.; Petrucelli, L.; Senjem, M. L.; Knopman, D. S.; Boeve, B. F.; Ivnik, R. J.; Smith, G. E.; Jack, C. R.; Parisi, J. E.; Petersen, R. C.; Dickson, D. W. TDP-43 is a key player in the clinical features associated with Alzheimer's disease. *Acta. Neuropathol.* **2014**, *127* (6), 811−824.
13. Josephs, K. A.; Murray, M. E.; Whitwell, J. L.; Parisi, J. E.; Petrucelli, L.; Jack, C. R.; Petersen, R. C.; Dickson, D. W. Staging TDP-43 pathology in Alzheimer's disease. *Acta. Neuropathol.* **2014**, *127* (3), 441−450.
14. Jo, M.; Lee, S.; Jean, Y.-M.; Kim, S.; Kwon, Y.; Kim, H.-J. The Role of TDP-43 propagation in neurodegenerative diseases: Integrating insights from clinical and experimental studies. *Exp. Mol. Med.* **2020**, *52*, 1652−1662.
15. Huang, W.; Zhou, Y.; Tu, L.; Ba, Z.; Huang, J.; Huang, N.; Luo, Y. TDP-43: From Alzheimer's disease to limbic-predominant age-related TDP-43 encephalopathy. *Front. Mol. Neurosci.* **2020**, *13*, 1−7.
16. Neumann M.; Sampathu D.M.; Kwong L.K.; Truax A.C.; Micsenyi M. C.;, Chou T.T.; Bruce J.; Schuck T.; Grossman M.; Clark C. M.; McCluskey L.F.; Miller B. L.; Masliah E.; Mackenzie I. R.; Feldman H.; Feiden W.; Kretzschmar H.A.;

Trojanowski J.Q.; Lee V.M. Ubiquitinated TDP-43 in frontotemporal lobar degeneration and amyotrophic lateral sclerosis. *Science*. **2006,** *314* (5796), 130-3.

17. Arai T.; Hasegawa M.; Akiyama H,; Ikeda K.; Nonaka T.; Mori H.; Mann D.; Tsuchiya K.; Yoshida M.; Hashizume Y.; Oda T. TDP-43 is a component of ubiquitin-positive tau-negative inclusions in frontotemporal lobar degeneration and amyotrophic lateral sclerosis. *Biochem. Biophys. Res. Commun.* **2006,** *351* (3), 602-11.
18. Shih, Y.-S.; Tu, L.-H.; Chang, T.-Y.; Ganesan, K.; Chang, W.-W.; Chang, P.-S.; fang, Y.-S.; Lin, Y.-T.; Jin, L.-W.; Chen, Y.-R. TDP-43 interacts with amyloid-beta, inhibits fibrillization, and worsens pathology in a model of Alzheimer's disease. *Nat. Commun.* **2020**, *11*, 5950−5965.
19. Zhu, L.; Xu, M.; Yang, M.; Yang, Y.; Li, Y.; Deng, J.; Ruan, L.; Liu, J.; Du, S.; Liu, X.; Feng, W.; Fushimi, K.; Bigio, E. H.; Mesulam, M.; Wang, C.; Wu, J. Y. An ALS-mutant TDP-43 neurotoxic peptide adopts an anti-parallel beta-structure and induces TDP-43 redistribution. *Hum. Mol. Genet.* **2014**, *23* (1), 6863−6877.
20. Pesiridis G. S.; Lee V. M.; Trojanowski J. Q. Mutations in TDP-43 link glycine-rich domain functions to amyotrophic lateral sclerosis. *Hum. Mol. Genet.* **2009,** *18* (R2), R156-62.
21. de Boer E. M. J.; Orie,V. K.; Williams, T.; Baker, M. R.; De Oliveira, H. M.; Polvikoski, T.; Silsby, M.; Menon, P.; van den Bos, M.; Halliday, G. M.; van den Berg, L. H.; Van Den Bosch, L.; can Damme, P.; Kiernan, M.; van Es, M. A.; Vucic, S. TDP-43 proteinopathies: a new wave of neurodegenerative diseases. *J. Neurol. Neurosurg. Psychiatry.* **2021,** *92,* 86–95.
22. Millucci L.; Ghezzi L.; Bernardini G.; Santucci A. Conformations and Biological Activities of Amyloid Beta Peptide 25-35. *Curr. Protein Pept. Sci.* **2010,** *11* (1), 54-67.
23. Pike, C.J.; Walencewicz-Wasserman, A.J.; Kosmoski, J.; Cribbs, D.H.; Glabe, C.G. and Cotman, C.W. Structure-activity analyses of beta-amyloid peptides: Contributions of the beta 25-35 region to aggregation and neurotoxicity. *J. Neurochem.* **1995**, 64, 253–265.

24. Smith, A.K.; Klimov, D.K. De novo aggregation of Alzheimer's Aβ25-35 peptides in a lipid bilayer. *Sci. Rep.* **2019,** *9*, 7161.
25. Wyttenbach, T.; Kemper, P. R.; and Bowers, M. T. Design of a new electrospray ion mobility mass spectrometer. *Int. J. Mass Spectrom.* **2001,** *212* (1−3), 13−23.
26. Laos V.; Bishop D.; Ganguly P.; Schonfeld, G.; Trapp, E.;Cantrell, K. L.; Buratto, S. K.; Shae, J. E.; Bowers, M. T. Catalytic Cross Talk between Key Peptide Fragments That Couple Alzheimer's Disease with Amyotrophic Lateral Sclerosis. *J. Am. Chem. Soc.* **2021,** *143* (9), 3494-3502.

VI. Self-Aggregation of the fALS-Related Protein SOD1

6.1 Introduction

Amyotrophic lateral sclerosis (ALS) is the most common motor neuron disease, with an estimated prevalence of approximately 5 in 100,000 in the United States.[1,2] It affects both upper and lower motor neurons, resulting in a progressive weakening of muscles that leads to paralysis, respiratory failure, and death. The mean life expectancy following the onset of symptoms is 2-5 years, though some patients may live significantly longer.[3,4] There is no cure for ALS, with current treatment options only improving outlook by a couple months in some patients. As with many neurodegenerative diseases, ALS is associated with the misfolding of protein.

Sporadic ALS (sALS) accounts for approximately 95% of cases, with no known cause. The remaining 5% of cases are inherited familial ALS (fALS), where an identifiable genetic cause can be linked to a family history of the disease.[5] 20% of fALS cases have been linked to mutations in superoxide dismutase 1 (SOD1). In general, ALS can be characterized by the formation of inclusion bodies in the cytoplasm of motor neuron cells. In sALS, the primary component of these inclusion bodies is TAR DNA-binding protein 43 where as in fALS, mutated SOD1 is the main component of theses inclusion bodies.[20-24] Additionally, wild-type (WT) SOD1 is present in smaller quantities in sALS inclusion bodies, with some studies suggesting it may play a toxic role there as well.[25-28]

SOD1 is a 153-residue, 32-kDa enzyme that exists as a homodimer and binds to molecules of copper and zinc to breakdown toxic charged oxygen radicals, essentially converting reactive oxygen into water.[13] Since its discovery more than 170 different mutations on this 153-residue long protein have been linked to fALS.[14] Many of these ALS-

related mutations retain their normal enzymatic activity, which suggests that a toxic gain in function as opposed to a loss of native function is responsible for the overall toxicity.[15,16]

Peptide	Primary Structure
Aβ	25 G S N K G A I I G L M 35
TDP-43	307 M G G G M N F G A F S I N 319
G314V	307 M G G G M N F V A F S I N 319

Table 6.1 Peptide sequence for SOD1$_{28-38}$ and associated mutants. Hydrophobic residues are highlighted in beige, Polar residues are highlighted in green, and positively charged residues are highlighted in grey.

Recent studies by have indicated that small soluble oligomers, not insoluble aggregates such as fibrils, are the proximal toxic agent in many protein misfolding diseases including ALS.[34-37] SOD1 residues 28-38 – SOD1(28-38) – were identified by cell viability studies to be sufficient for cytotoxicity (**Table 6.1**). X-ray crystallography of SOD1(28-38) P28K revealed an out of register, antiparallel β-sheet structure with a channel through the middle termed a corkscrew. The corkscrew bears structural similarities to another soluble oligomer, the cylindrin,[43] with the notable exception that while the cylindrin is a closed β-barrel the corkscrew is an open structure that can extend indefinitely, making a full rotation every 16 strands (**Figure 6.1**). Cylindrin-like structures have been postulated to be the proximal toxic agent in several protein misfolding diseases.[44,23] The P28K mutation was used to increase solubility and facilitate crystal formation, but was shown not to change toxicity or the stability of the corkscrew structure.

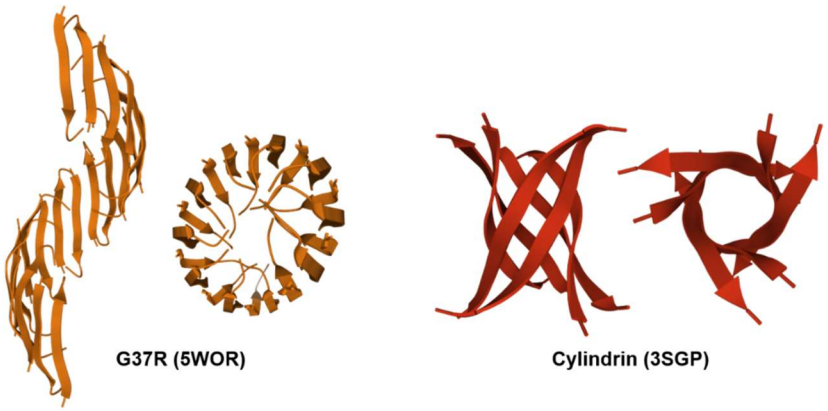

Figure 6.1 Side and top view of the crystal structures of (left) SOD1(28-38) P28K G37R corkscrew (PDB 5WOR) and (right) the cylindrin of K11V peptide segment of αB-Crystallin (PDB 3SGP).

The central glycine at residue 33 was identified as being essential for the stability of the corkscrew structure. The synthetic mutation G33W, which replaces the central glycine with a tryptophan, introduces a bulky side chain and was shown to disrupt the formation of the corkscrew structure. Critically, in cell viability studies the G33W mutation inhibits the toxicity of both SOD1(28-38) and the full length SOD1, even when paired with other ALS-related mutations. This result implies that SOD1(28-38) is necessary for toxicity and that this toxicity is linked to the formation of the corkscrew structure.[24]

It is important to note that SOD1(28-38) is a relatively conserved region of the protein, with only 6 ALS-related mutations. Of these mutations, G37R is of particular interest because transgenic mice studies have shown an enhanced rate of aggregation in full length SOD1.[26] In addition, X-ray crystallography of SOD1(28-38) P28K G37R shows that it forms a corkscrew structurally similar to what is observed in WT SOD1, with a full rotation ever 20 strands.[25]

While these earlier studies are highly informative, they do not address the mechanism for SOD1 aggregation that leads to the proposed toxic structures which is essential to the development of effective therapeutics. Here, we aim to use ion mobility-mass spectroscopy (IM-MS) in conjunction with atomic force microscopy (AFM) to correlate the crystal structure to the soluble phase and elucidate the early-stage aggregation pathway of WT $SOD1_{28-38}$ and the G37R and G33W mutations.

6.2 Experimental Methods

6.2A Peptide Preparation

All SOD1(28-38) peptides were purchased from GenScript (New Jersey, USA). To reduce peptides to their monomeric state, peptides were dissolved in hexafluoroisopropanol (HFIP) to concentrations of 100 mg/mL, which was completely evaporated off before final sample preparation.

6.2B Ion-Mobility Mass Spectrometry

Ion mobility-mass spectrometry (IM-MS) was used to deduce oligomer development and determine collision cross sections. IM-MS separates species of a specific $[m]^{+z}$ (m = mass, z = charge) with different $[n]^{+z}$ (n = oligomer number) by measuring arrival time distributions (ATDs). Experiments were performed on a home-built high resolution ion mobility mass spectrometer that consists of a nano-electrospray ionization source, ion funnel, a 200 cm-long drift cell, and a quadrupole mass filter mass spectrometer. Ions are generated at the nano-electrospray ionization source, captured and stored in a home-built hourglass ion funnel, then pulsed into the 200 cm drift cell filled with ~10 torr of helium gas. The ions exit the drift cell continue to the quadrupole mass filter and finally reach the detector. The long

drift cell allows for improved separation of conformers as well as oligomers of different sizes, results in incredibly well resolved and detailed ATDs.[27]

6.2C Far- UV Circular Dichroism

CD data was collected using a Jasco J-810 CD Spectrometer. $SOD1_{28-38}$ samples of all peptides were prepared at peptide concentrations of 100 μM in 10 mM ammonium acetate, pH 7.4. Measurements were collected at wavelengths from 260-190 nm with 0.5 nm intervals, a 4 s response time, and a 1 nm bandwidth. All spectra were collected in a 1 mm quartz cuvette at 295 K. Data represents an average of 5 scans with a buffer baseline subtracted and the curves baseline corrected.

6.2D Thioflavin T Fluorescence Assay

Thioflavin T stock solutions were prepared using the method described by Khurana et al.[26] SOD1(28-38) peptides were prepared at a concentration 100 μM peptide and 98 μM thioflavin T in 10 mM ammonium acetate, pH 7.4. Peptides were incubated in a 37° C water bath for two weeks. Fluorescence was then measured (λex = 446 nm, λem = 460-540 nm) on a ThermoSpectronic Aminco Bowman Series 2 Luminescence Spectrometer with excitation and emission bandwidths set to 2 nm and a photomultiplier voltage of 600. Samples were pipetted gently at the beginning of the experiment. An increase in the fluorescence of thioflavin T at 490 nm is associated with the formation of β-sheet amyloid fibrils. The buffer background was subtracted from all data points. A standard consisting of a 100 μM thioflavin T solution in dimethylformamide was run prior to each experiment and the fluorescence intensity at 490 nm was used to normalize the data.[27]

6.2E Atomic Force Microscopy

Atomic force microscopy (AFM) was used to characterize TDP-43(307-319) fibril growth and morphology, and correlate these with oligomeric assembly. Experiments were conducted using an MFP-3D AFM (Asylum Research, Goleta, CA) and Cantilever C on HQ:XSC11/Al BS AFM probes (NanoAndMore USA Corp, Watsonville, CA). Images were acquired in air using repulsive tapping mode. Samples were prepared for imaging by depositing 5 μL of solution on freshly cleaved V1-grade muscovite mica discs (Ted Pella, Edding, CA) and drying in a vacuum desiccator. Samples were visibly dry in approximately 5 minutes but were allowed to dry over-night.

6.3 Results and Discussion

6.3A Ion Mobility-Mass Spectrometry

Ion mobility-mass spectrometry (IM-MS) is a useful tool for studying soluble oligomer species in protein aggregation. Because an oligomers arrival time is related to its collision cross section, this technique is capable of revealing interesting conformational information. Solutions of WT SOD1(28-38), the ALS-related mutant SOD1(28-38) G37R, and the corkscrew disrupting mutant SOD1(28-38) G33W were each incubated at 100 μM peptide concentrations in 10 mM ammonium acetate, pH 7.4, at room temperature. MS reveals several major and minor peaks for all peptides (**Figure 6.2**).

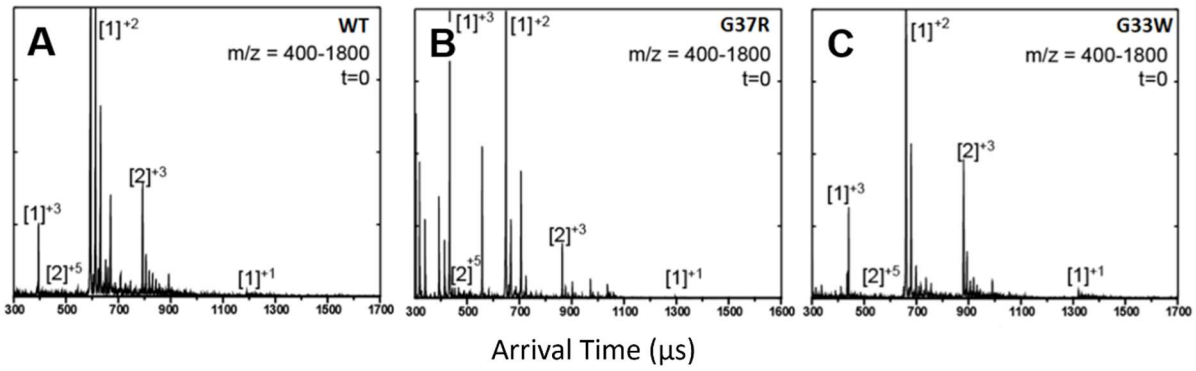

Figure 6.2 Mass spectra at t=0 for (A) WT SOD1(28-38), (B) G37R, and (C) G33W. All mass spectra have major peaks corresponding to the $[2]^{+3}$, $[1]^{+2}$, and $[1]^{+3}$ charge states and minor peaks corresponding to the $[1]^{+1}$ and $[2]^{+5}$ charge states. All experiments performed by Dr. Veronica Laos.[32]

Of particular interest is the $[2]^{+5}$ charge state as the arrival time distributions (ATDs) reveal oligomers with multiple conformations. Both WT SOD1(28-38) and SOD1(28-38) G37R were observed to form extended and compact structures (**Figure 6.3A-D**). Because compact structures experience fewer buffer gas collisions in the drift cell of the instrument, they will have an earlier arrival time than extended structures. The compact structures observed here have collision cross sections consistent with the corkscrew structures described by Eisenberg et al.[43,25] SOD1(28-38) G37R was observed to have a greater preference for the compact conformation than WT SOD1(28-38). Both peptides experienced a shift towards compact conformations at longer incubation times. SOD1(28-38) G33W was not observed to form a compact structure (**Figure 6.3E, F**). Taking the corkscrew to be a toxic structure, these results are consistent with the G37R mutation causing ALS and the G33W mutation being non-toxic.

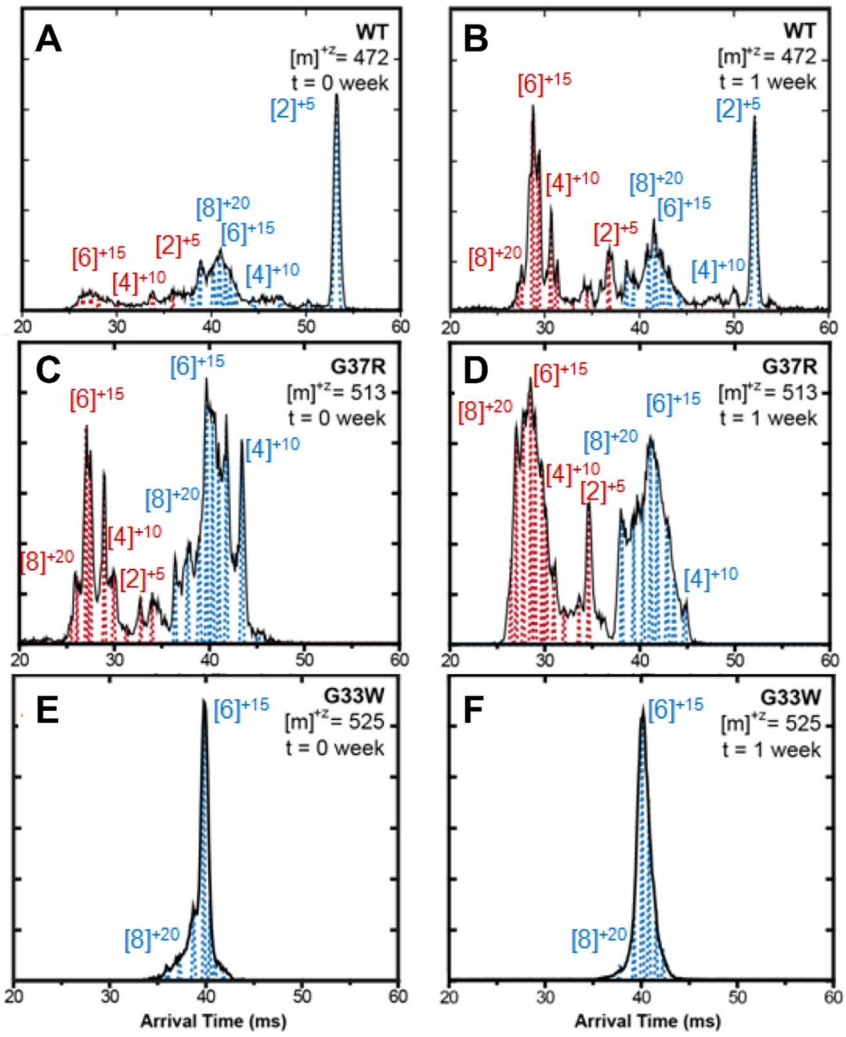

Figure 6.3 ATD of the $[2]^{+5}$ charge state at t=0 and t=1 week for (A, B) WT SOD1(28-38), (C, D) G37R, and (E, F) G33W. Oligomers are present in two series for both WT SOD1(28-38) and SOD1(28-38) G317R representing different conformations. Species in red are consistent with a compact conformation and species in blue are consistent with an extended conformation. Distributions for both peptides shift towards compact conformations after 1 week. G33W shows only oligomers consistent with an extended conformation. All experiments performed by Dr. Veronica Laos.[32]

6.3B Secondary Structure Characterization

SOD1(28-38) peptides were investigated using far-UV circular dichroism (CD) and the thioflavin T (ThT) fluorescence assay. Both these techniques are commonly used to identify and quantify fibril formation by tracking beta sheet formation. CD spectra of all SOD1(28-38) spectra were not observed to change over the course of 3 weeks. Both WT SOD1(28-38) (**Figure 6.4A**) and SOD1(28-38) G37R (**Figure 6.4C**) only demonstrated a negative band around 196 nm, characteristic of random coil secondary structure. SOD1(28-38) demonstrates this band in addition to a negative band around 225 nm, characteristic of alpha helix formation (**Figure 6.4B**). None of the peptides demonstrated fluorescence in the ThT assay (**Figure 6.4D**). These results suggest a lack of substantial fibril formation.

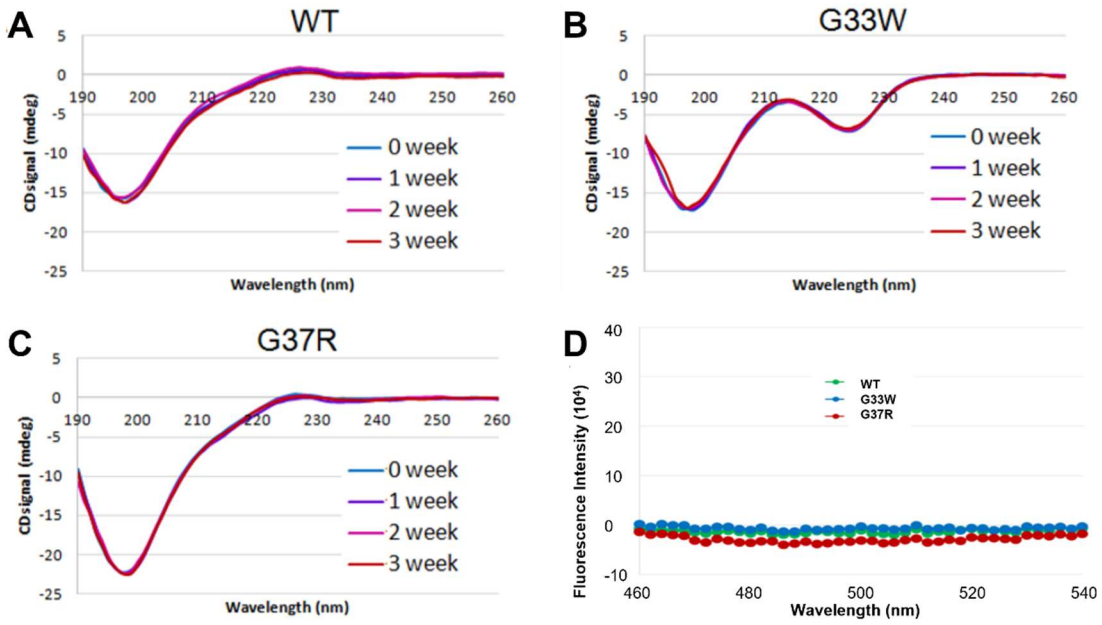

Figure 6.4 Secondary structure analysis for SOD1(28-38) does not predict fibril formation. Far-UV CD spectra of (A) WT SOD1$_{28-38}$, (B) G37R, and (C) G33W show no evolution over time and are inconsistent beta sheet formation. WT SOD1(28-38) and SOD1(28-38) G37R both demonstrate bands corresponding to random coil secondary structure and SOD1 demonstrates bands consistent with random coil and alpha helix

secondary structures. (D) None of the peptides were shown to fluoresce using the ThT fluorescence assay after 2 weeks of incubation.

6.3C Atomic Force Microscopy

Atomic force microscopy (AFM) is useful for studying the transition from soluble oligomers to larger, insoluble aggregates including fibrils. AFM phase imaging can also give relative information about the mechanical properties of individual features to complement the bulk secondary structure analysis of CD and ThT fluorescence. In repulsive mode phase imaging, harder features such as β-sheets will have a lower phase. All peptides were incubated at concentrations of both 100 μM and 10 μM in 10 mM ammonium acetate, pH 7.4, for up to 5 weeks.

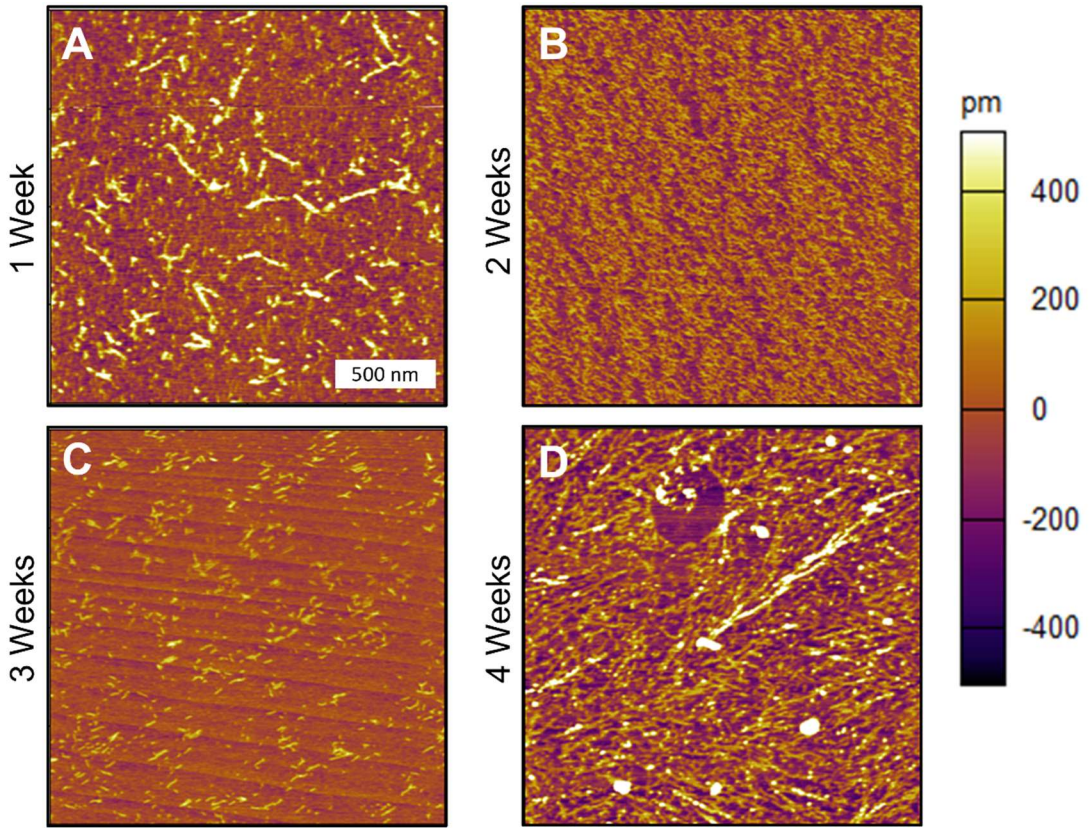

Figure 6.5 AFM height images of 10 µM WT SOD1(28-38) after incubating for (A) 1 week, (B) 2 weeks, (C) 3 weeks, and (D) 4 weeks. Very short, linear aggregates are observable at all time points

At 10 µM peptide concentrations, WT SOD1(28-38) was observed to uncommonly form high aspect ratio aggregates within 1 week and persist through 4 weeks (**Figure 6.5**). Height analysis of these features reveals that they commonly have significant, semi-regular height variation (**Figure 6.6**). The interval of this variation is inconsistent with the pitch of the corkscrew crystal structure. Instead, this is likely a beads-on-a-string mechanism of peptide assembly into larger structures. Phase imaging of these aggregates indicates that they are harder than the background peptide film, suggesting some level of beta sheet formation (**Figure 6.7A**). At 100 µM concentrations, only a peptide film is observable. This film is disordered at 1 week (**Figure 6.8A**), but by 3 weeks has developed a somewhat ordered pattern (**Figure 6.8B**). This likely indicates that the features observed at 10 µM are non-fibrillar in nature, a conclusion supported by secondary structure characterization.

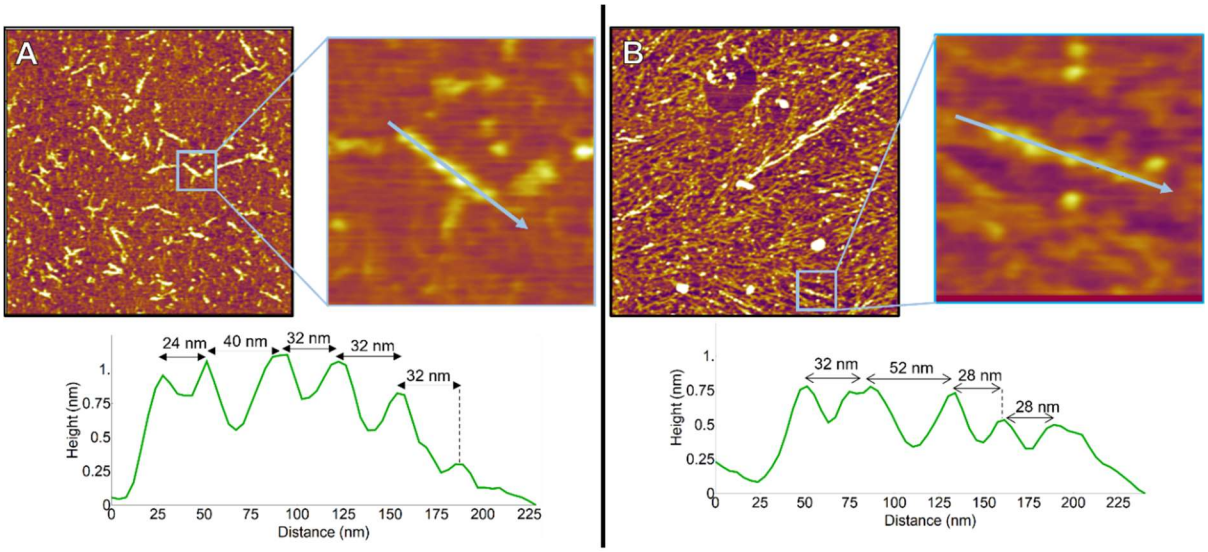

Figure 6.6 Height profiles of features observed in AFM height images of 10 µM WT SOD1(28-38) after incubating for (A) 1 week and (B) 4 weeks. Both profiles reveal semi0regular height variations consistent with a beads-on-a-string assembly mechanism.

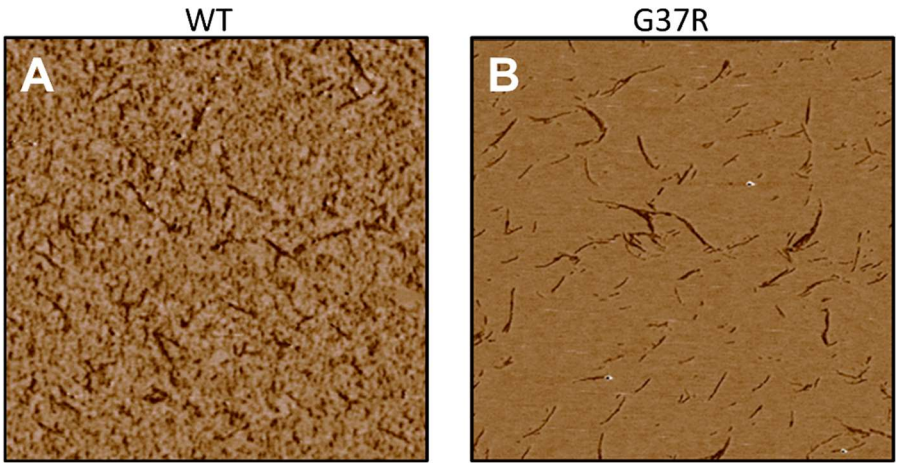

Figure 6.7 AFM repulsive mode phase images of discrete features observed in (A) 10 µM WT SOD1(28-38) after 15 minutes and (D) 10 µM SOD1(28-38) G37R after 5 weeks. Lower phases are associated with harder features, while higher phases are associated with softer features. Both images show features that are harder than the peptide film background suggesting some level of beta sheet formation.

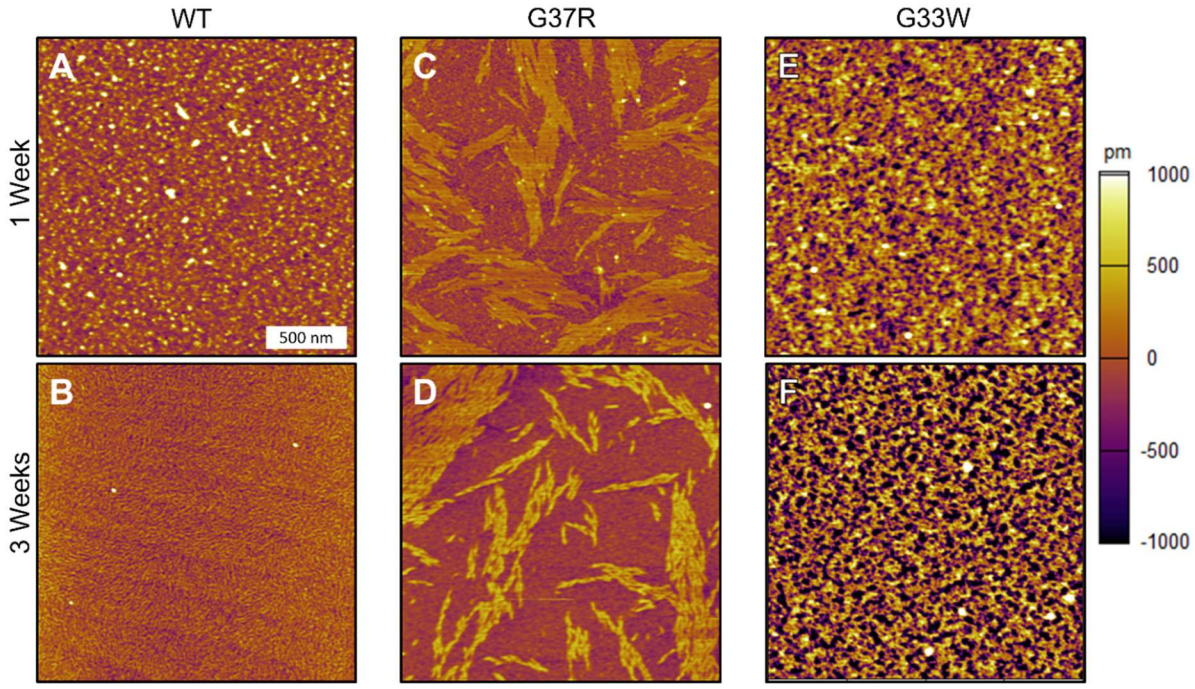

Figure 6.8 AFM height images of 100 µM (A, B) WT SOD1(28-38), (C, D) SOD1(28-38) G37R, and (E, F) SOD1(28-38) G33W. WT SOD1(28-38) demonstrates a peptide film at 1 week that demonstrates a small degree of order after 3 weeks. SOD1(28-38) G317R forms flat features with regular height. Corkscrew disrupting mutant SOD1(28-38) G33W was only observed to demonstrate a disordered peptide film.

SOD1(28-38) G37R begins to exhibit discreet, high aspect ratio aggregates after 2 weeks when incubated at 10 µM. These aggregates are fully separated from the background peptide film after 5 weeks (**Figure 6.9**). Similar to the WT, phase imaging indicates the aggregates observed are β-sheet rich relative to the peptide film background (**Figure 6.7B**). After increasing peptide concentration to 100 µM, SOD1(28-38) G37R formed flake-like, non-fibrillar features with a largely consistent height of approximately 500pm on top of a disordered film of peptide at both 1 week and 3 weeks (**Figure 6.8C, D**). Phase contrast between these flakes and the background suggest a higher proportion of β-sheets in the flakes

(**Figure 6.10**). These features are consistent with the evolution of the aggregates observed at 10 µM. These results indicate that G37R is more prone to forming organized structures than WT. Considering that G37R is a fALS related mutation, it is not surprising to see a higher degree of ordered aggregation.

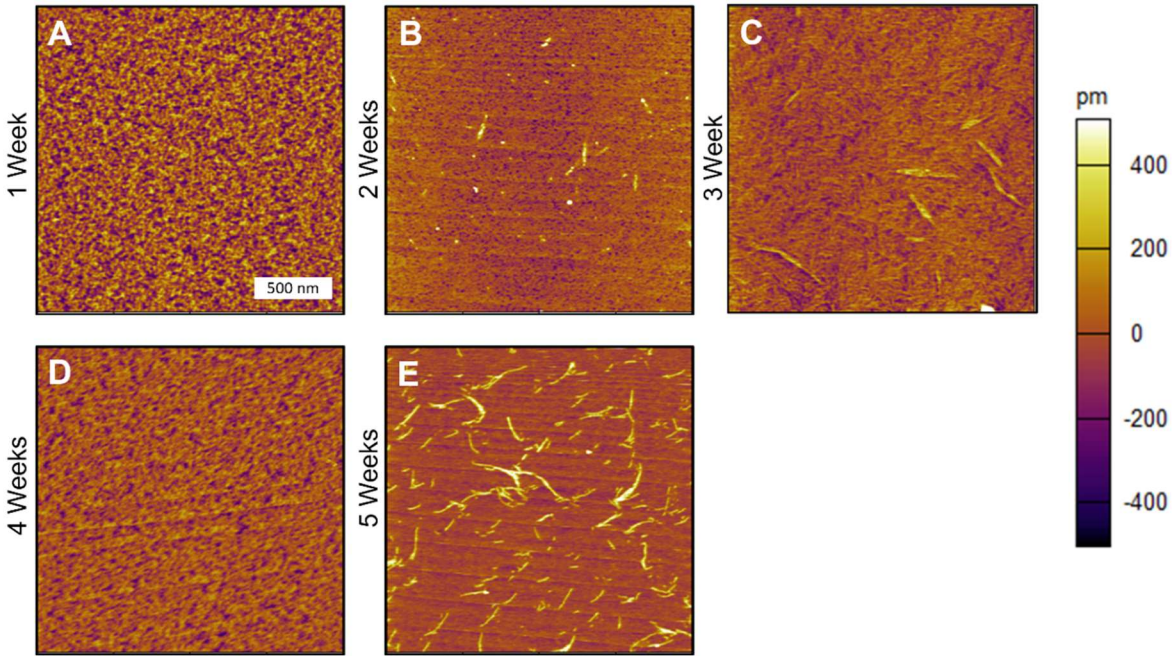

Figure 6.9 AFM height images of 10 µM SOD1(28-38) G37R after incubating for (A) 1 week, (B) 2 weeks, (C) 3 weeks, (D) 4 weeks, and (E) 5 weeks. Short linear features associated with the background peptide film are observable at 2 and 3 weeks. At 5 weeks these features are distinct from the background.

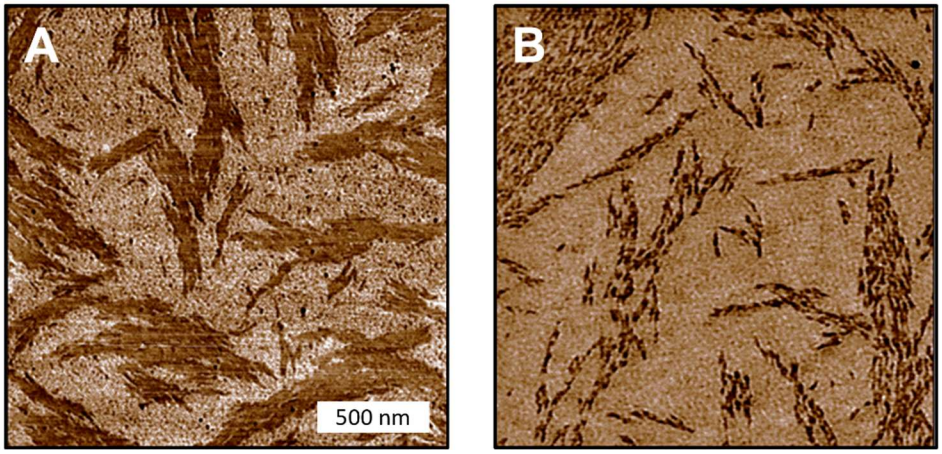

Figure 6.10 AFM repulsive mode phase images of 100 μM SOD1(28-38) G37R after incubating for (A) 1 week and (B) 3 weeks. Lower phases are associated with harder features, while higher phases are associated with softer features. Both images show features that are harder than the peptide film background suggesting beta sheet formation.

At both 10 μM (**Figure 6.11**) and 100 μM (**Figure 6.8E, F**) the corkscrew disrupting mutant SOD1(28-38) G33W was observed to form an amorphous peptide film. In some areas, portions of this film are relatively rough, however, discrete, high aspect ratio aggregates such as those observed in WT SOD1(28-38) and SOD1(28-38) G37R are never observed. This suggests that those aggregates observed in WT and G37R may either be directly related to the corkscrew or dependent on the same intermolecular interactions.

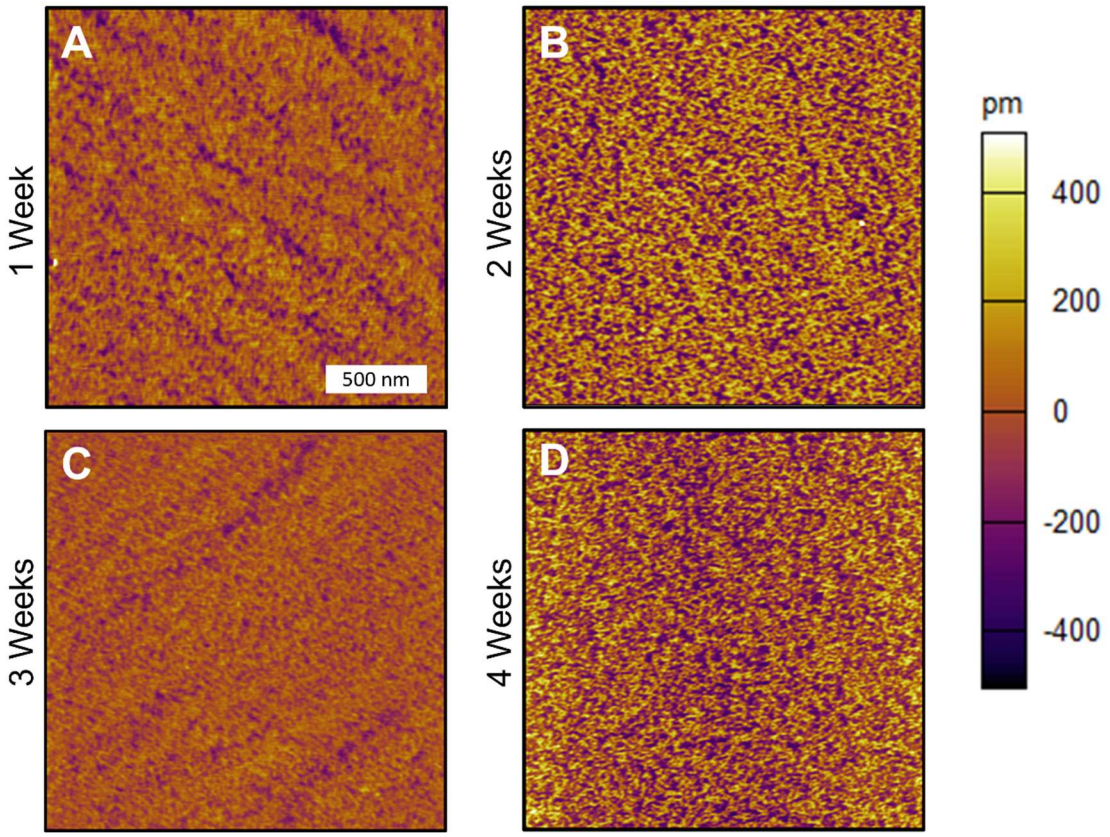

Figure 6.11 AFM height images of 10 µM SOD1(28-38) G33W after incubating for (A) 1 week, (B) 2 weeks, (C) 3 weeks, and (D) 4 weeks. Only a disordered peptide film is ever observable.

6.4 Conclusion

Recent studies have highlighted the ability of SOD1(28-38) to form a corkscrew structure similar to the cylindrin structure previously described. This fragment is of particular interest because it is both highly conserved, with relatively few naturally occurring mutations, and is sufficient for toxicity. The toxicity is believed to be tied to the corkscrew structure due to its similarities with the cylindrin and because the synthetic corkscrew-disrupting mutation G33W is non-toxic. Understanding the aggregation properties and

corkscrew formation of this fragment may thus elucidate information on the pathology of ALS. [43,25]

In this work, IM-MS was shown to support that WT SOD1(28-38) and SOD1(28-38) G37R both form a corkscrew structure, while SOD1(28-38) G33W does not. Additionally, secondary structure characterization shows the bulk solutions of all peptides do not contain structures with long range order over the course 3 weeks. AFM demonstrates that the corkscrew structures were also not observed to be on pathway to fibril formation. Despite this, SOD1(28-38) G37R is predisposed to forming more ordered aggregates while SOD1(28-38) G33W reduces aggregation propensity. Given that only corkscrew forming peptides were observed to form extended aggregates via AFM, it's possible that these are related to the presence of corkscrew structures.

6.5 References

1. Mehta, P.; Kaye, W.; Raymond, J. Punjani, R.; Larson, T.; Cohen, J.; Muravov, O.; Horton, K. Prevalence of Amyotophic Lateral Sclerosis – United States. Rep, 2015. *Morb Mortal Wkly Rep.* **2018**, *67* (46), 1285-9.
2. Mehta, P.; Raymond, J.; Punjani, R.; Han, M.; Larson, T.; Kaye, W.; Nelson, L. M.; Topol, B.; Muravov, O.; Genson, C.; Horton, K. Prevalence of amyotrophic lateral sclerosis in the United States Using Established and Novel Methodologies, 2017. *Amyotroph Lateral Scler Frontotemporal Degener* **2022,** Advanced online publication.
3. Millul, A.; Beghi, E.; Logroscino, G.; Micheli, A.; Vitelli, E.; Zardi, A. Survival of patients with amyotrophic lateral sclerosis in a population-based registry. *Neuroepidemiology* **2005**, *25* (3), 114-9.
4. Del Aguila, M. A.; Longstreth, W. T. Jr.; McGuire, V.; Koepsell, T. D.; van Belle, G. Prognosis in amyotrophic lateral sclerosis, a population-based study. *Neurology* **2003**,*60* (5), 813-9.

5. Byrne, S.; Walsh, C.; Lynch, C.; Bede, P. Elamin, M. Kenna, K. McLaughlin, R. Hardiman, O. Rate of familial amyotrophic lateral sclerosis: a systematic review and meta-analysis. *J Neurol Neurosurg Psychiatry* **2011**, *82*, 623-7.
6. Pasinelli, P.; Brown, Robert H. B. Molecular Biology of Amyotrophic Lateral Sclerosis: Insight from Genetics. *Nat Rev Neurosci* **7**, 710-23.
7. Chattopadhyay, M.; Valentine, J. S. Aggregation of Copper-Zinc Superoxide Dismutase in Familial and Sporadic ALS. *Antioxid Redox Signal*. **2009**, *11* (7), 1603-1614.
8. Blokhuis, A. M.; Groen, E. J. N.; Koppers, M.; van den Berg, L. H.; Pasterkamp, R. J. Protein aggregation in amyotrophic lateral sclerosis. *Acta Neuropathol* **2013**, *125*, 777-794.
9. Gagliardi, S.; Cova, E.; Davin, A.; Guareschi, S.; Abel, K.; Alvisi, E.; Laforenza, U.; Ghidoni, R.; Cashman, J. R.; Ceroni, M.; Cereda, C. SOD1 mRNA expression in sporadic amyotrophic lateral sclerosis. *Neurobiol Dis* **2010**, *39* (2), 198-203.
10. Forsberg, K.; Jonsson, P. A.; Anderson, P. M.; Bergemalm, D.; Graffmo, K. S.; Hultdin, M.; Jacobsson, J.; Rosquist, R.; Marklund, S. L.; Brännström, T. Novel Antibodies Reveal Inclusions Containing Non-Native SOD1 in Sporadic ALS Patients. *PLoS One* **2010** *5* (7), e11552.
11. Rotunno, M. S.; Bosco, D. A. An emerging role for misfolded wild-type SOD1 in sporadic ALS pathogenesis. *Front Cell Neurosci* **2013**, *7*.
12. Ivanova, M. I.; Sievers, S. I.; Guenther, E. L.; Johnson, L. M.; Winkler, D. D.; Galaleldeen, A.; Saway, M. R.; Hart, P. J.; Eisenberg, D. S. Aggregation-triggered segments of SOD1 fibril formation support a common pathway for familial and sporadic ALS. *Proc Natl Acad Sci USA* **2014** *111* (1), 197-210.
13. Fridovich, I. Superoxide dismutase. An adaptation to a paramagnetic Gas. *J Biol Chem* **1989** *264* (14), 7761-4.
14. Rosen, D. R.; Siddique, T.; Patterson, D.; Figlewicz, D. A.; Sapp, P. Hentati, A.; Donaldson, D.; Goto, J.; O'Regan, J. P.; Deng, H. X.; Rahmani, Z.; Krizus, A.; McKenna-Yasek, D.; Cayabyab, A.; Gaston, S. M.; Berger, R.; Tanzi, R. E.; Halperin, J. J.; Herzfeldt, B.; Van den Bergh, R.; Hung, W. Y.; Bird, T.; Deng, G.; Mudler, D. W.; Smyth, C.; Laing, N. G.; Soriano, E.; Pericake-Vance, M. A.; Haines,

J. Rouleau, G. A.; Gusella, J. S.; Gorvitz, H. R.; Brown Jr, R. H. Mutations in Cu/Zn superoxide dismutase gene are associated with familial amyotrophic lateral sclerosis. *Nature* **1993**, *362* 59-62.

15. Gurney, M. E.; Pu, H.; Chiu, A. Y.; Dal Canto, M. C.; Polchow, C. Y.; Alexander, D. D.; Caliendo, J.; Hentati, A.; Kwon, Y. W.; Deng, H. X.; Chen, W.; Zhai,P.; Sufit, R. L.;Siddique, T. Motor neuron degeneration in mice that express a human Cu, Zn superoxide dismutase mutation. *Science* **1995**, 264 (5166), 1772–1775.
16. Brujin, L. I.; Houseweart, M. K;, Kato, S.; Answerson, K. L.; Anserson, S. D.; Ohama, E.; Reaume, A. G.; Scott, R. W.; Cleveland, D. W. Aggregation and motor neuron toxicity of an ALS-linked SOD1 mutant independent from wild-type SOD1. *Science* **1998,** *281* (5384), 1851-4.
17. Proctor, E. A.; Fee, L. Tao, Y. Redler, R. L.; Fay, J. M.; Zhang, Y.; Lv, Z.; Mercer, I. P.; Deshmukh, M.; Lyubchenko, Y. L.; Dokholyan, N. V. Nonnative SOD1 trimer is toxic to motor neurons in a model of amyotrophic lateral sclerosis. *Proc Natl Acad Sci USA* **2015**, *113* (3) 614-9.
18. Sengupta, U.; Nilson, A. N.; Kayed, R. The Role of Amyloid-β Oligomers in Toxicity, Propagation, and Immunotherapy. *EBioMedicine* **2016**, *6*, 42-9.
19. Fang Y.S.; Tsai K. J.; Chang Y. J.; Kao P.; Woods R.; Kuo P. H.; Wu C. C.; Liao J. Y.; Chou S. C.; Lin V.; Jin L. W.; Yuan H. S.; Cheng I. H.; Tu P. H.; Chen Y. R. Full-length TDP-43 forms toxic amyloid oligomers that are present in frontotemporal lobar dementia-TDP patients. *Nat Commun* **2014,** *5,* 4824.
20. Ghag,G.; Bhatt, N.; Cantu, D. V.; Guerrero-Munoz, M. J.; Ellsworth, A.; Sengupta, U.; Kayed, R. Soluble tau aggregates, not large fibrils, are toxic species that display seeding and cross-seeding behavior. *Protein Sci* **2018**, *27* (11), 1901-9.
21. Laganowsky, A.; Liu, C.; Saway, M. R.; Whitelegge, J. P.; Park, J.; Zhao, M.; Pensalfini, A.; Soriaga, A. B.; Landau, M.; Teng, P. K.; Cascio, D.; Glabe, C.; Eisenberg, D.; Atomic View of a Toxic Amyloid Small Oligomer. *Science* **2012** *355* (6073), 1228-31.
22. Do, T. D.; LaPOinte, N. E.; Nelson, R.; Krotee, P.; Hayden, E. Y.; Ulrich, B.; Quan, S.; Feinstein, S. C.; Teplow, D. B.; Eisenberg, D.; Shea, J.; Bowers, M. T. Amyloid

β-Protein C-terminal Fragments: Formation of Cylindrins and β-Barrels. *J Am Chem Soc* **2016** *138* (2), 549-57.

23. Laos, V.; Do, T. D.; Bishop, D.; Jin, Y.; Marsh, N. M.; Quon, B.; Fetters, M.; Contrell, K. L.; Buratto, S. K., Bowers, M. T.; Characterizing TDP-43$_{307-319}$ Oligomeric Assembly Mechanistic and Structural Implications Involved in Etiology of Amyotrophic Lateral Sclerosis. *ACS Chem Neurosci* **2019** *10* (9), 4112-23.
24. Sangwan, S.; Zhao, A.; Adams, K. L.; Jayson, C. K.; Sawaya, M. R.; Guenther, E. L.; Pan, A. C.; Ngo, J.; Moore, D. M.; Soriage, A. B.; Do, T. D.; Goldschmidt, L.; Nelson, R.; Bowers, M. T.; Koehler, C. M.; Shaw, D. E.; Novitch, B. G.; Eisenberg, D. S. Atomic structure of a toxic, oligomeric segment of SOD1 linked to amyotrophic lateral sclerosis (ALS) *Proc Natl Acad Sci USA* **2017** *114* (33), 8770-5.
25. Sangwang, S.; Sawaya, M. R.; Murray, K. A.; Hughes, M. P.; Eisenberg, D. S. Atomic structures of corkscrew forming segments of SOD1 reveal varied oligomer conformations, *Protein Sci* **2018** *27* (7), 1231-42.
26. Wong, P. C.; Pardo, C. A.; Borchelt, D. R., Lee, M. K.; Copeland, N. G.; Jenkins, N. A; Sisodia, S. S.; Cleveland, D. W.; Price, D. L. An Adverse Property of a Familial ALS-Linked SOD1 Mutation Causes Motor Neuron Disease Characterized by Degeneration of Mitochondria. *Neuron* **1995** *14*, 1105-16.
27. Wyttenbach, T.; Kemper, P. R.; Baykut, G.; Park, M. A.; Bowers, M. T. A new instrument with high mass and high ion mobility resolution. *Int J of Mass Spectrom* **2018** *434*, 108-115.
28. Mason, E. A. Transport Properties of Ions in Gases, 99th ed. John Wiley & Sons, **1988**.
29. Gidden, J.; Ferzoco, A.; Baker, E. S.; Bowers, M. T. Duplex Formation and the Onset of Helicity in Poly d(CG)n Oligonucleotides in a Solvent-Free Environment. *J Am Chem Soc* **2004** *126* (46), 15132-15140.
30. Khurana, R.; Coleman, C.; Ionescu-Zanetti, C.; Carter, S. A.; Krishna, V.; Grover, R. K.; Roy, R.; Singh, S.; Mechanism of thioflavin T binding to amyloid fibrils. *J Struct Biol* **2005** *3* (141), 229-38.

31. Williams, A. T. R.; Winfield, S. A.; Miller, J. N. Relative Fluorescence Quantum Yields Using a Computer-controlled Luminescence Spectrometer. *Analyst* **1983** *108*, 1067-71.
32. Laos, V. Characterizing Oligomeric Assembly of ALS-related Proteins Utilizing Ion Mobility Mass Spectrometry. Ph.D. Dissertation, University of California – Santa Barbara, Santa Barbara, CA, **2020**. https://escholarship.org/uc/item/5pc2w0hj

VII. Summary and Future Work

7.1 Summary

Protein misfolding is related to numerous neurodegenerative diseases, including amyotrophic lateral sclerosis (ALS), Alzheimer's disease (AD), and Parkinson's disease. In these diseases, proteins adopt non-native conformations and aggregate into soluble oligomers and insoluble fibrils. Atomic force microscopy (AFM) is a powerful tool for imaging the early-stage assembly of these features when used in combination with ion mobility-mass spectrometry (IM-MS). The research presented in this work focuses on using these techniques to elucidate the structural assembly for the ALS-related protein fragments TDP-43(307-319) and SOD1(28-38). Additional focus was given to modulating TDP-43(307-319) through inhibitor molecules and cross talk with the AD-related protein amyloid beta (Aβ).

Interestingly, self-aggregation of TDP-43(307-319) was observed to occur via a bifurcated pathway. Fibrilization was found to be independent of oligomers implicated in disease. While ALS related mutations A315T and A315E were observed to rapidly form both higher order oligomers and fibrils, WT and the synthetic non-toxic mutation G314V were both observed to form fibrils in the absence of higher order toxic oligomers.[28] This result was notably different from recent work studying Aβ42 that showed the toxic dodecamer species seeding fibril formation.[2]

Having determined the self-aggregation propensity of TDP-43(307-319), potential inhibitor molecules were tested to determine their effect on higher order oligomers and fibrils. In collaboration with Ambuj Singh, (University of California Santa Barbara, Computer Science Department,) molecules generated using the novel Joint Pharmacophore Space (JPS) were shown to have a profound impact on oligomerization while having almost

no effect on fibrils or their formation.[40] As oligomers are suspect to be responsible to disease, this is an exciting result that may lead to new treatments for ALS. Additionally, these results support the conclusion that TDP-43(307-319) aggregation occurs via a bifurcated pathway.

TDP-43(307-319) was further studies to explain the association of TDP-43 aggregation with cognitive decline in AD. Co-aggregation experiments with the physiologically relevant fragment Aβ revealed significant cross talk between the two peptides. This resulted in rapid oligomerization and the formation of hetero-oligomers. Co-aggregation did not conclusively lead to a change in fibril formation when using WT TDP-43(307-319). However, in co-aggregation experiments with the non-toxic mutant G314V fibrils were observed at earlier time points than they were for self-aggregation experiments.[26] This suggests that co-aggregation may enhance fibrillization similarly to oligomerization.

Finally, the corkscrew-forming peptide SOD1(28-38) was investigated for its toxic role in familial ALS. IM-MS experiments were indicative of corkscrew formation in both WT SOD1(28-38) and SOD1(28-38) G37R and showed that SOD1(28-38) G37R disrupts corkscrew formation by replacing the central glycine that provides necessary flexibility. While AFM imaging revealed that none of these peptides formed fibrils, corkscrew formation was linked to nonfibrillar ordered aggregates.

7.2 Future Work

Neurodegenerative diseases remain one the least understood medical problems in the modern world. While the work here aims to shed light on certain aspects of several of these diseases, significant progress will be required to develop effective therapeutics. The presented research shows that IM-MS and AFM can be effective tools in studying these

diseases and should be further utilized to investigate abhorrent protein assembly and evaluating the modulating effects of drug molecules and other amyloidogenic proteins.

Studying protein fragments is necessary when utilizing mass-dependent tools like IM-MS. However, selecting the correct disease-relevant fragment can be non-trivial, and many studies choose to focus on different areas of the same protein. Both TDP-43(277-414) and TDP-43(286-331) have been previously identified as larger fragments that may be involved in disease.[5-6] Studying these fragments may provide additional insight into assembly of TDP-43, and confirm that TDP-43(307-319) is representative of aggregation observed in disease. While IM-MS may struggle with larger fragments, AFM is not gated in the same manner. Larger peptides may even allow individual oligomers to be imaged.

An aspect of physiologically observed protein aggregation that is not touched upon in this work is that pathological TDP-43 is typically heaving phosphorylated and ubiquitinated. The role of these post translational modifications in aggregation is not well established and understanding their impact could be important in the development of therapeutics.

Finally, significant work remains to be done on studying JPS inhibitor molecules. In addition to further training of the JPS machine learning algorithm to refine potential drug molecules, consideration must be given to these molecules' ability to modulate co-aggregation of TDP-43 and Aβ. The significant cross talk between these two peptides exemplifies the complex aggregation mechanism occurring in diseases like AD. Simply modulating self-aggregation may not be sufficient to combat aggregation *in vivo* where potential aggregation enhancers may be working to counteract the effect. The first steps to show that these inhibitors will remain effective include studying their effect on co-aggregation ofTDP-43(307-319) and Aβ(25-35).

7.3 References

1. Laos, V.; Do, T. D.; Bishop, D.; Jin, Y.; Marsh, N. M.; Quon, B.; Fetters, M.; Cantrell, K. L.; Buratto, S. K.; Bowers, M. T. Characterizing TDP-43(307-319) Oligomeric Assembly to Elucidate Mechanistic and Structural Implications Involved in the Etiology of ALS. *ACS Chem. Neurosci.* **2019**, *10* (9), 4112−4123.
2. Economou, N. J.; Giammona, M. J., Do, T. D.; Zheng, X.; Teplow, D. B.; Buratto, S. K.; Bowers, M. T. Amyloid β-Protein Assembly and Alzheimer's Disease: Dodecamers of Aβ42, but Not of Aβ40, Seed Fibril Formation. J. Am. Chem. Soc. 2016, 138 (6), 1772-5.
3. Laos, V.; Bishop, D.; Lang, A. C.; Marsh, N. M.; Cantrell, K. L.; Buratto, S. K.; Singh, A. K.; Bowers, M. T. Modulating ALS-Related Amyloidogenic TDP-43$_{307-319}$ Oligomeric Aggregation with Computationally Derived Therapeutic Molecules. *Biochemistry*. **2020**, *59* (4), 499-508.
4. Laos, V.; Bishop D.; Ganguly P.; Schonfeld, G.; Trapp, E.;Cantrell, K. L.; Buratto, S. K.; Shae, J. E.; Bowers, M. T. Catalytic Cross Talk between Key Peptide Fragments That Couple Alzheimer's Disease with Amyotrophic Lateral Sclerosis. *J. Am. Chem. Soc.* **2021,** *143* (9), 3494-3502.
5. Cushman M.; Johnson B. S.; King O.D.; Gitler A.D.; Shorter J. Prion-like disorders: blurring the divide between transmissibility and infectivity. *J. Cell Sci.* **2010**, 123 (Pt 8), 1191-201.
6. Chen A.K.; Lin R.Y.; Hsieh E.Z.; Tu P.H.; Chen R.P.; Liao T.Y.; Chen W.; Wang C.H.; Huang J.J.; Induction of amyloid fibrils by the C-terminal fragments of TDP-43 in amyotrophic lateral sclerosis. *J. Am. Chem. Soc*. **2010**, *132* (4), 1186–1187.